Supporting Information

Bimetallic CuFe nanoparticles as active and stable catalyst for chemoselective hydrogenation of biomass derived platform molecules

Karen S. Arias,† Lichen Liu,† Andrea Garcia-Ortiz, Maria J. Climent, Patricia Concepcion, Sara Iborra,*Avelino Corma*,

Instituto de Tecnología Química, Universidad Politécnica de Valencia-Consejo Superior de Investigaciones Científicas (UPV-CSIC), Av. de los Naranjos s/n, 46022 Valencia, Spain

† These authors contribute equally to this work.

*Corresponding authors. E-mail: acorma@itq.upv.es (A.C.) siborra@itq.upv.es (S.I.)

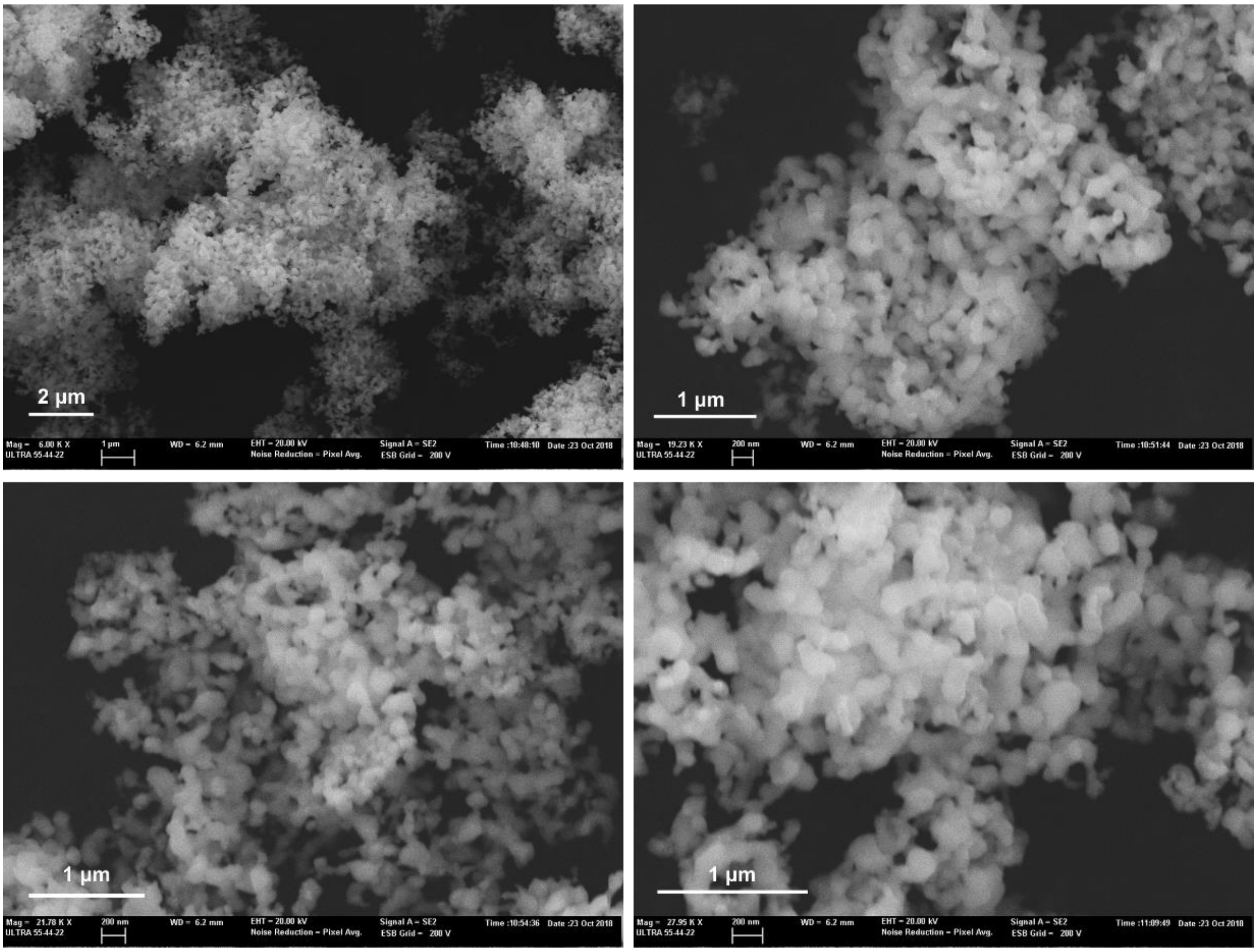

Figure S1. FESEM images of Fe@C sample. Fe nanoparticles of 50-200 nm can be observed.

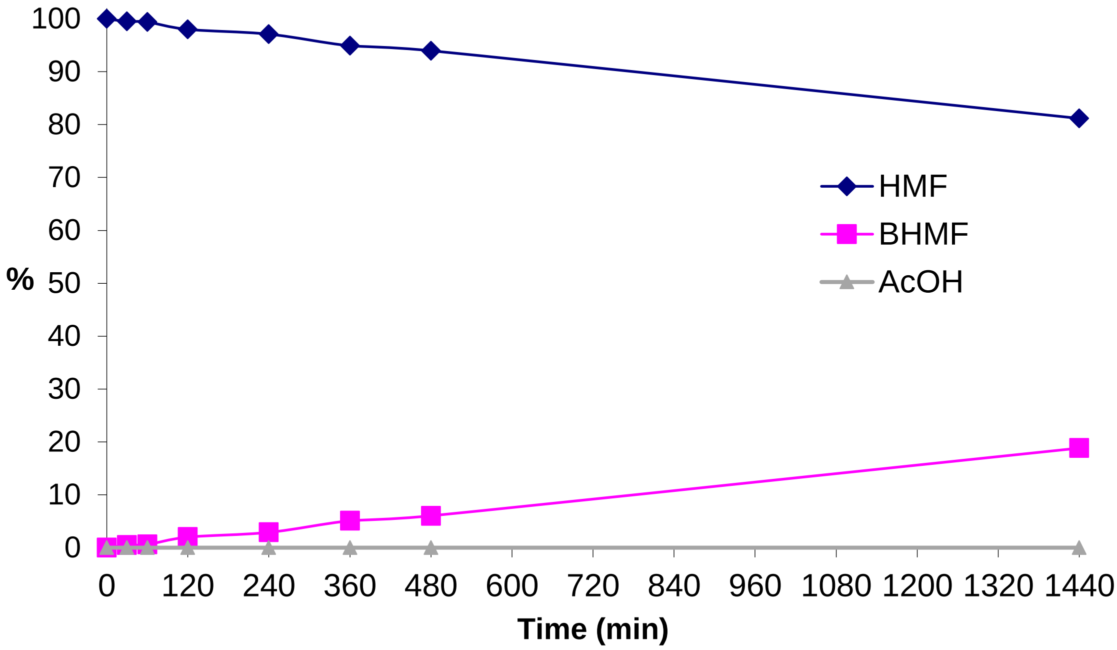

Figure S2. Catalytic performance of Fe@C catalyst after pre-reduction treatment.

The catalyst (10 mg) has been pre-reduced by H_2 (10 bar) at 260 ºC for 6 h in autoclave before of reaction. HMF, dodecane and MeOH were dried previously with molecular sieves and N_2 flow. After the pre-reduction treatment, a solution of HMF (0.5 mmol) in MeOH (5 mL) and dodecane as standard was transferred to autoclave at room temperature with a syringe and was purged three times with H_2. Then the autoclave was pressurized with 10 bar of H_2. The stirring speed is kept at 1000 rpm and the reactor was heated at 110 ºC.

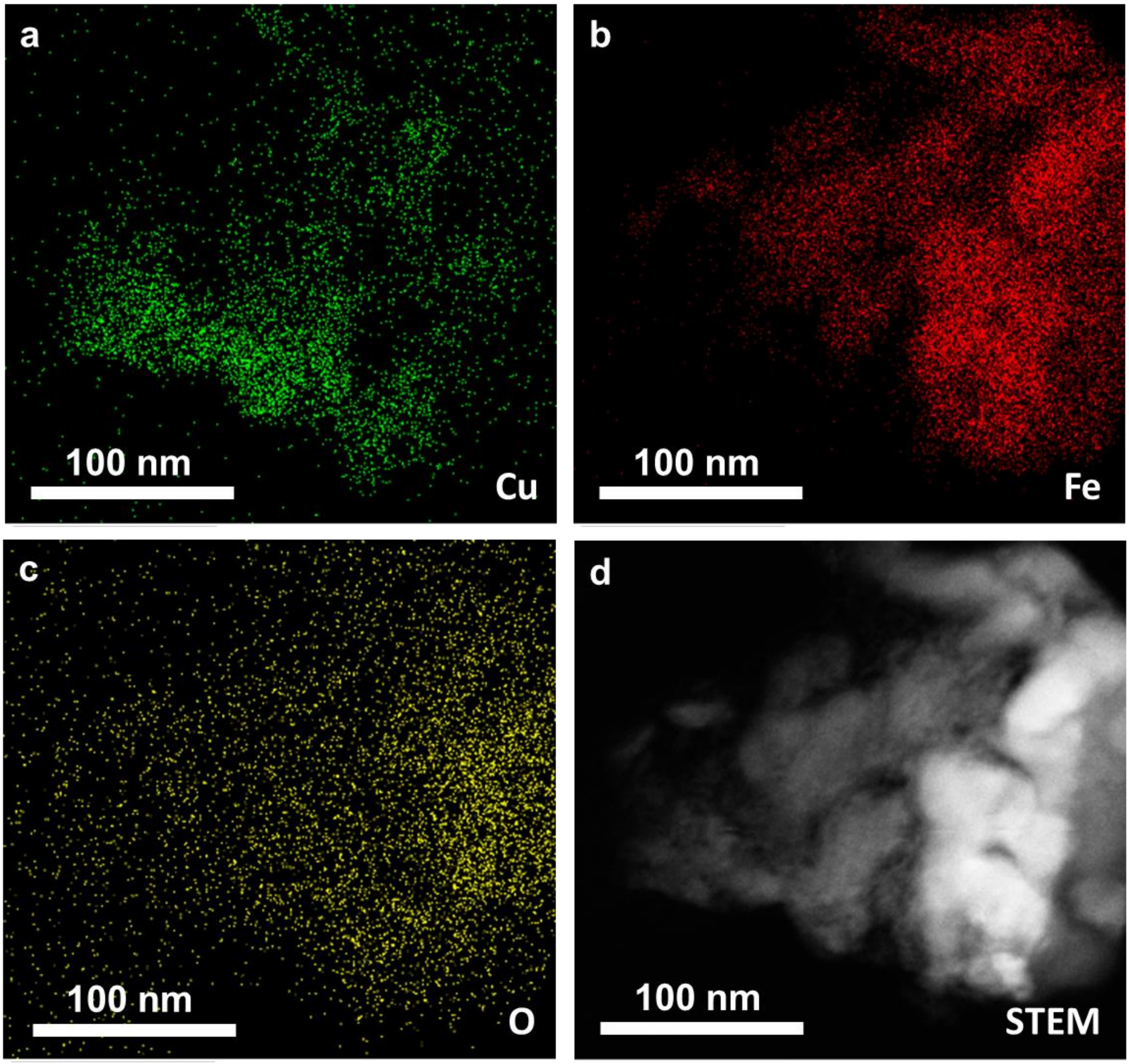

Figure S3. Morphological characterization of 25Cu/Fe@C sample by STEM-EDS mapping with 25 wt% of Cu. In these images, Cu nanoparticles as well as highly dispersed Cu species on Fe@C nanoparticles can be observed.

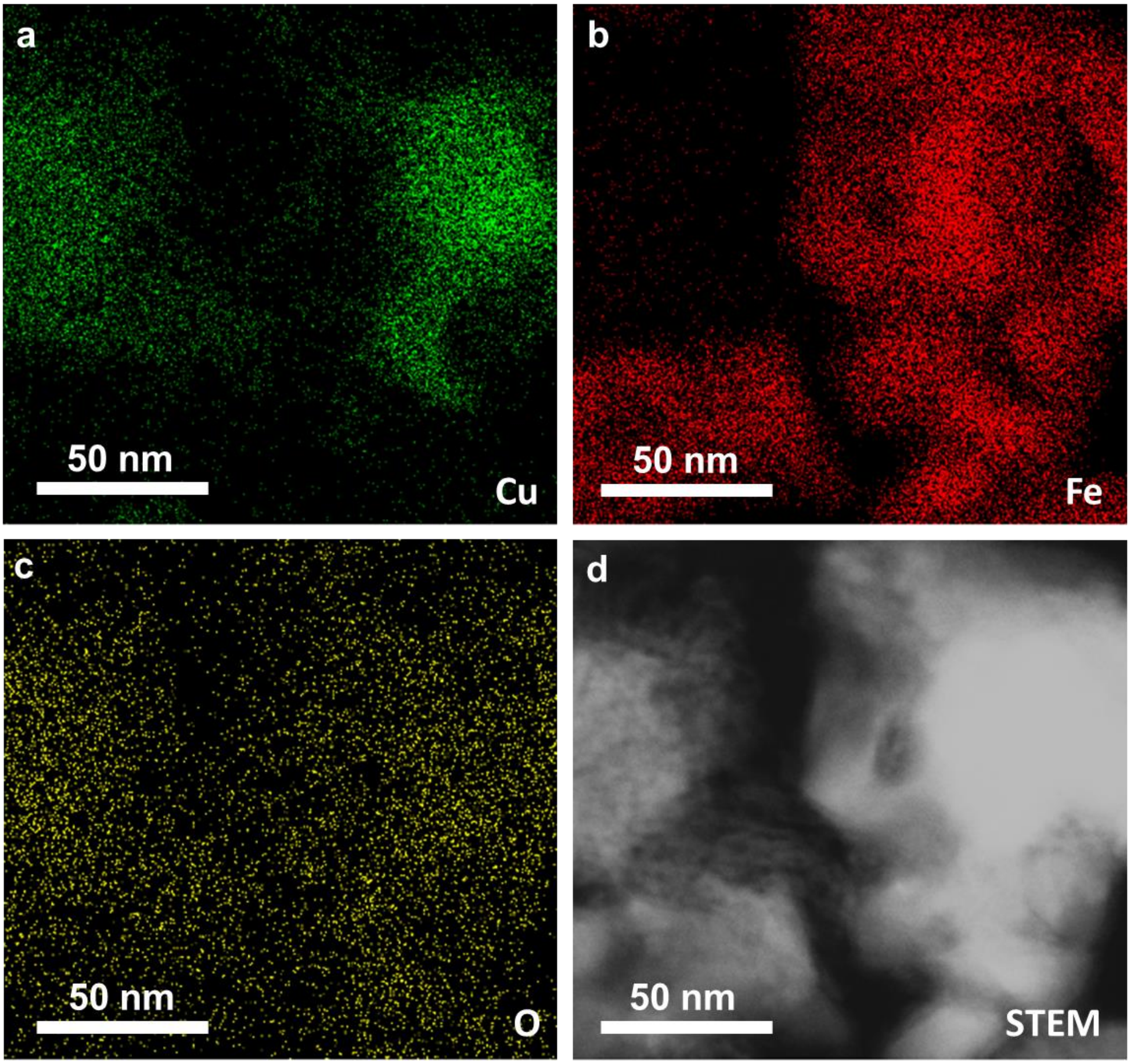

Figure S4. Morphological characterization of 25Cu/Fe@C sample by STEM-EDS mapping with 25 wt% of Cu. In these images, Cu nanoparticles as well as highly dispersed Cu species on Fe@C nanoparticles can be observed.

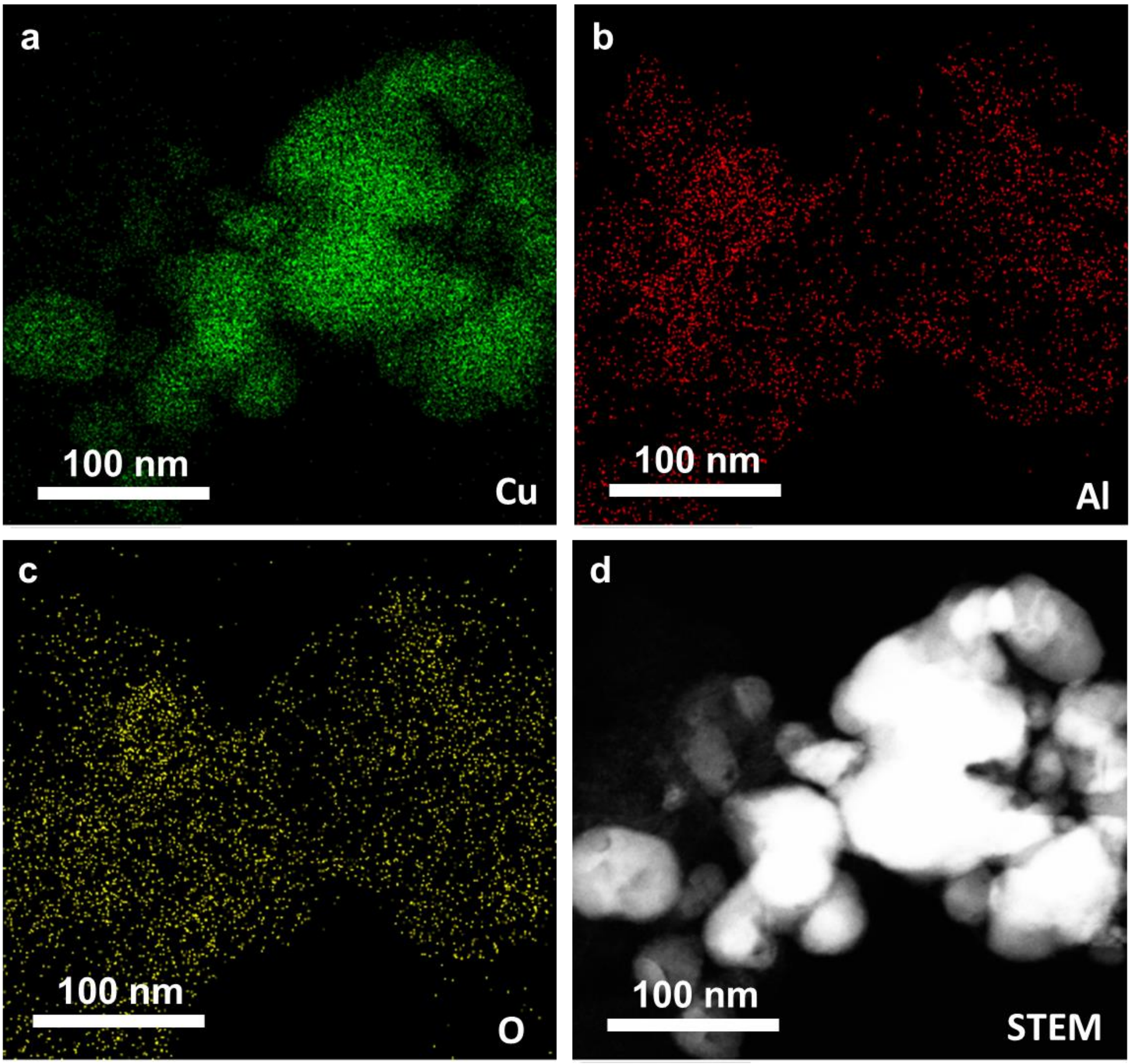

Figure S5. Morphological characterization of $25Cu/Al_2O_3$ sample by STEM-EDS mapping. In these images, Cu nanoparticles as well as highly dispersed Cu species on Al_2O_3 can be observed.

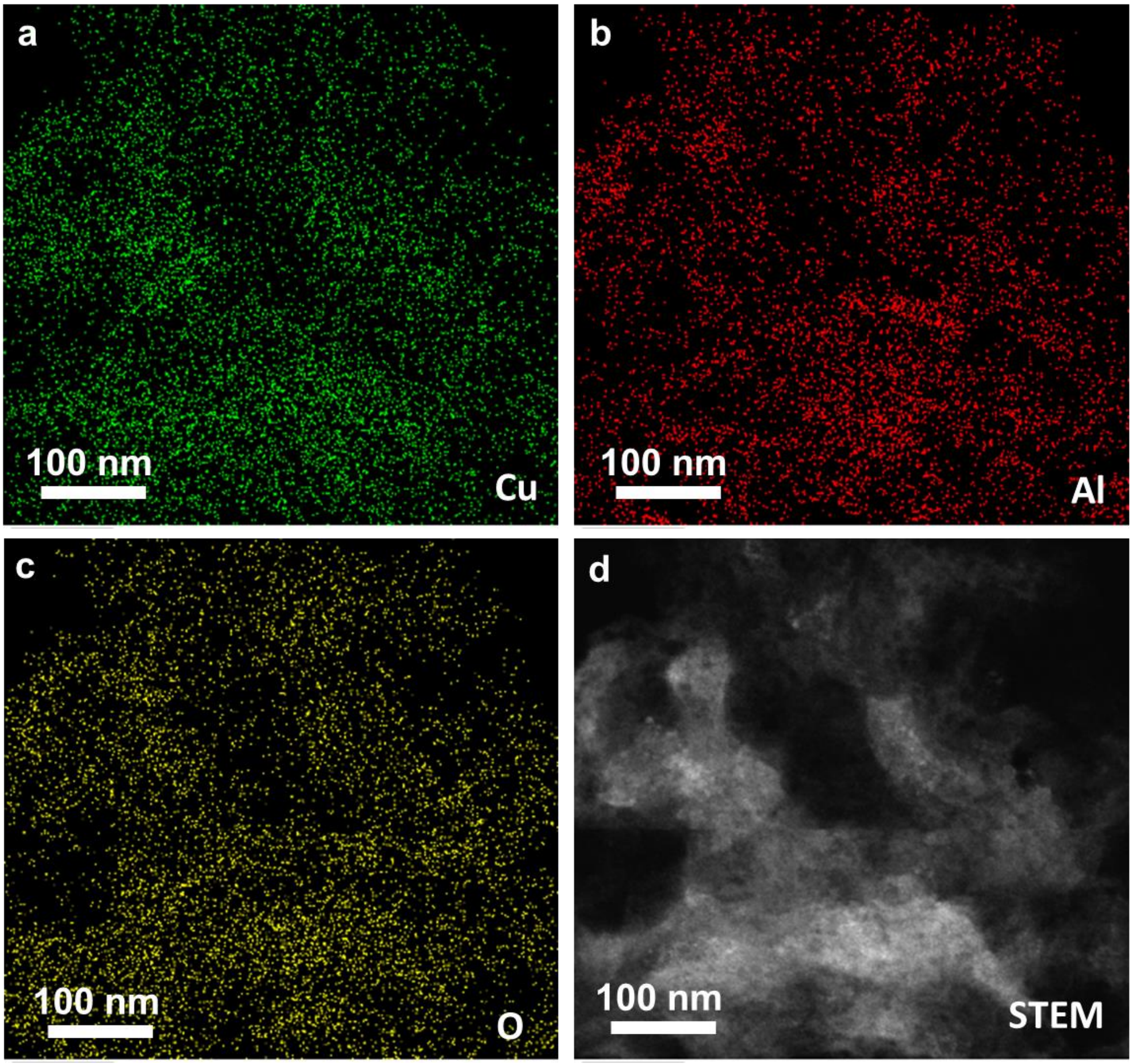

Figure S6. Morphological characterization of 25Cu/Al_2O_3 sample by STEM-EDS mapping. In these images, Cu nanoparticles as well as highly dispersed Cu species on Al_2O_3 can be observed.

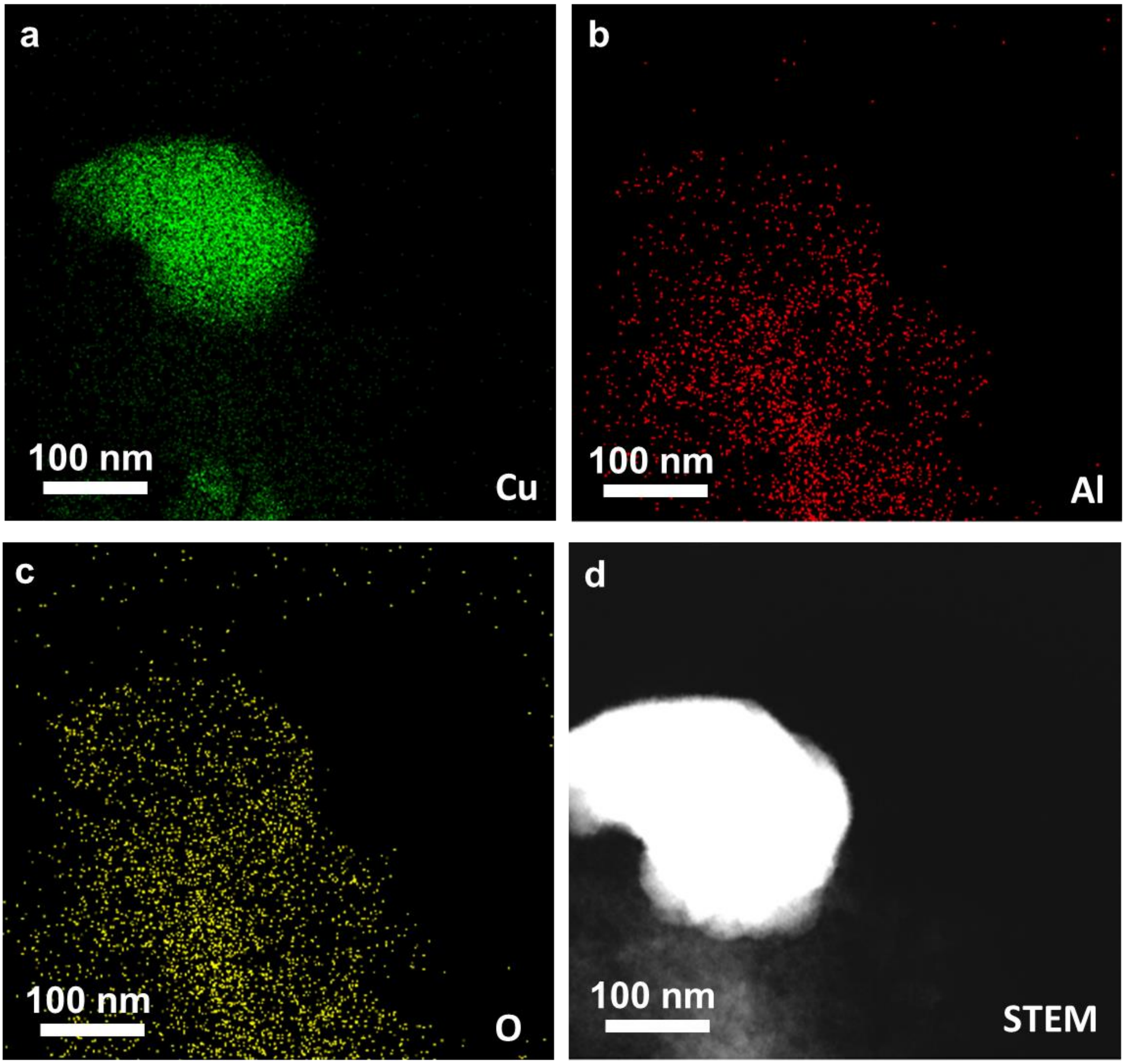

Figure S7. Morphological characterization of $25Cu/Al_2O_3$ sample by STEM-EDS mapping. In these images, Cu nanoparticles as well as highly dispersed Cu species on Al_2O_3 can be observed.

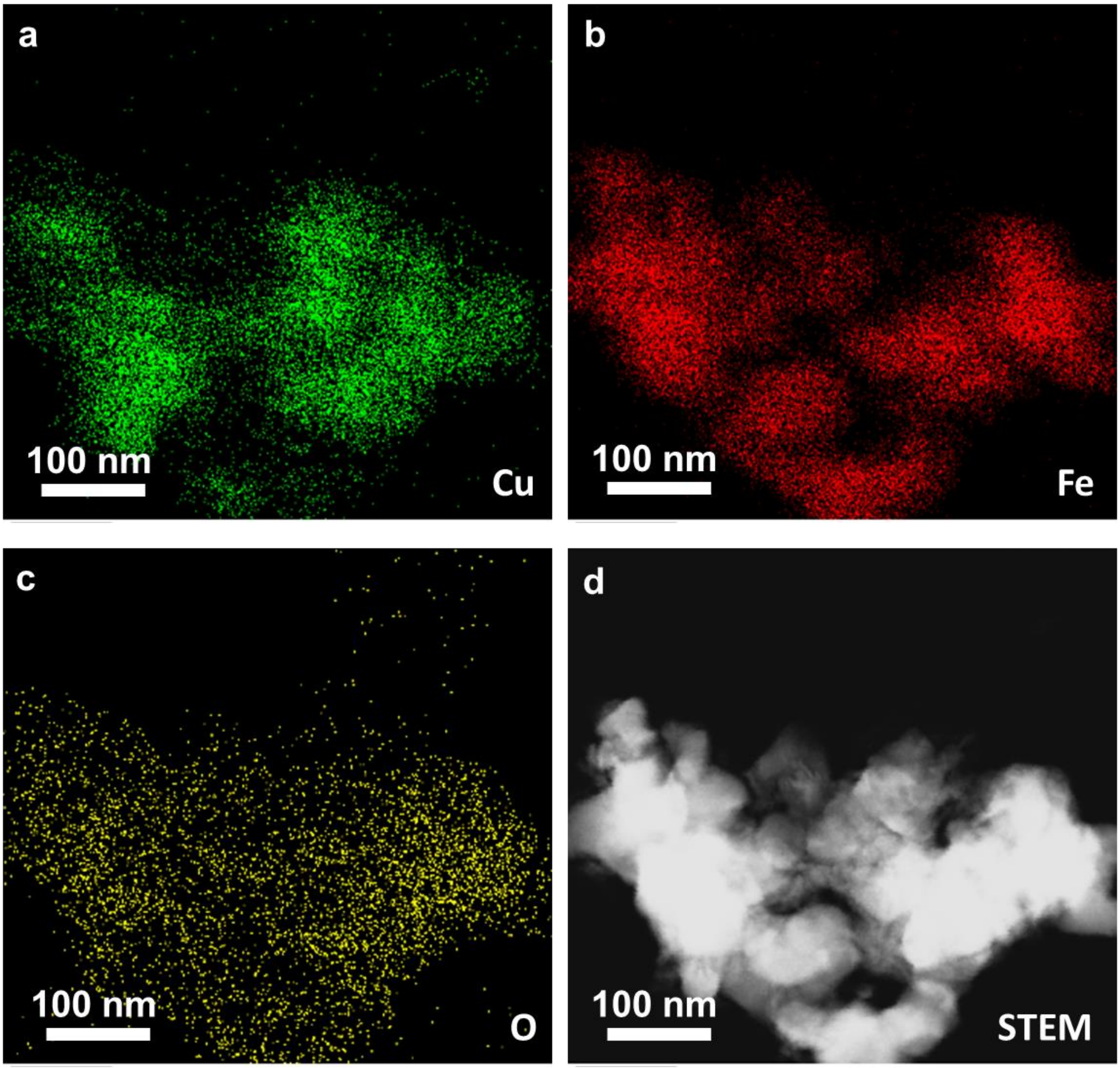

Figure S8. Morphological characterization of $25Cu/Fe_2O_3$ sample by STEM-EDS mapping. In these images, Cu nanoparticles as well as highly dispersed Cu species on the Fe support can be observed.

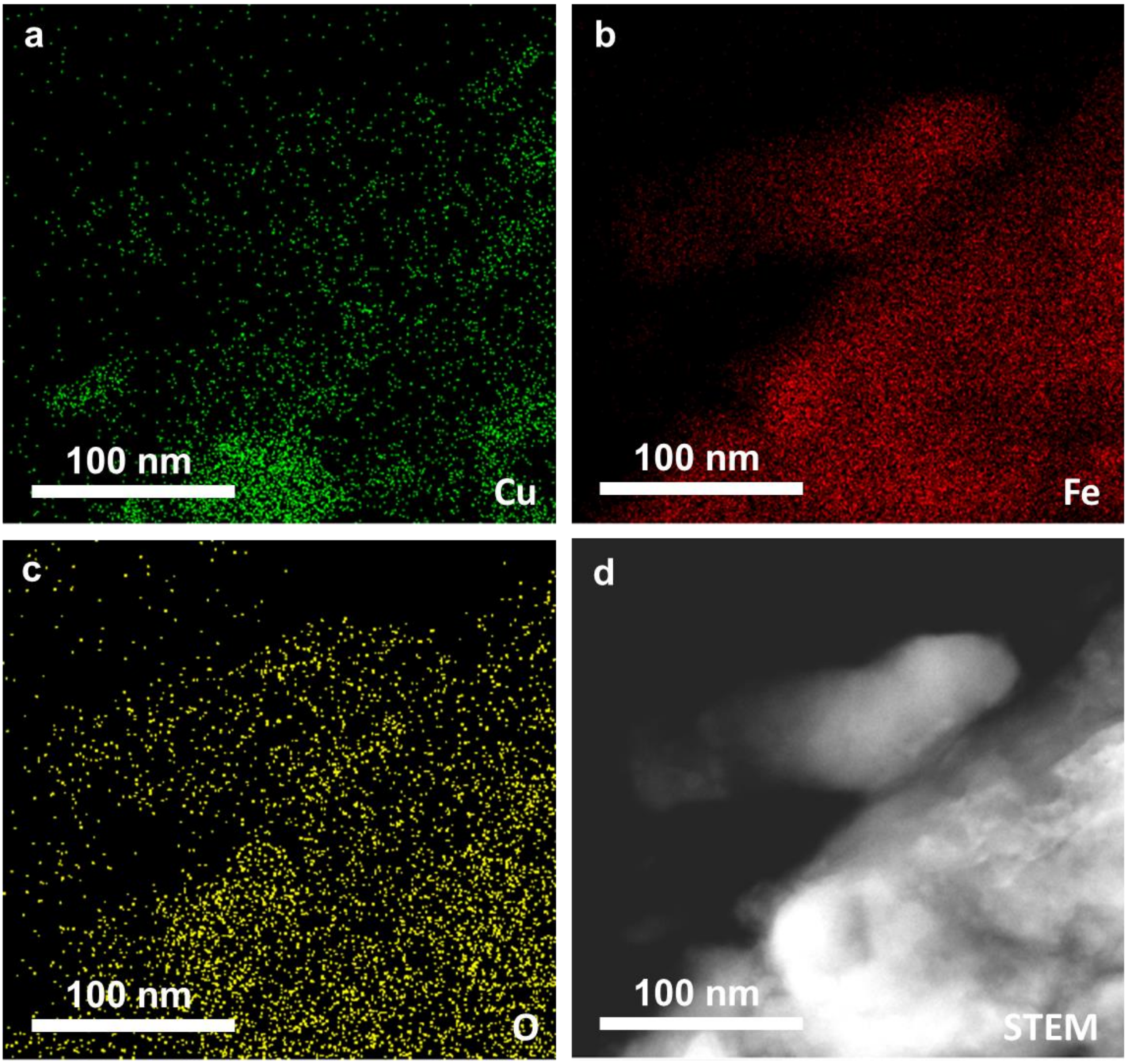

Figure S9. Morphological characterization of $25Cu/Fe_2O_3$ sample by STEM-EDS mapping. In these images, Cu nanoparticles as well as highly dispersed Cu species on the Fe support can be observed.

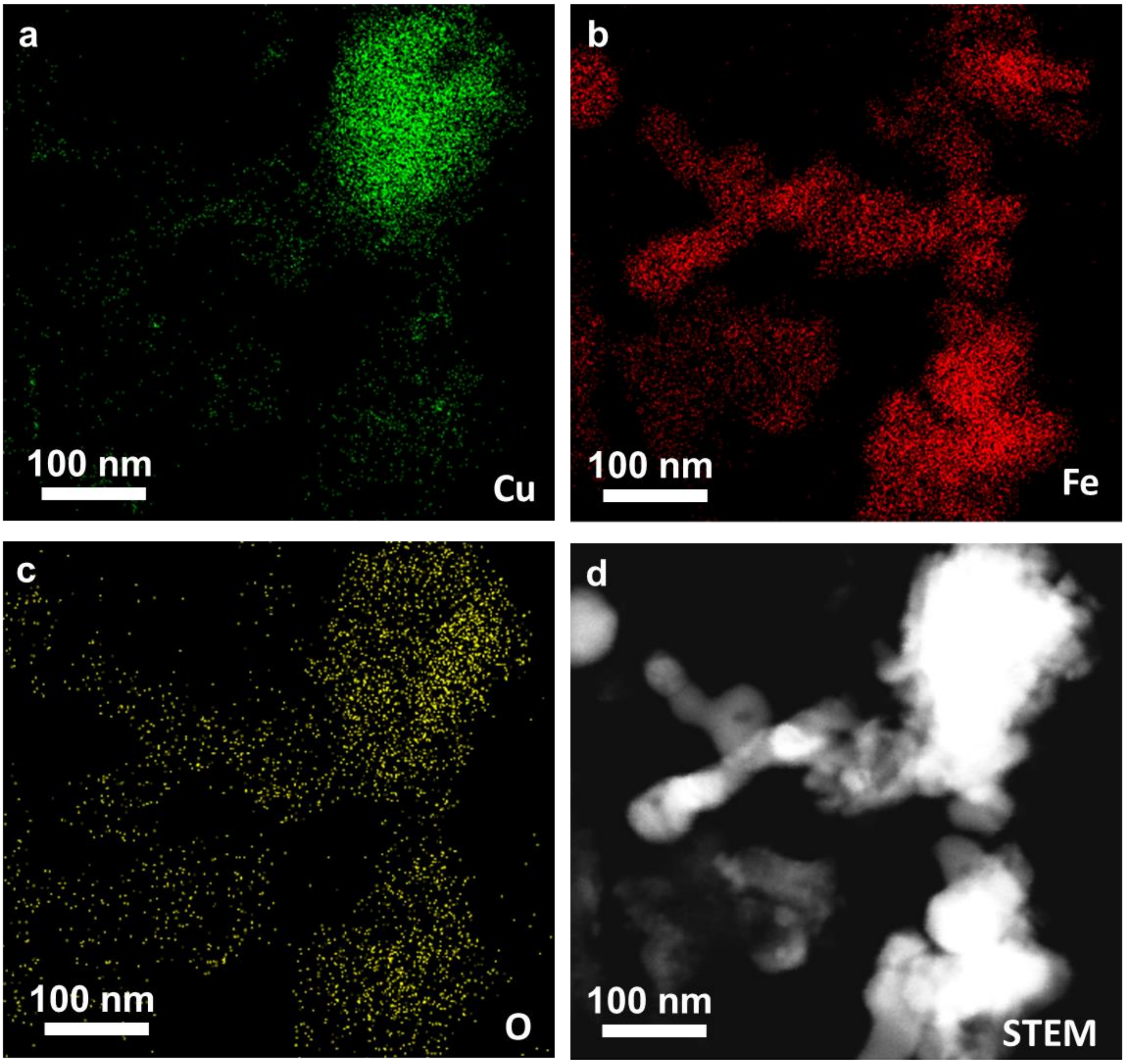

Figure S10. Morphological characterization of $25Cu/Fe_2O_3$ sample by STEM-EDS mapping. In these images, Cu nanoparticles as well as highly dispersed Cu species on the Fe support can be observed.

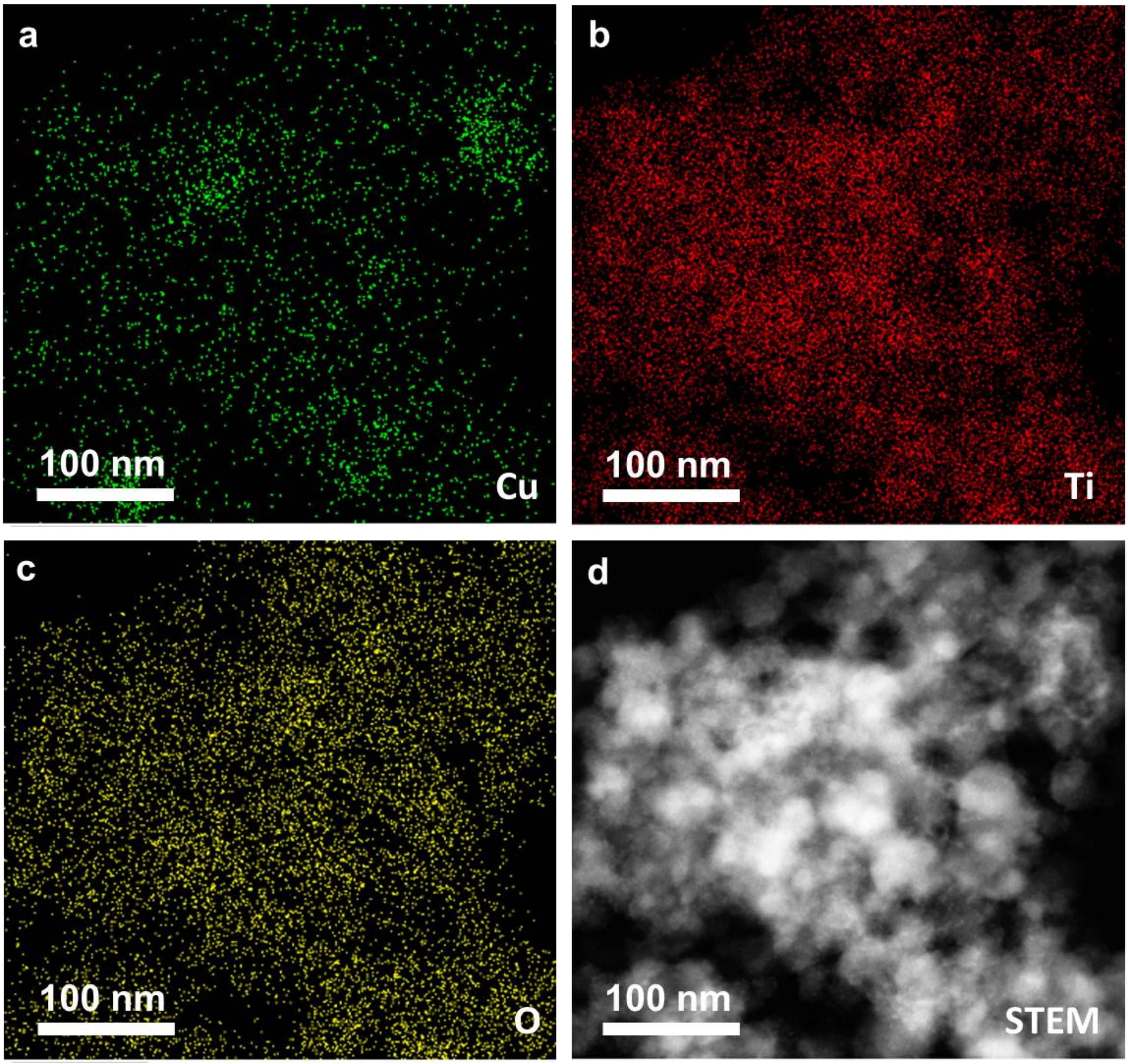

Figure S11. Morphological characterization of 25Cu/TiO_2 sample by STEM-EDS mapping. In these images, Cu nanoparticles as well as highly dispersed Cu species on TiO_2 can be observed.

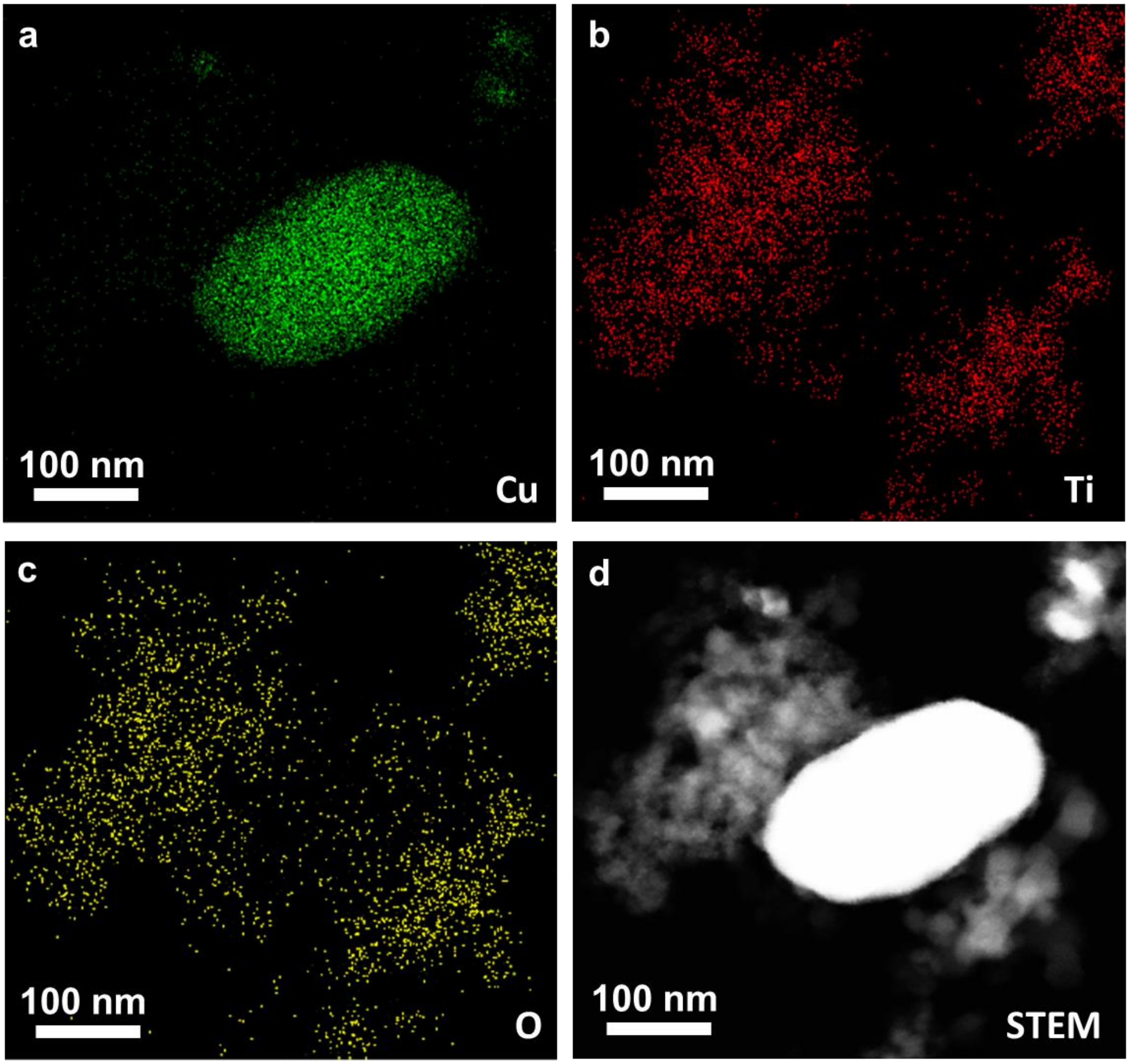

Figure S12. Morphological characterization of $25Cu/TiO_2$ sample by STEM-EDS mapping. In these images, Cu nanoparticles as well as highly dispersed Cu species on TiO_2 can be observed.

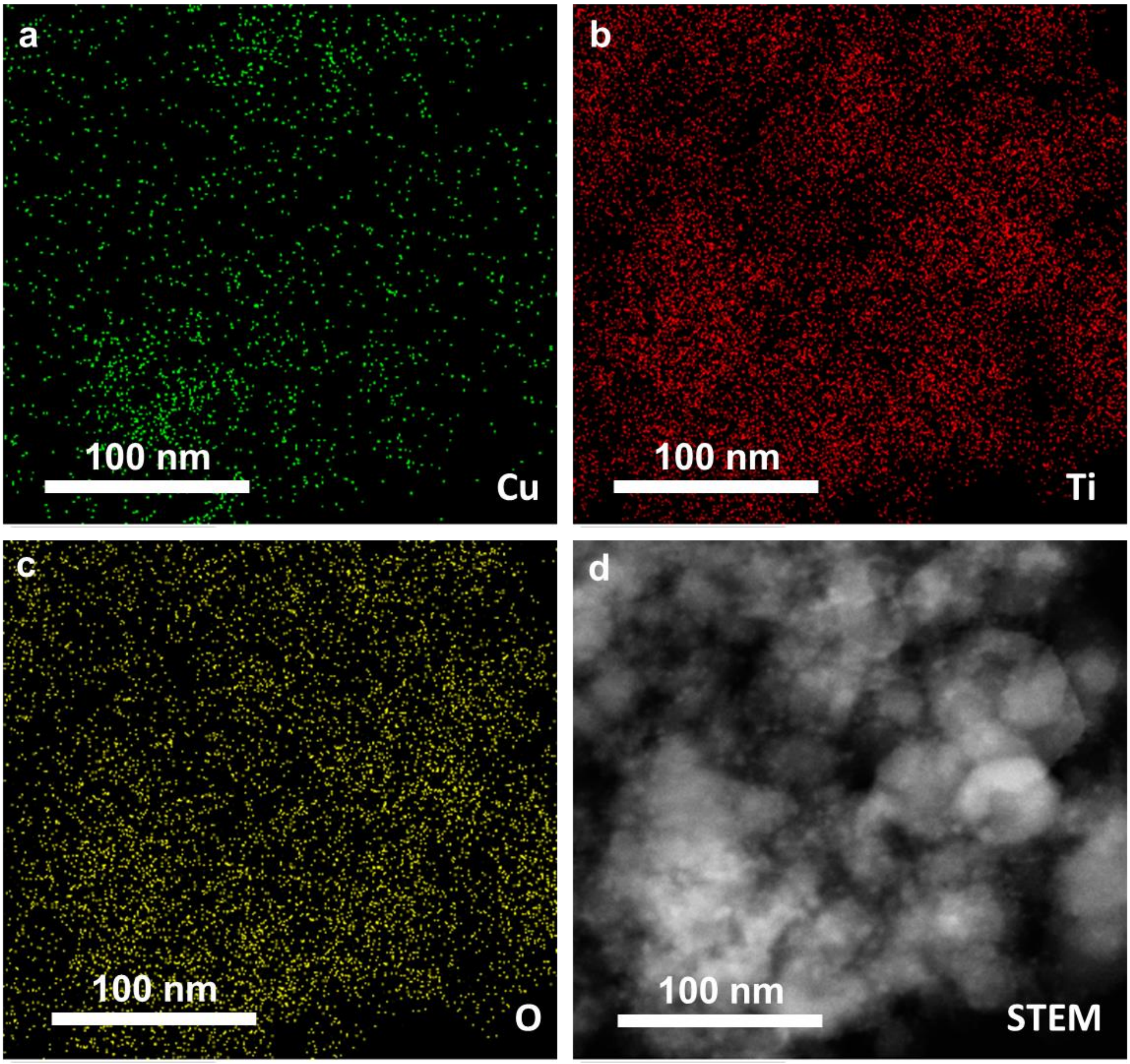

Figure S13. Morphological characterization of $25Cu/TiO_2$ sample by STEM-EDS mapping. In these images, Cu nanoparticles as well as highly dispersed Cu species on TiO_2 can be observed.

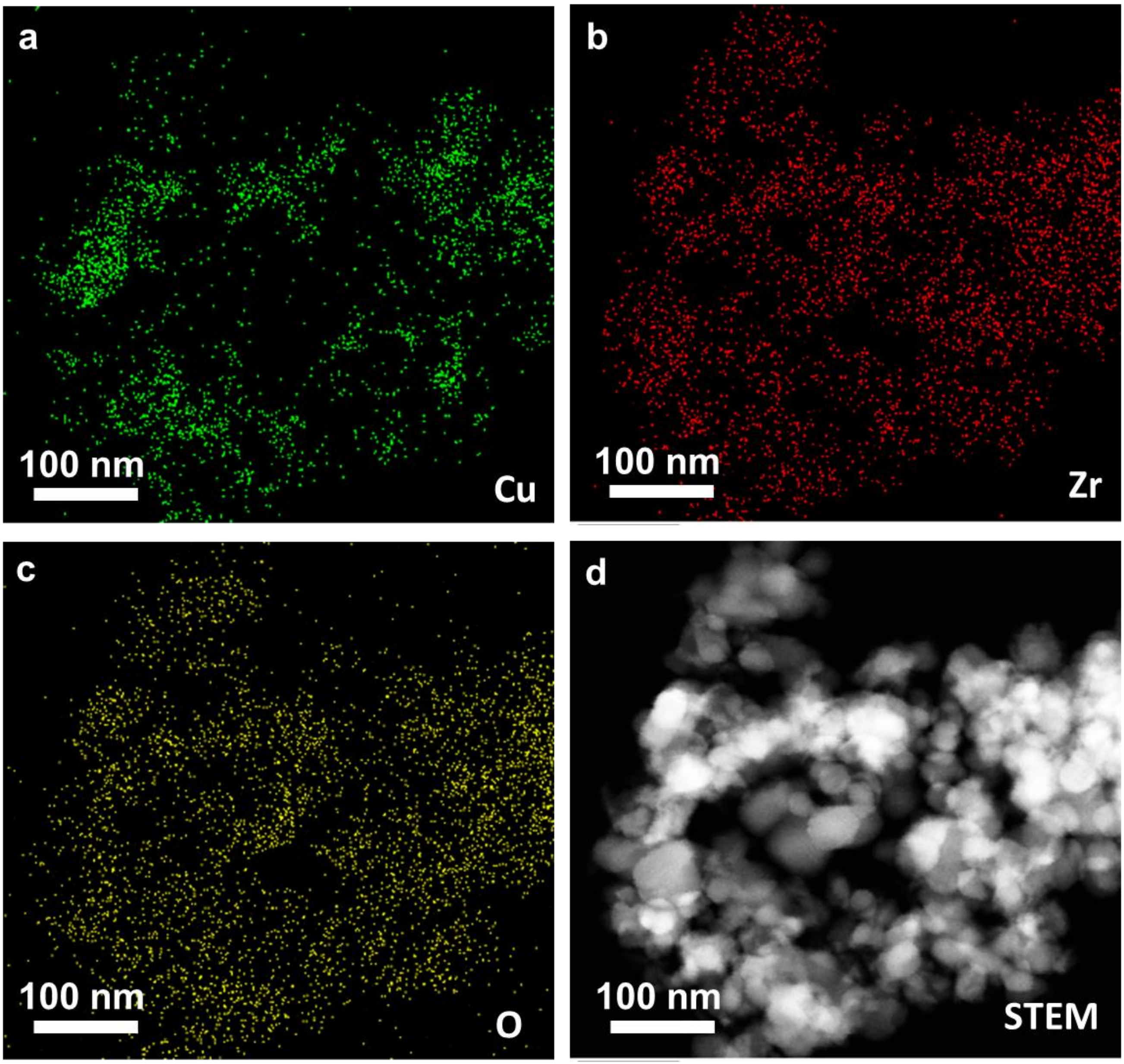

Figure S14. Morphological characterization of $25Cu/ZrO_2$ sample by STEM-EDS mapping. In these images, Cu nanoparticles as well as highly dispersed Cu species on ZrO_2 can be observed.

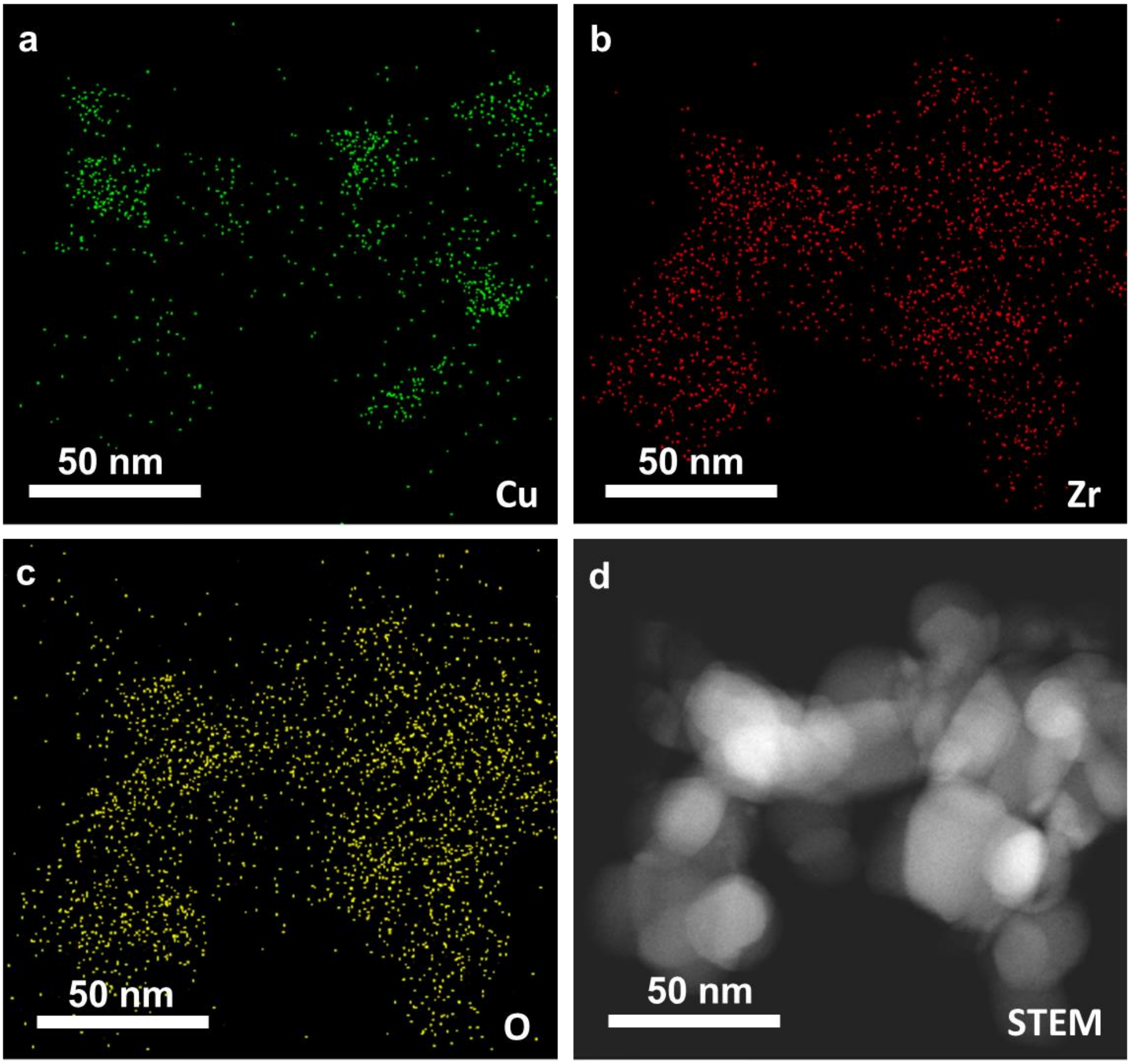

Figure S15. Morphological characterization of 25Cu/ZrO_2 sample by STEM-EDS mapping. In these images, Cu nanoparticles as well as highly dispersed Cu species on ZrO_2 can be observed.

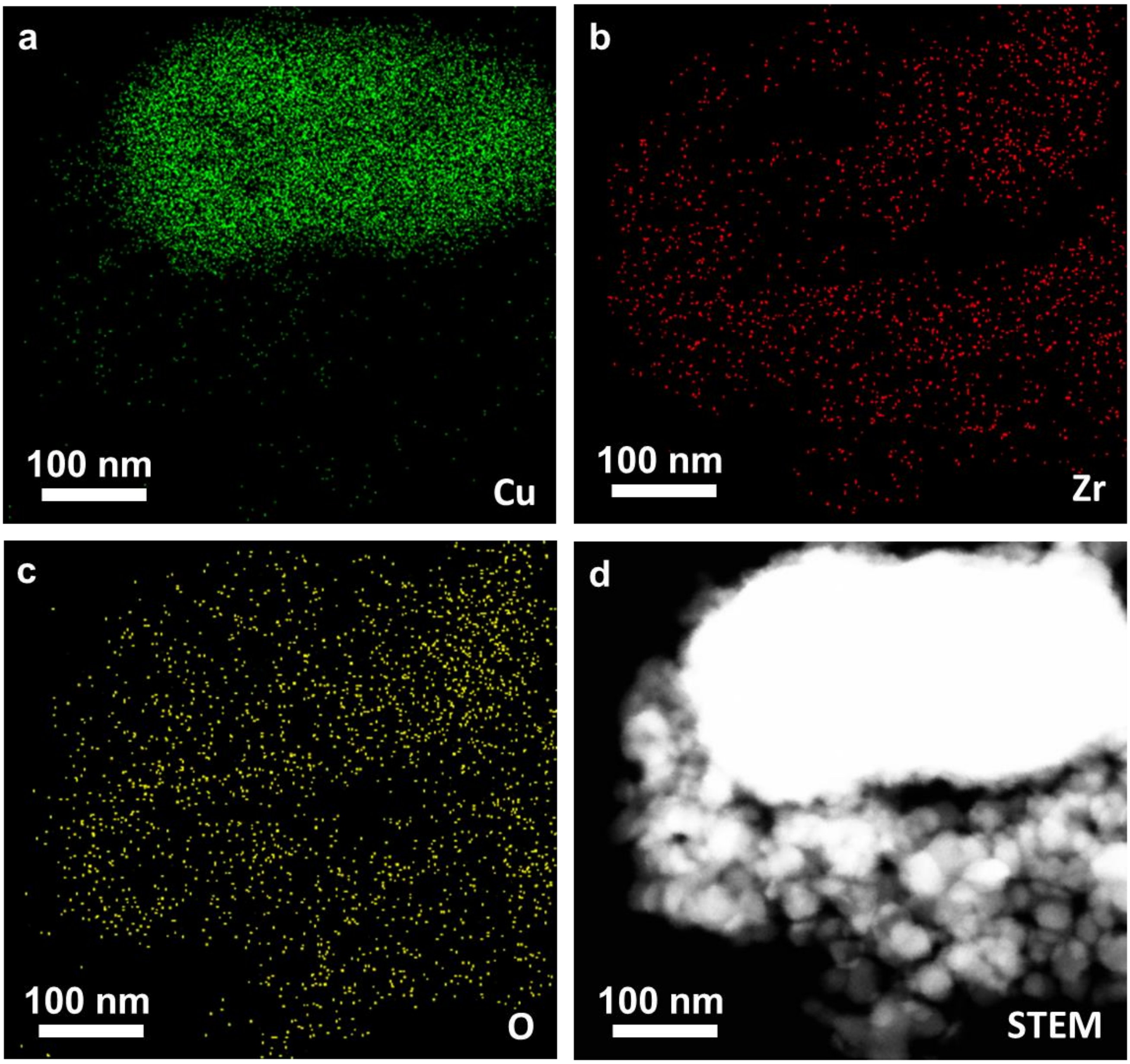

Figure S16. Morphological characterization of $25Cu/ZrO_2$ sample by STEM-EDS mapping. In these images, Cu nanoparticles as well as highly dispersed Cu species on ZrO_2 can be observed.

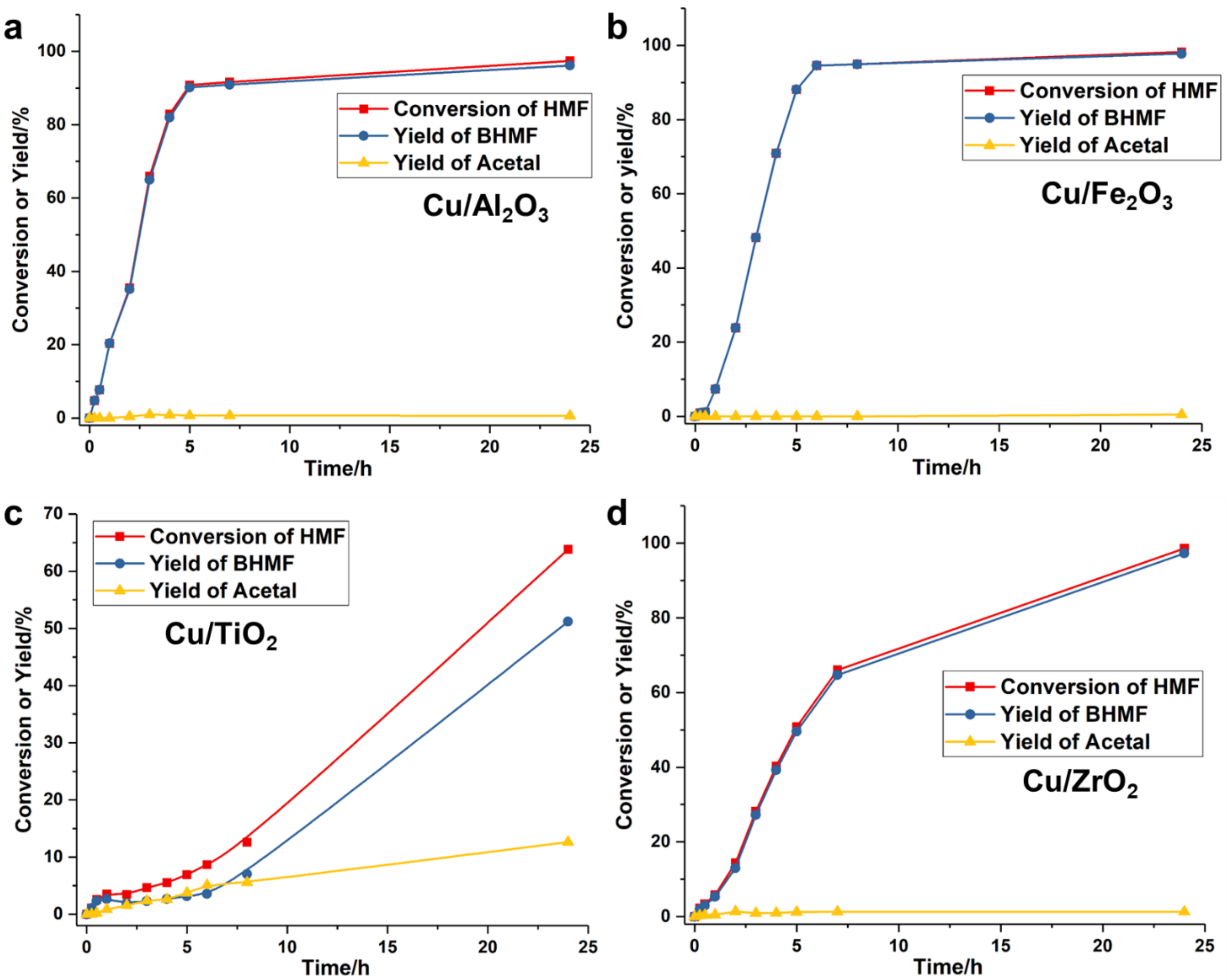

Figure S17. Catalytic performance of Cu catalysts supported on conventional solid carriers for hydrogenation of HMF. (a) 25Cu/Al_2O_3, (b) 25Cu/Fe_2O_3, (c) 25Cu/TiO_2 and (d) 25Cu/ZrO_2. Reaction conditions: 10 mg solid catalyst, 0.5 mmol HMF, 5 mL methanol as solvent, 110 ºC and 10 bar of H_2.

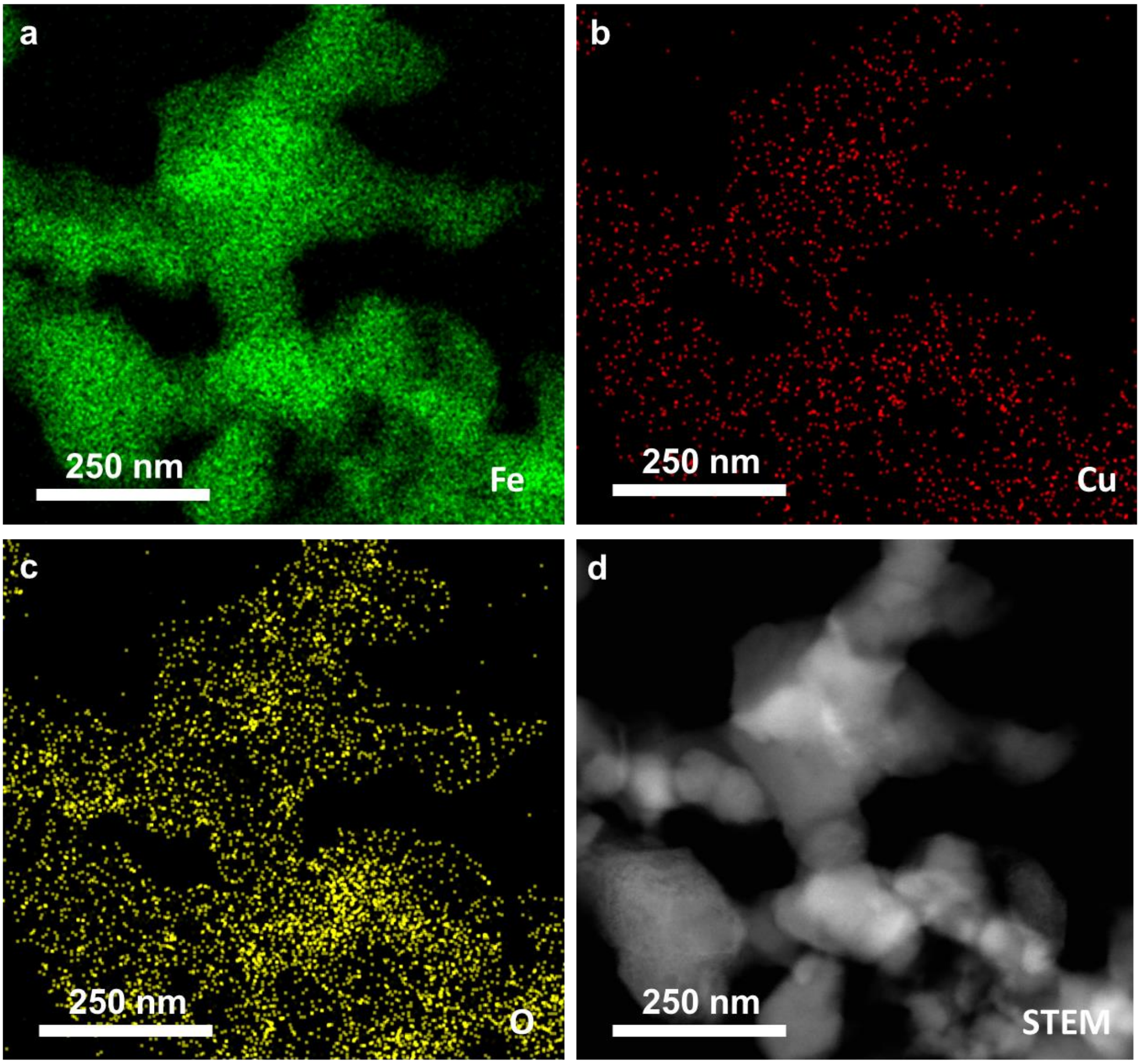

Figure S18. Morphological characterization of 5Cu/Fe@C sample by STEM-EDS mapping with 5 wt% of Cu. In these images, Cu nanoparticles as well as highly dispersed Cu species on Fe@C nanoparticles can be observed.

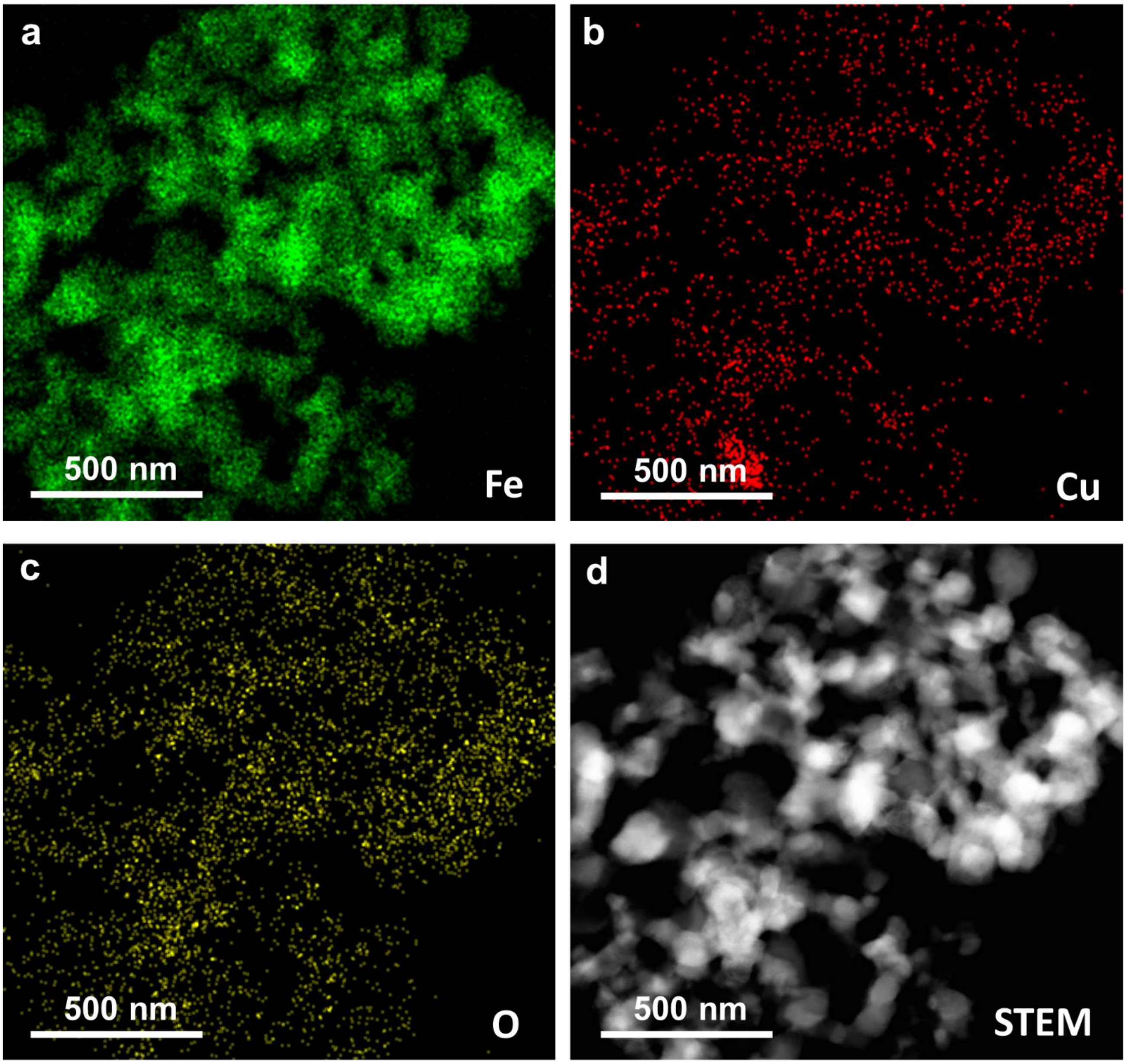

Figure S19. Morphological characterization of 5Cu/Fe@C sample by STEM-EDS mapping with 5 wt% of Cu. In these images, Cu nanoparticles as well as highly dispersed Cu species on Fe@C nanoparticles can be observed.

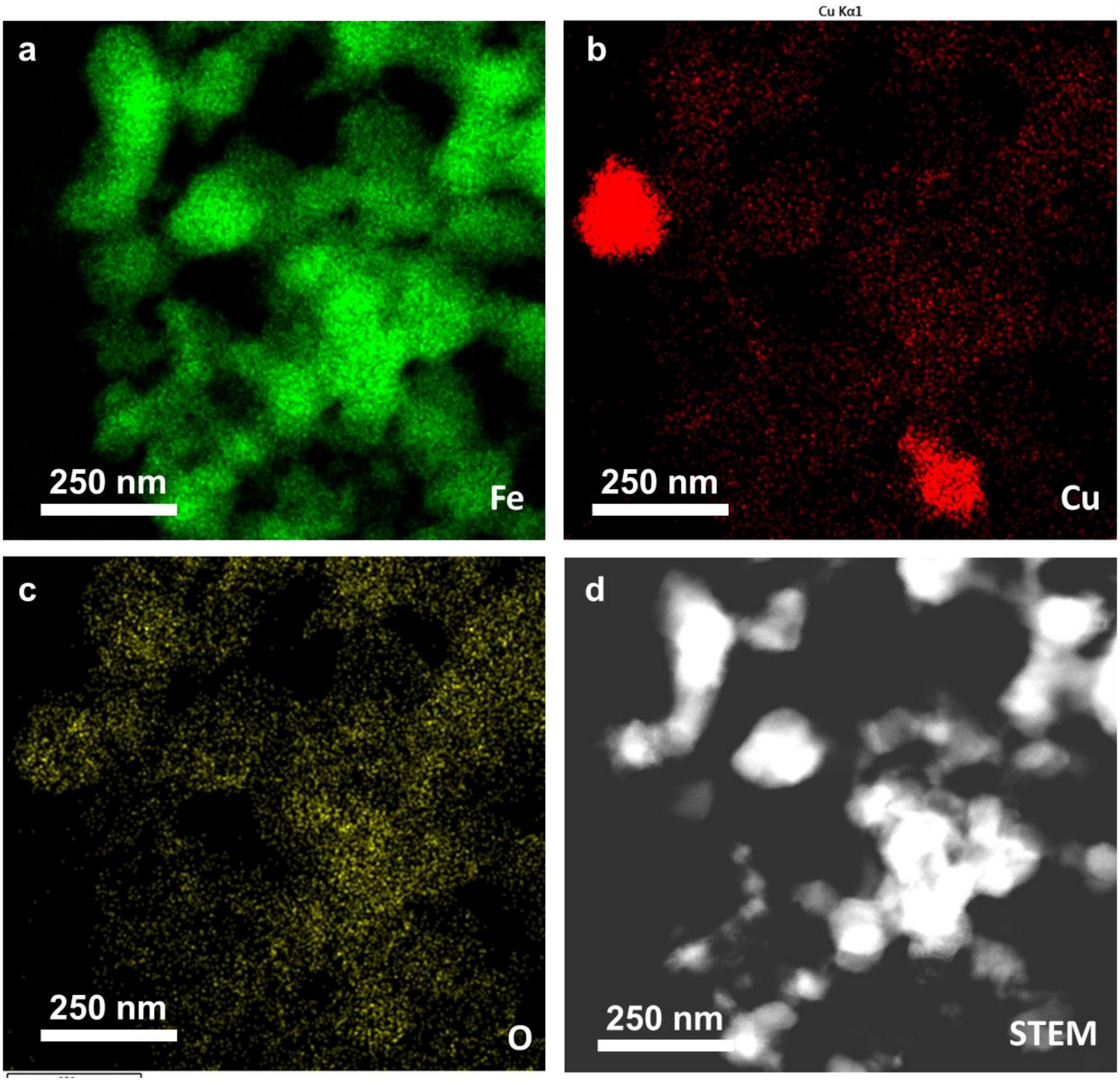

Figure S20. Morphological characterization of 5Cu/Fe@C sample by STEM-EDS mapping with 5 wt% of Cu. In these images, Cu nanoparticles as well as highly dispersed Cu species on Fe@C nanoparticles can be observed.

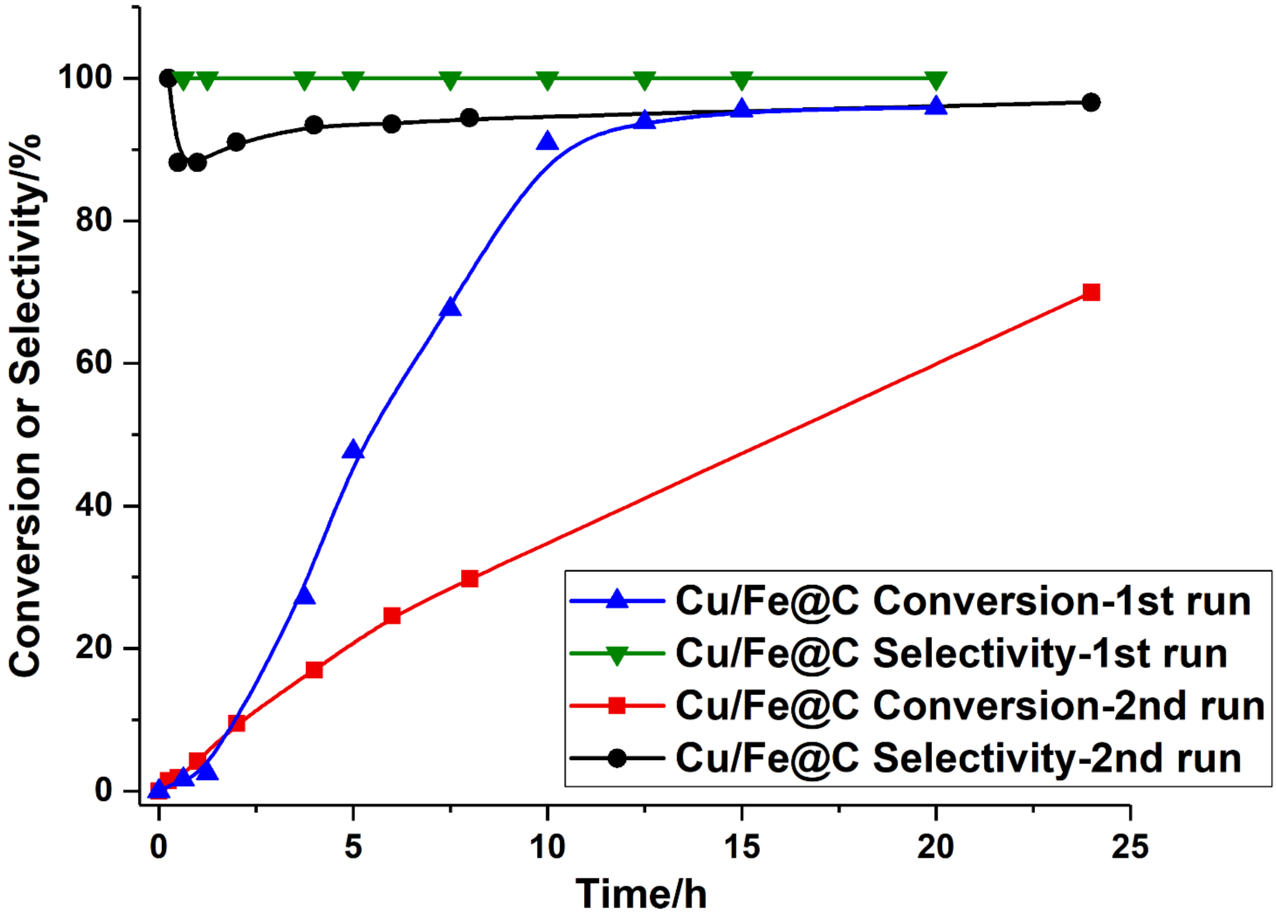

Figure S21. Stability test of Cu/Fe@C sample for hydrogenation of HMF.

Table S1. Chemical compositions of various CuFe bimetallic catalysts, determined by ICP.

Sample	Mole percentage of Fe	Mole percentage of Cu
$Fe_{0.92}Cu_{0.08}$	0.92	0.08
$Fe_{0.88}Cu_{0.12}$	0.88	0.12
$Fe0_{.76}Cu_{0.24}$	0.76	0.24
$Fe_{0.50}Cu_{0.50}$	0.50	0.50
$Fe_{0.25}Cu_{0.75}$	0.25	0.75

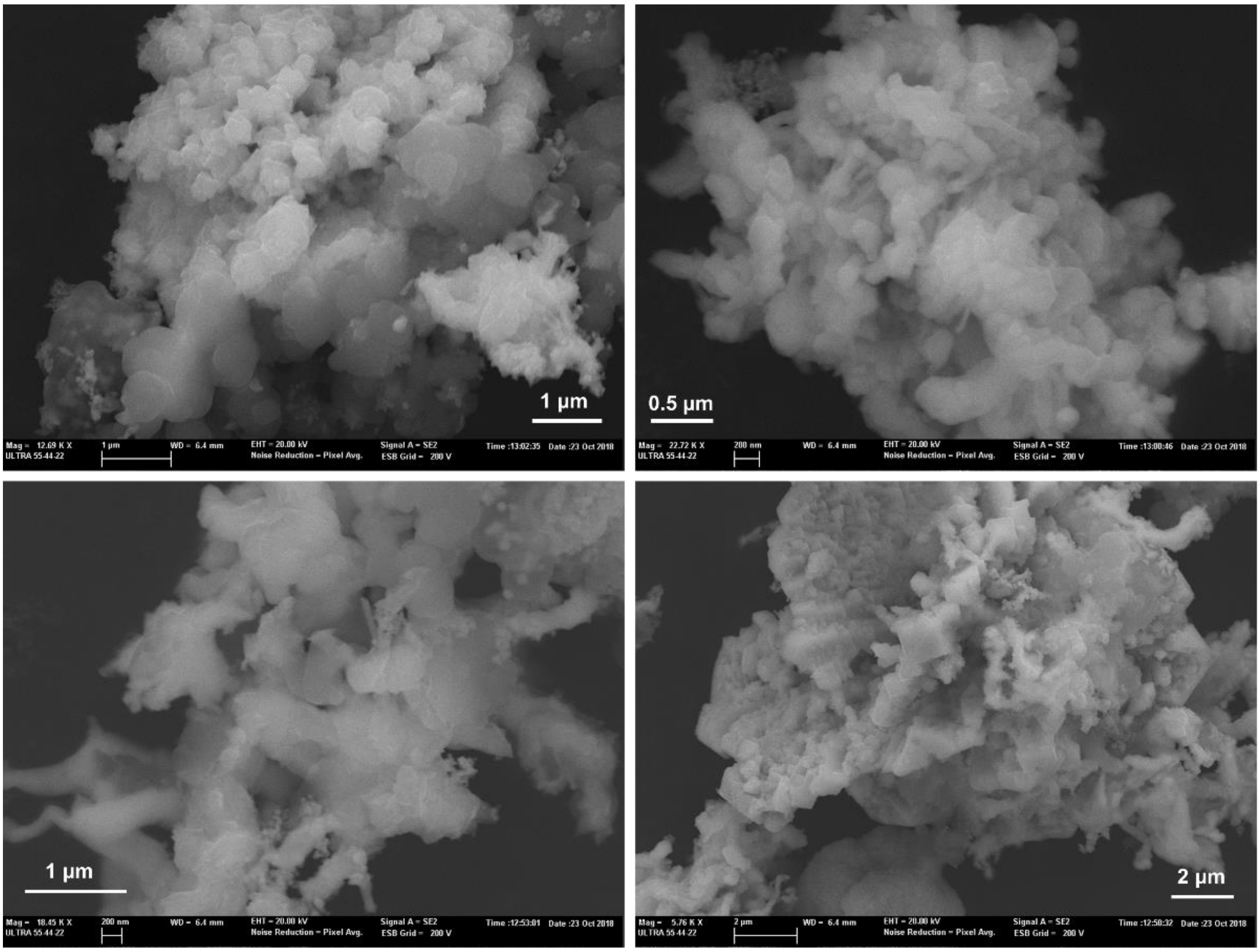

Figure S22. FESEM images of Cu@C sample. Cu nanoparticles of 50-500 nm can be observed.

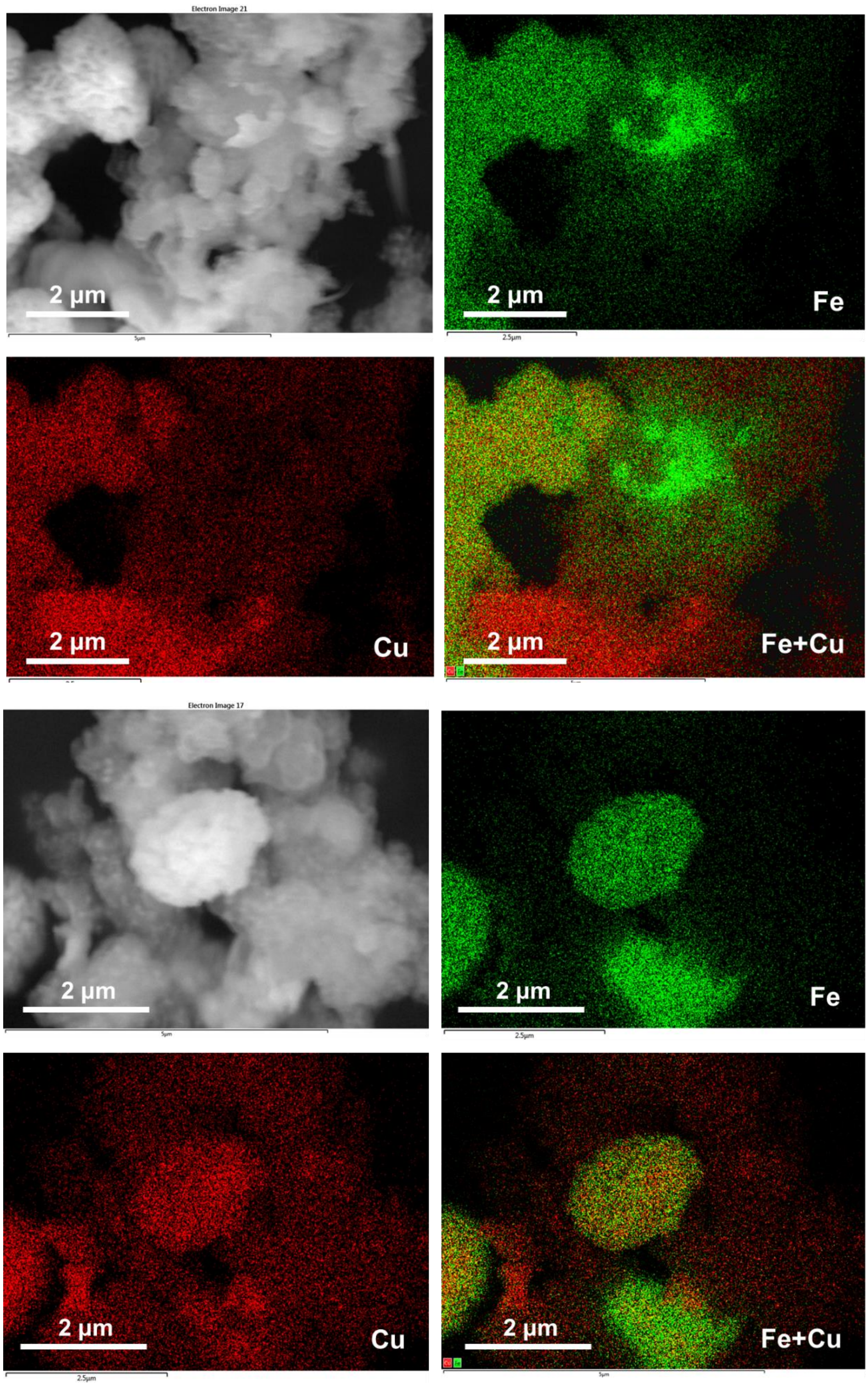

Figure S23. FESEM-EDS mapping of $Cu_{0.75}Fe_{0.25}$@C sample in two different areas.

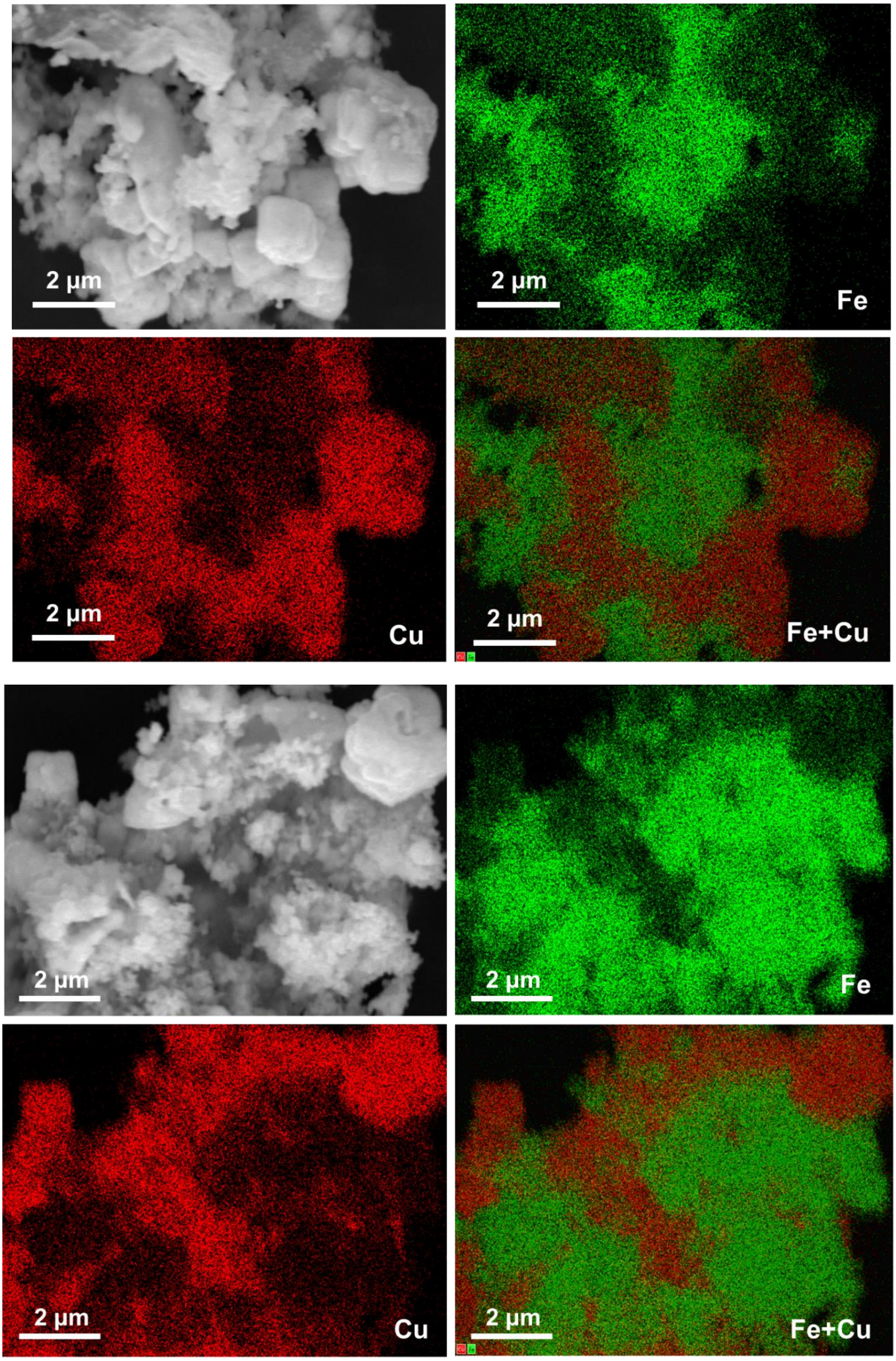

Figure S24. FESEM-EDS mapping of $Cu_{0.50}Fe_{0.50}@C$ sample in two different areas.

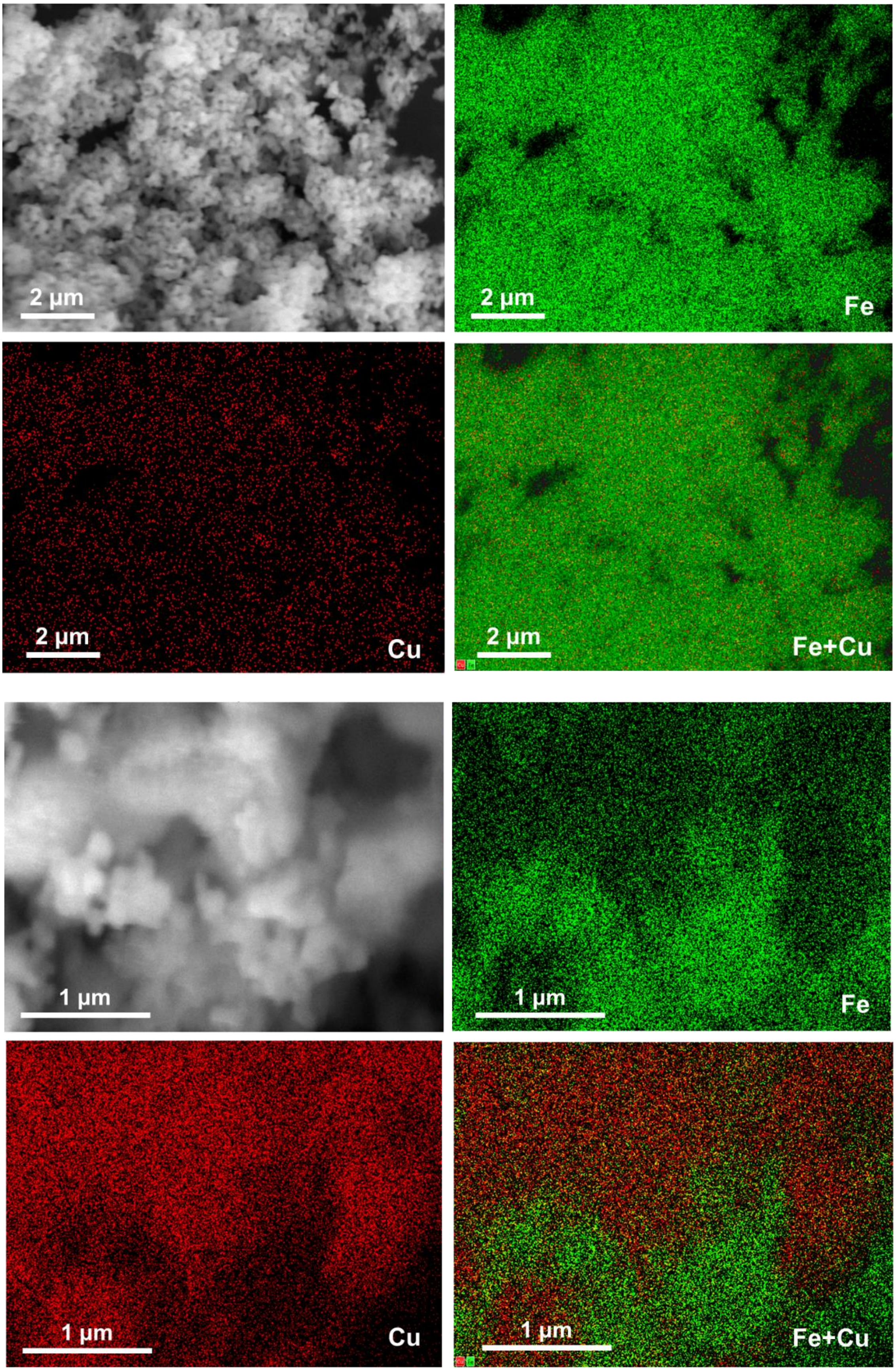

Figure S25. FESEM-EDS mapping of $Cu_{0.24}Fe_{0.76}$@C sample in two different areas.

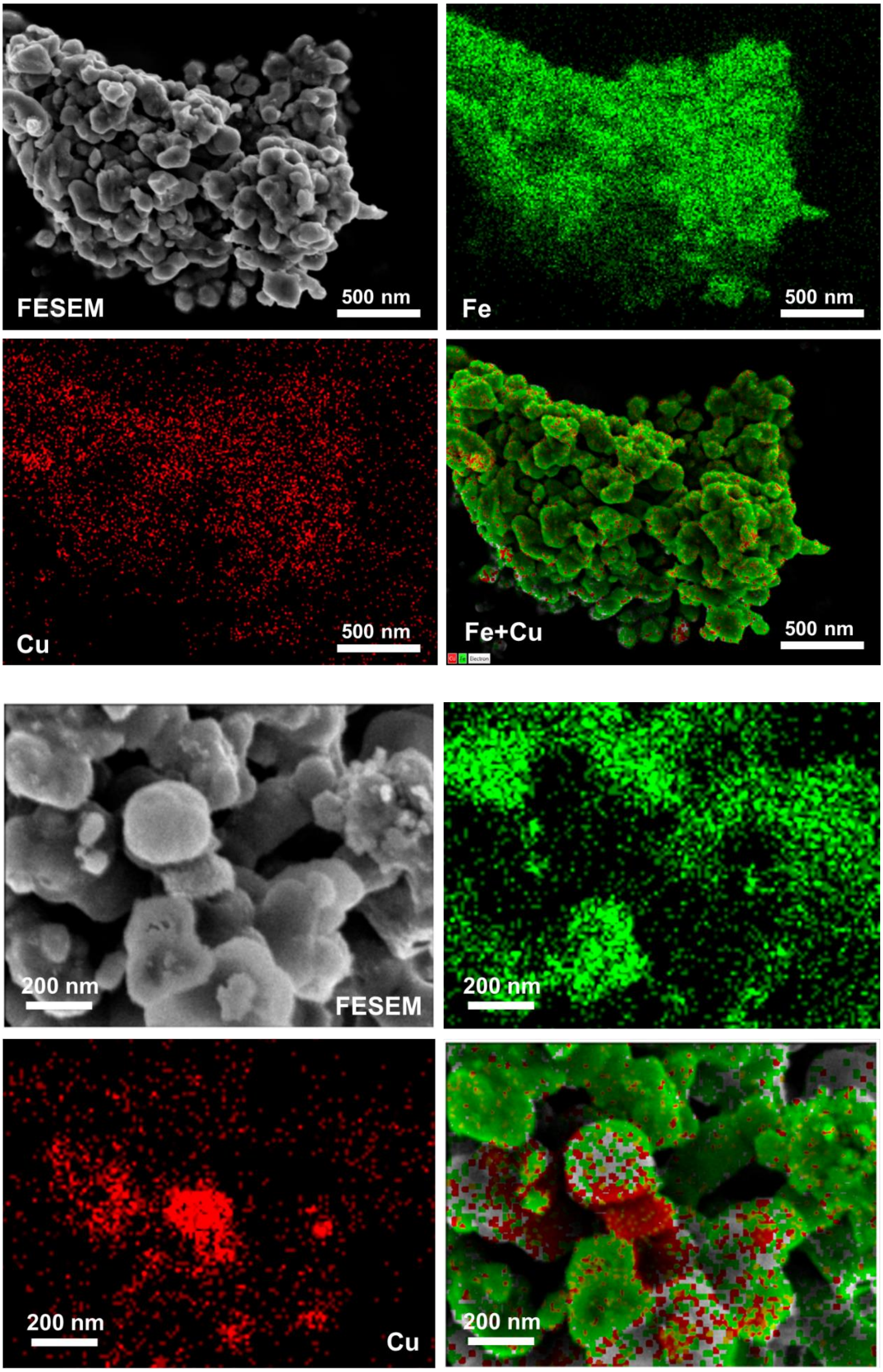

Figure S26. FESEM-EDS mapping of $Cu_{0.12}Fe_{0.88}@C$ sample in two different areas.

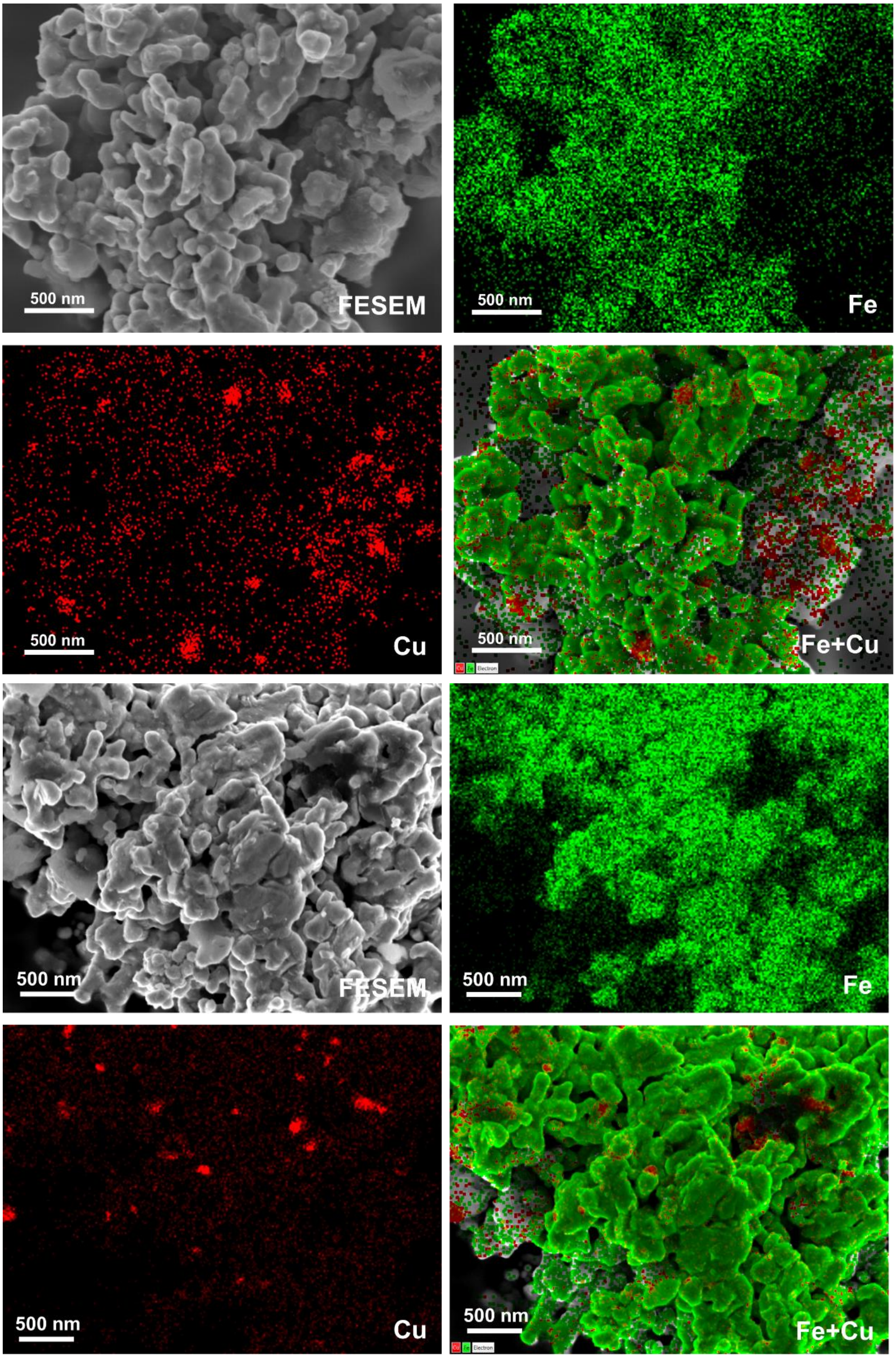

Figure S27. FESEM-EDS mapping of $Cu_{0.08}Fe_{0.92}$@C sample in two different areas.

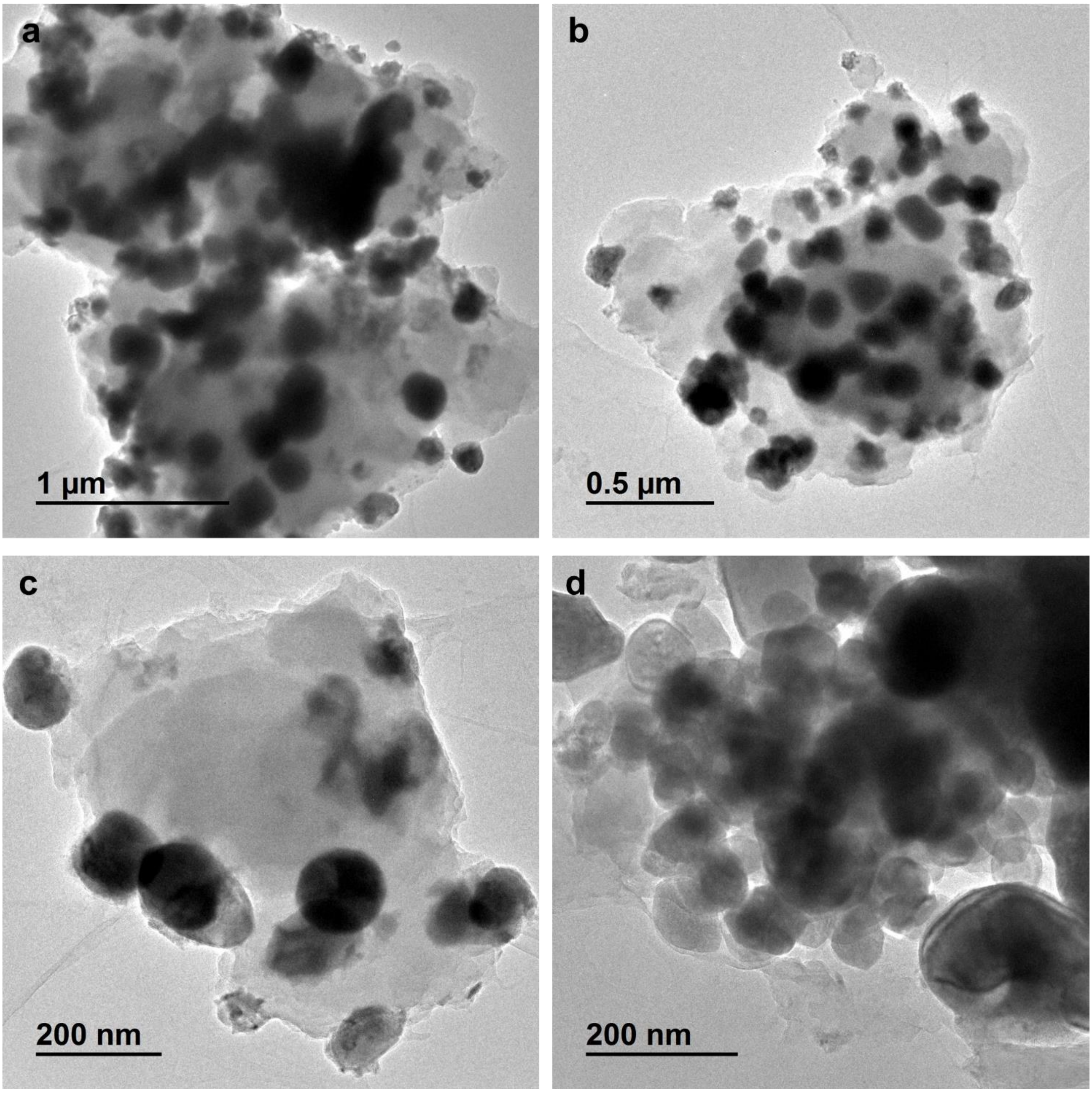

Figure S28. Low-magnification TEM images of $Cu_{0.08}Fe_{0.92}$@C sample.

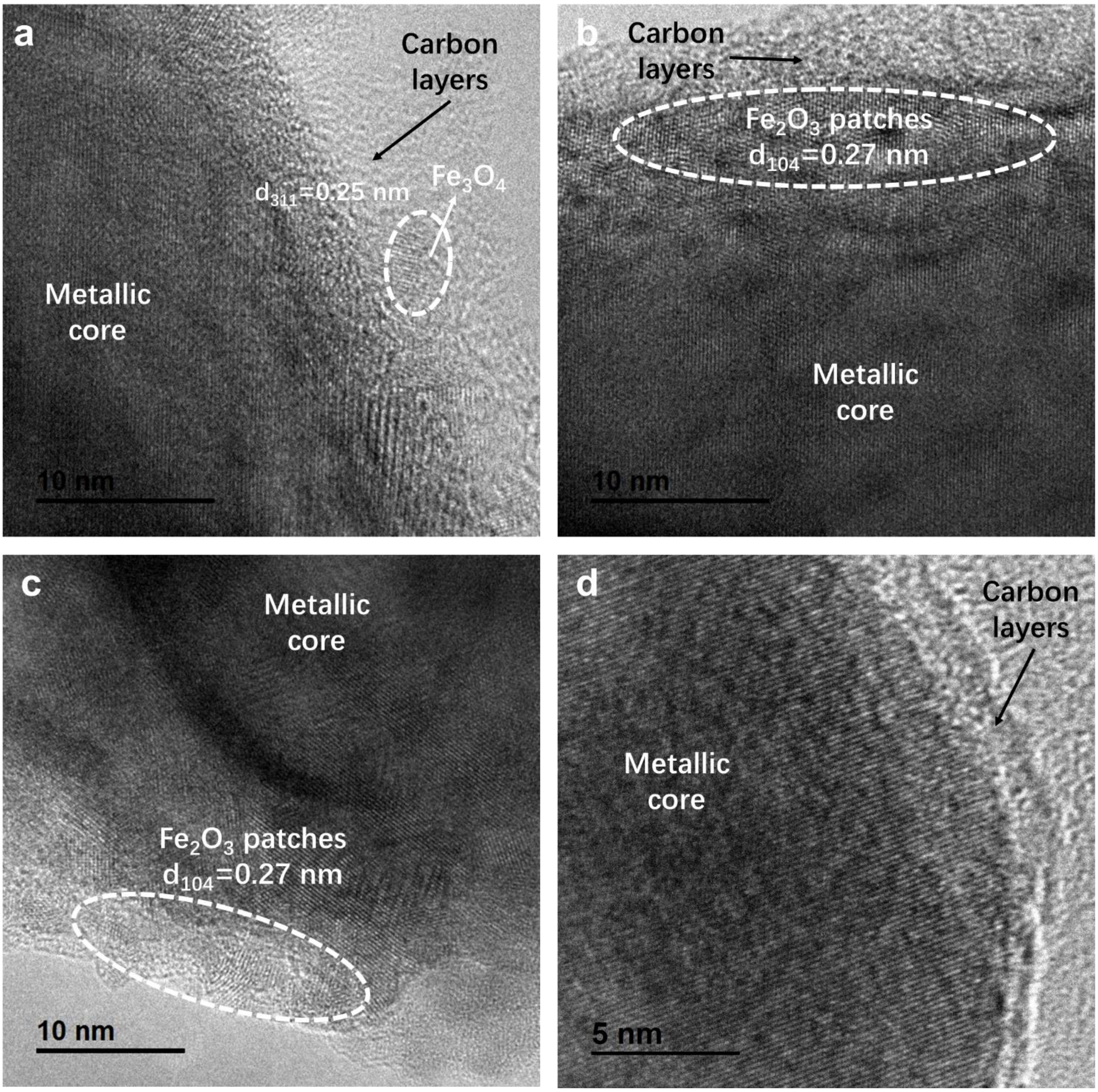

Figure S29. High-magnification TEM images of $Cu_{0.08}Fe_{0.92}$@C sample.

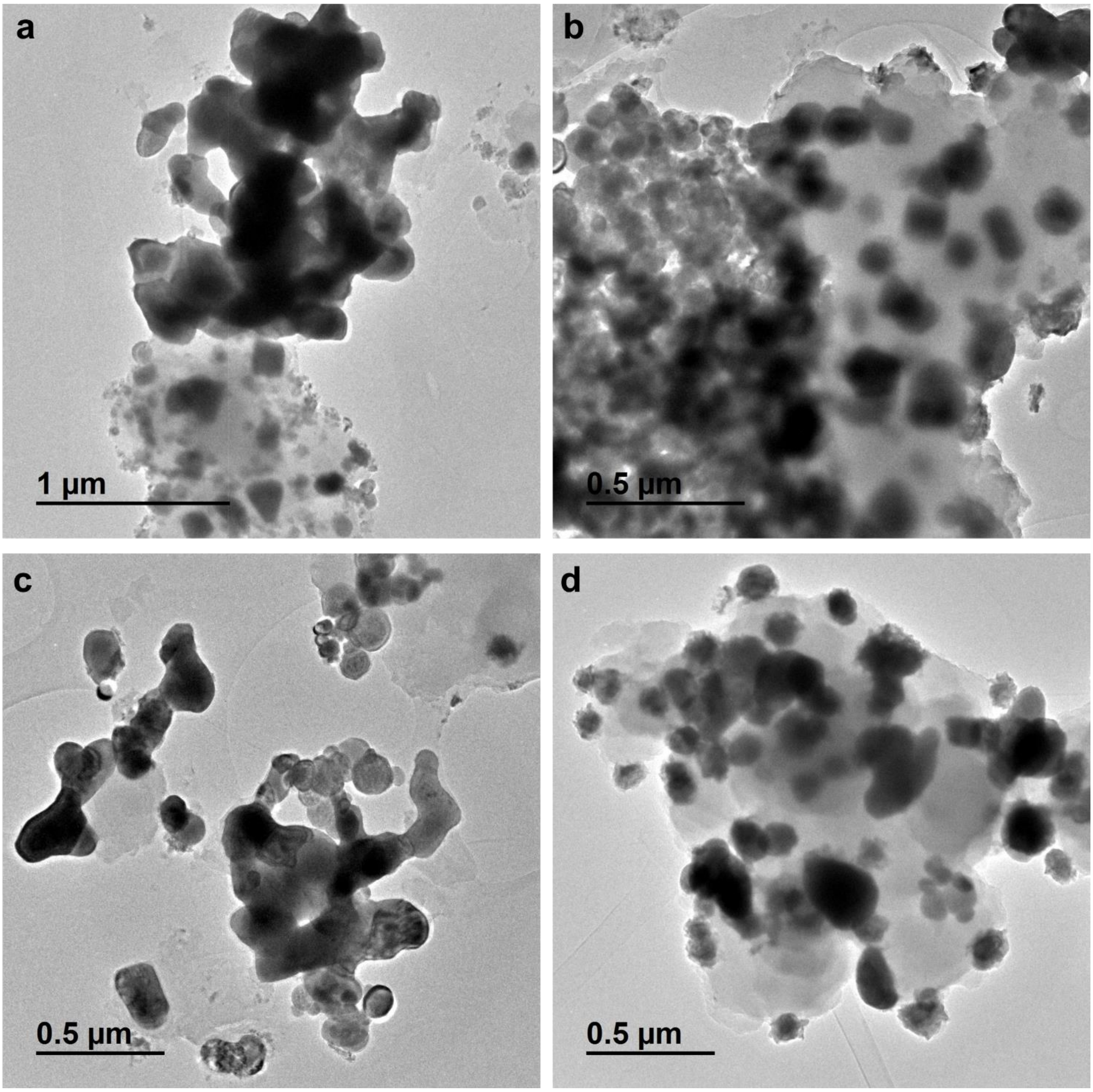

Figure S30. Low-magnification TEM images of $Cu_{0.12}Fe_{0.88}$@C sample.

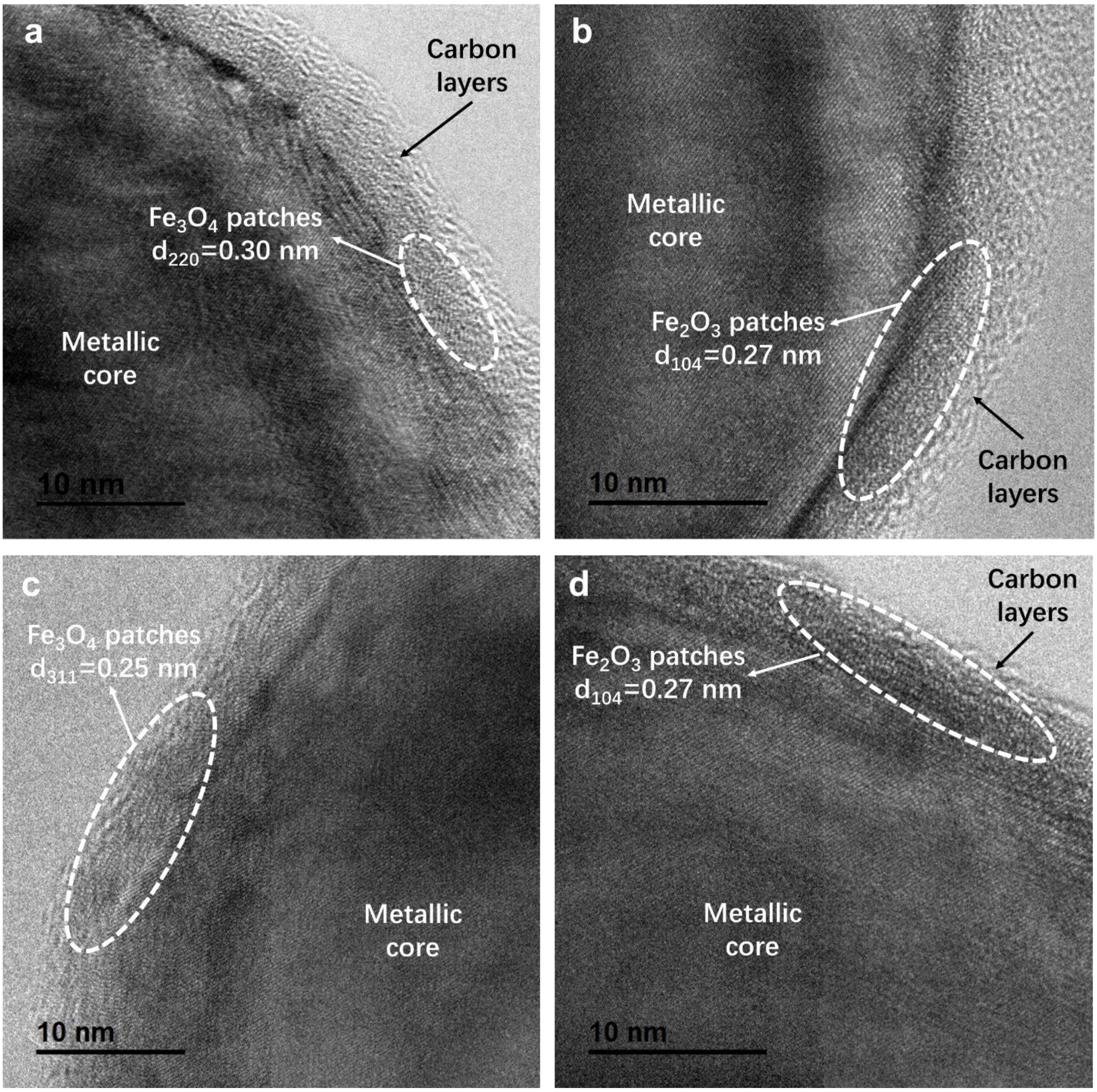

Figure S31. High-resolution TEM images of $Cu_{0.12}Fe_{0.88}$@C sample.

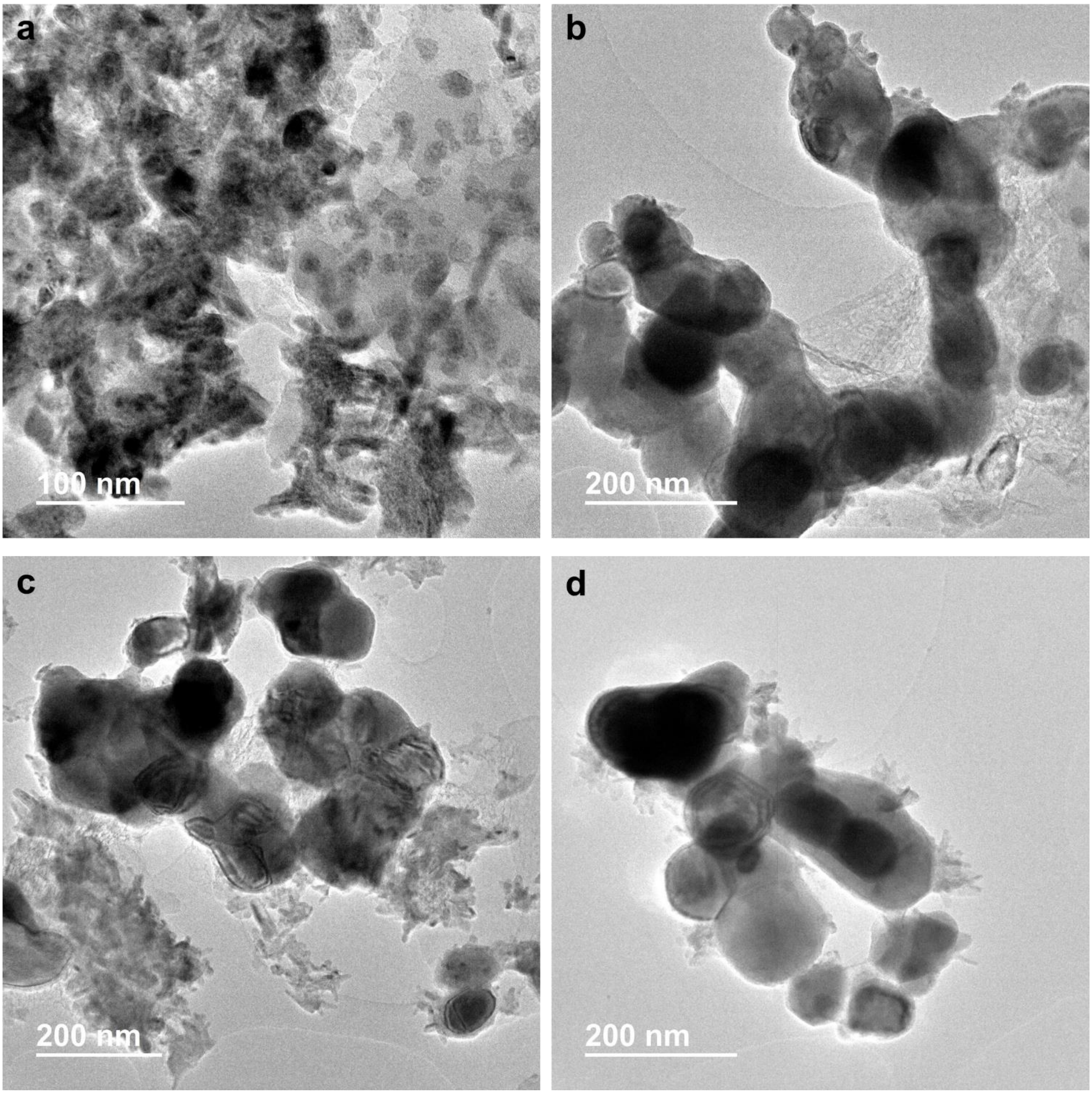

Figure S32. Low-magnification TEM images of $Cu_{0.24}Fe_{0.76}$@C sample.

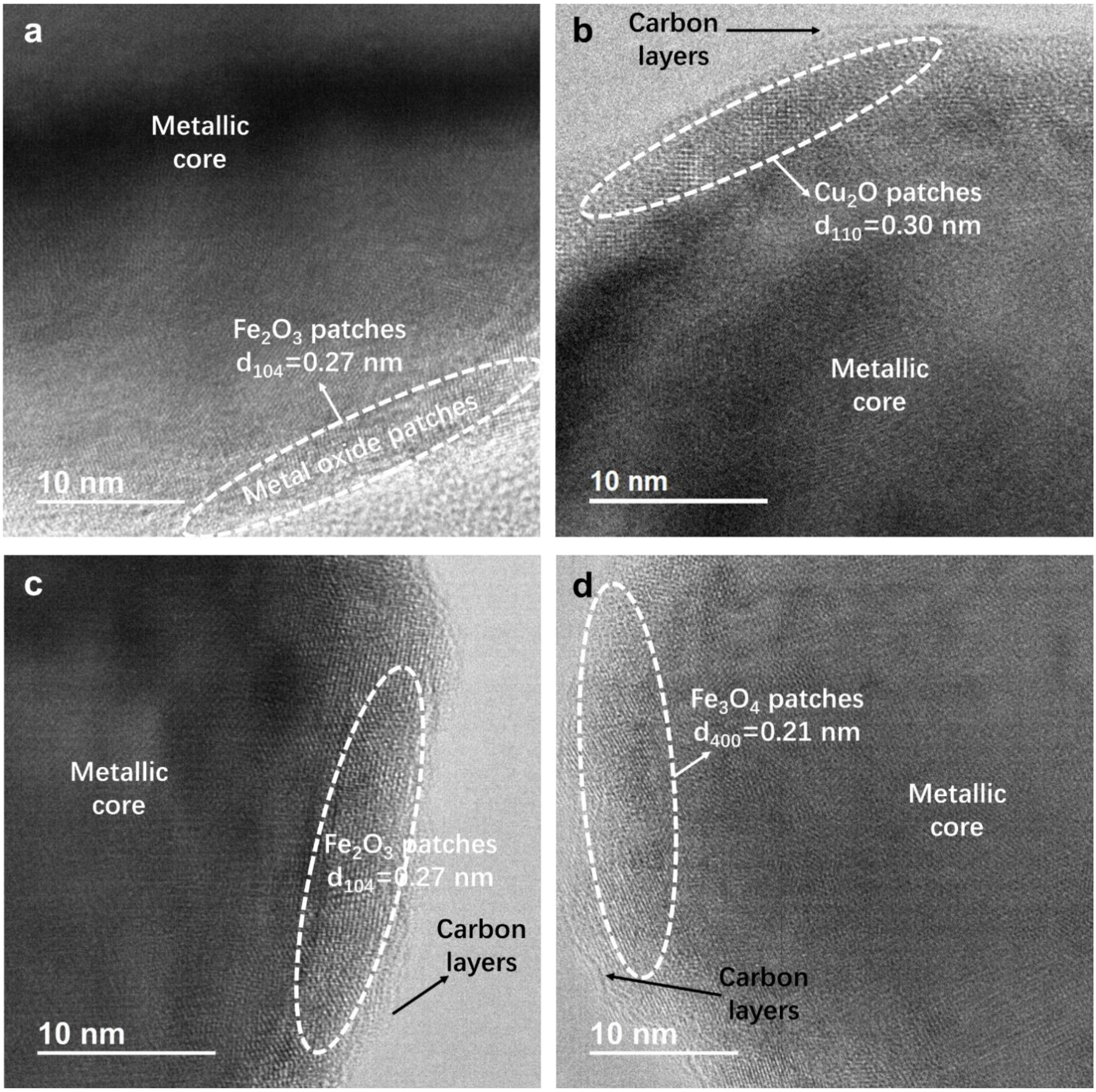

Figure S33. High-resolution TEM images of $Cu_{0.24}Fe_{0.76}$@C sample.

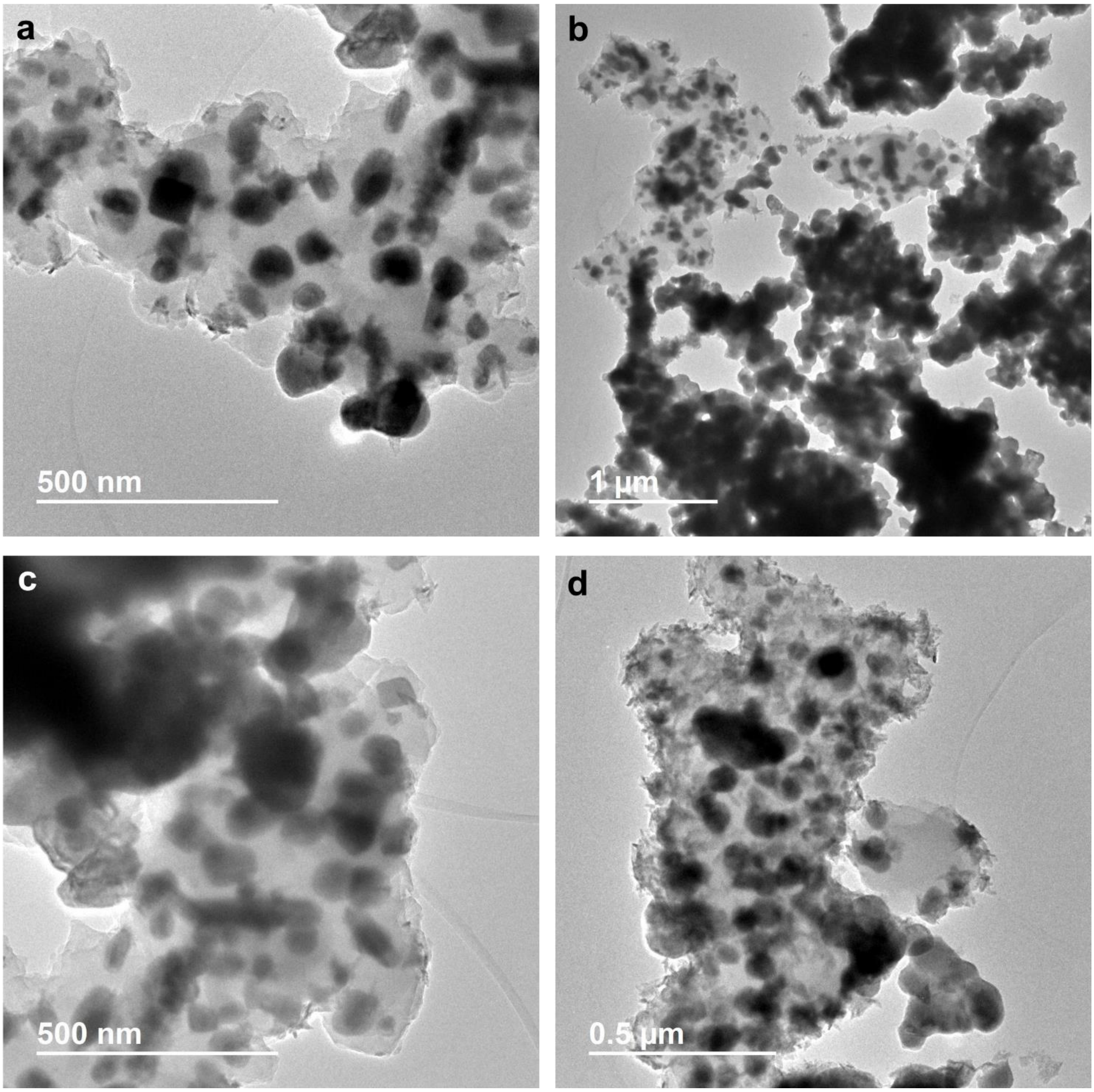

Figure S34. Low-magnification TEM images of $Cu_{0.50}Fe_{0.50}$@C sample.

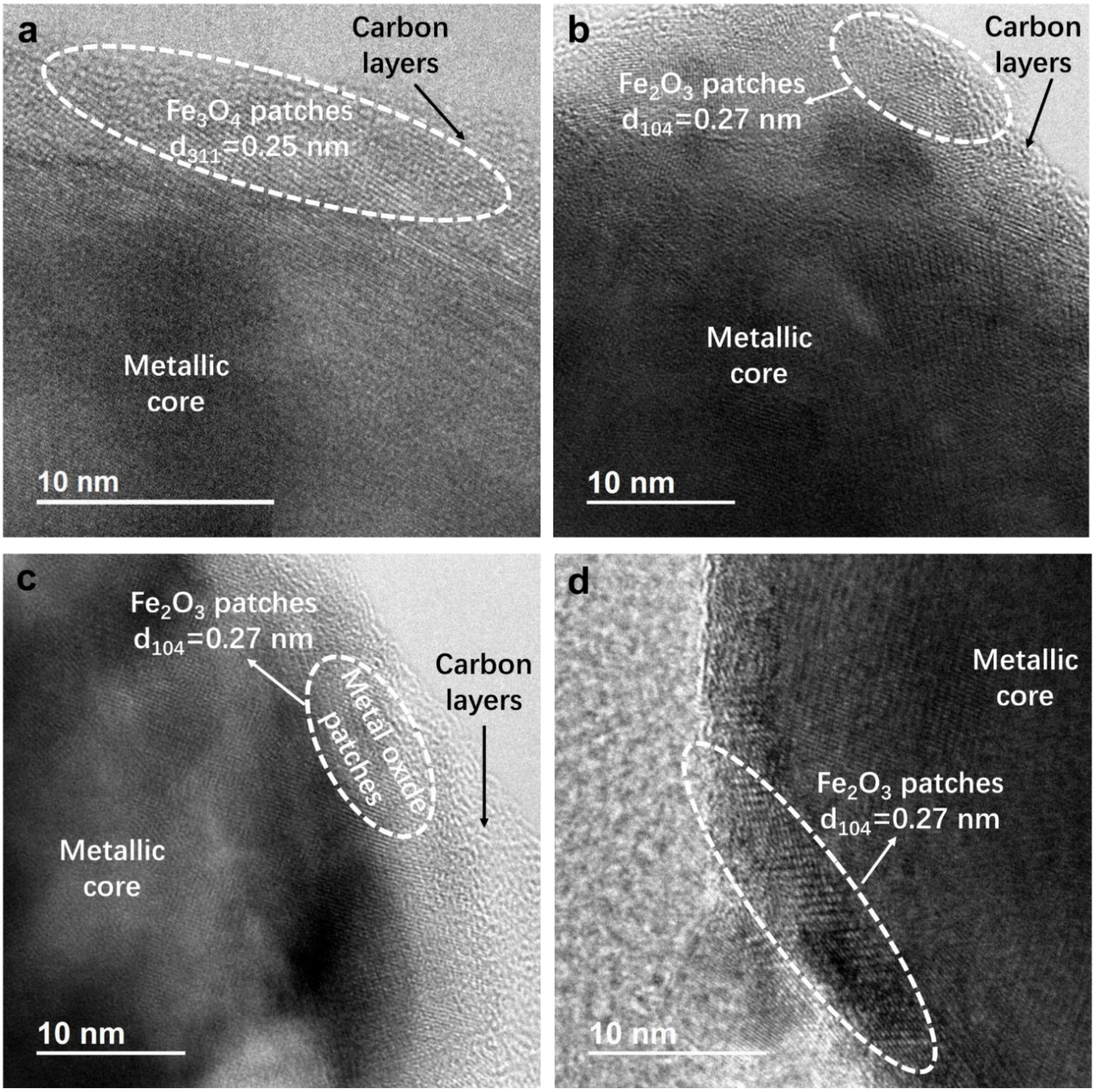

Figure S35. High-resolution TEM images of $Cu_{0.50}Fe_{0.50}$@C sample.

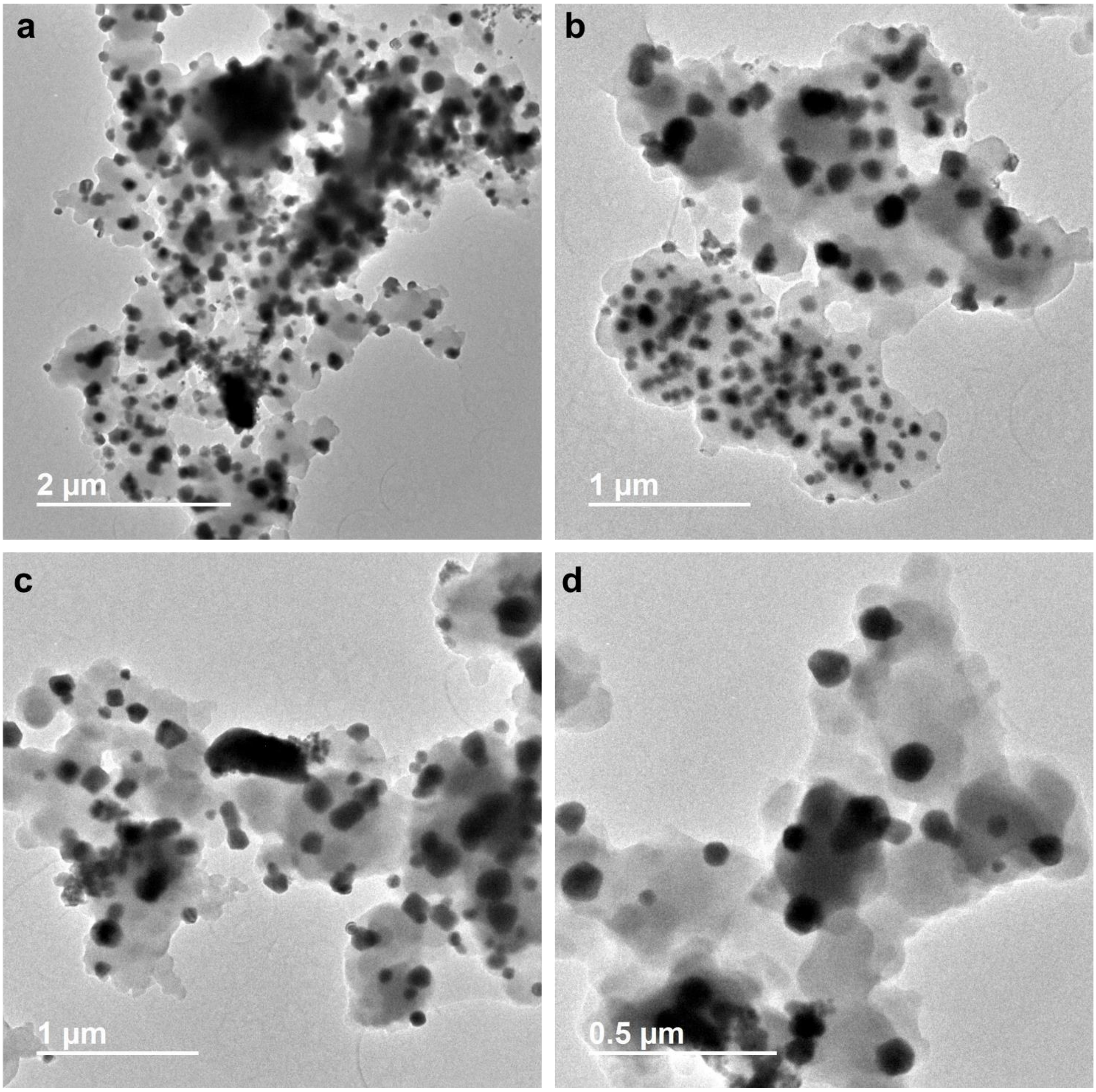

Figure S36. Low-magnification TEM images of $Cu_{0.75}Fe_{0.25}$@C sample.

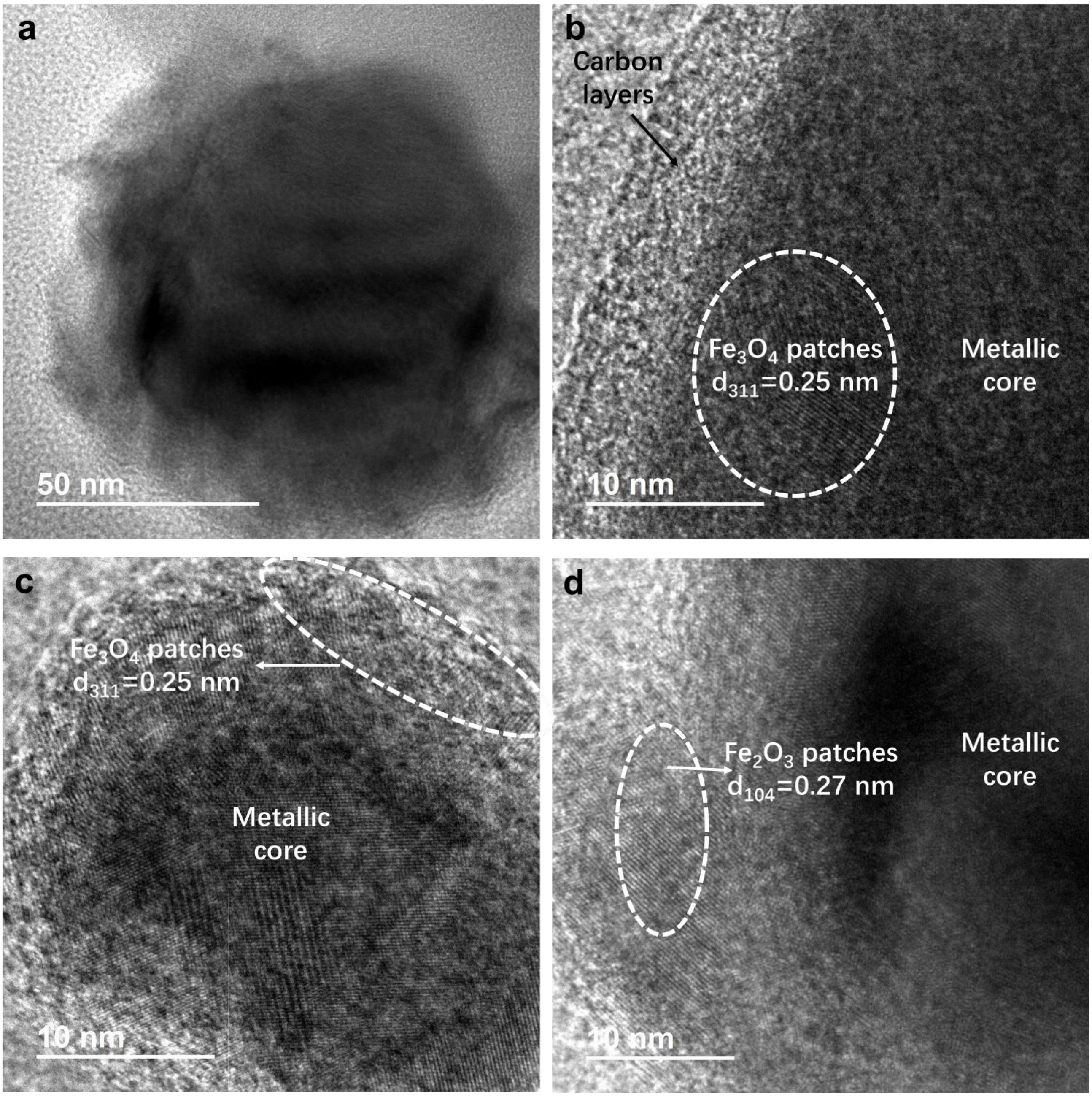

Figure S37. High-resolution TEM images of $Cu_{0.75}Fe_{0.25}$@C sample.

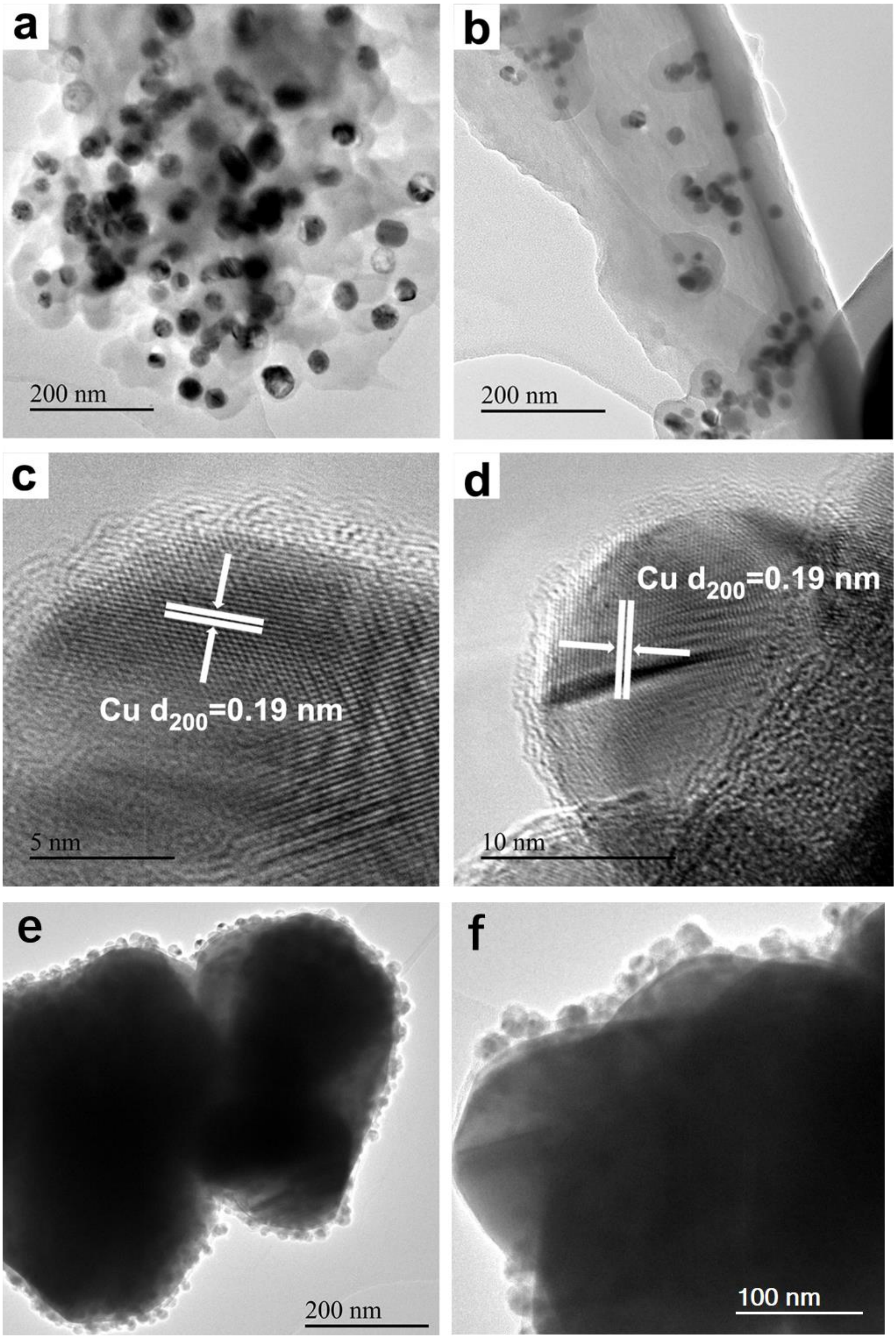

Figure S38. High-resolution TEM images of Cu@C sample. It should be noted that, there are also very big Cu nanoparticles present in the Cu@C sample.

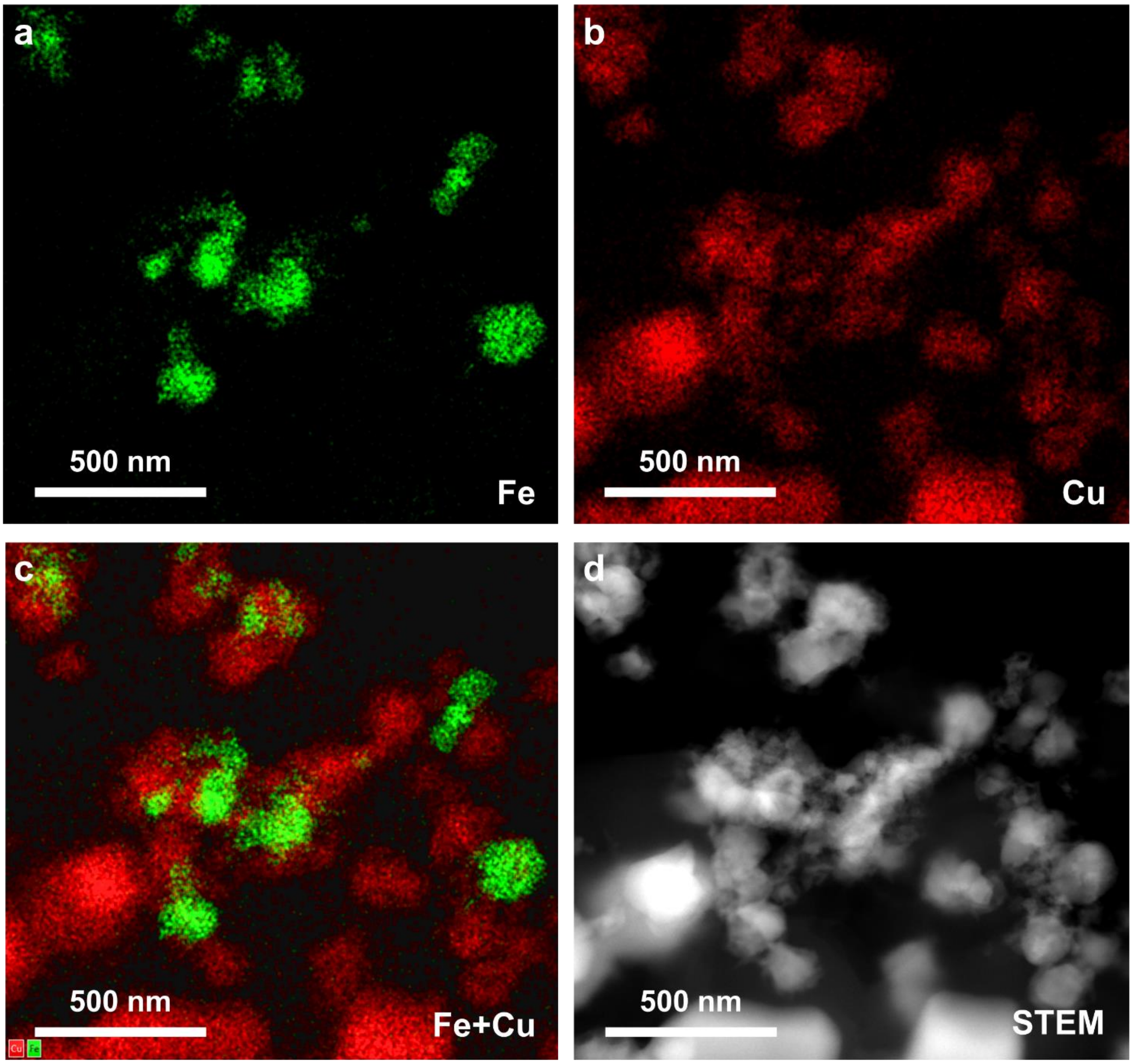

Figure S39. STEM-EDS mapping of Cu and Fe in the $Cu_{0.76}Fe_{0.24}$ sample. (a-c) mapping of Cu and Fe in this area and the corresponding HAADF-STEM image (d).

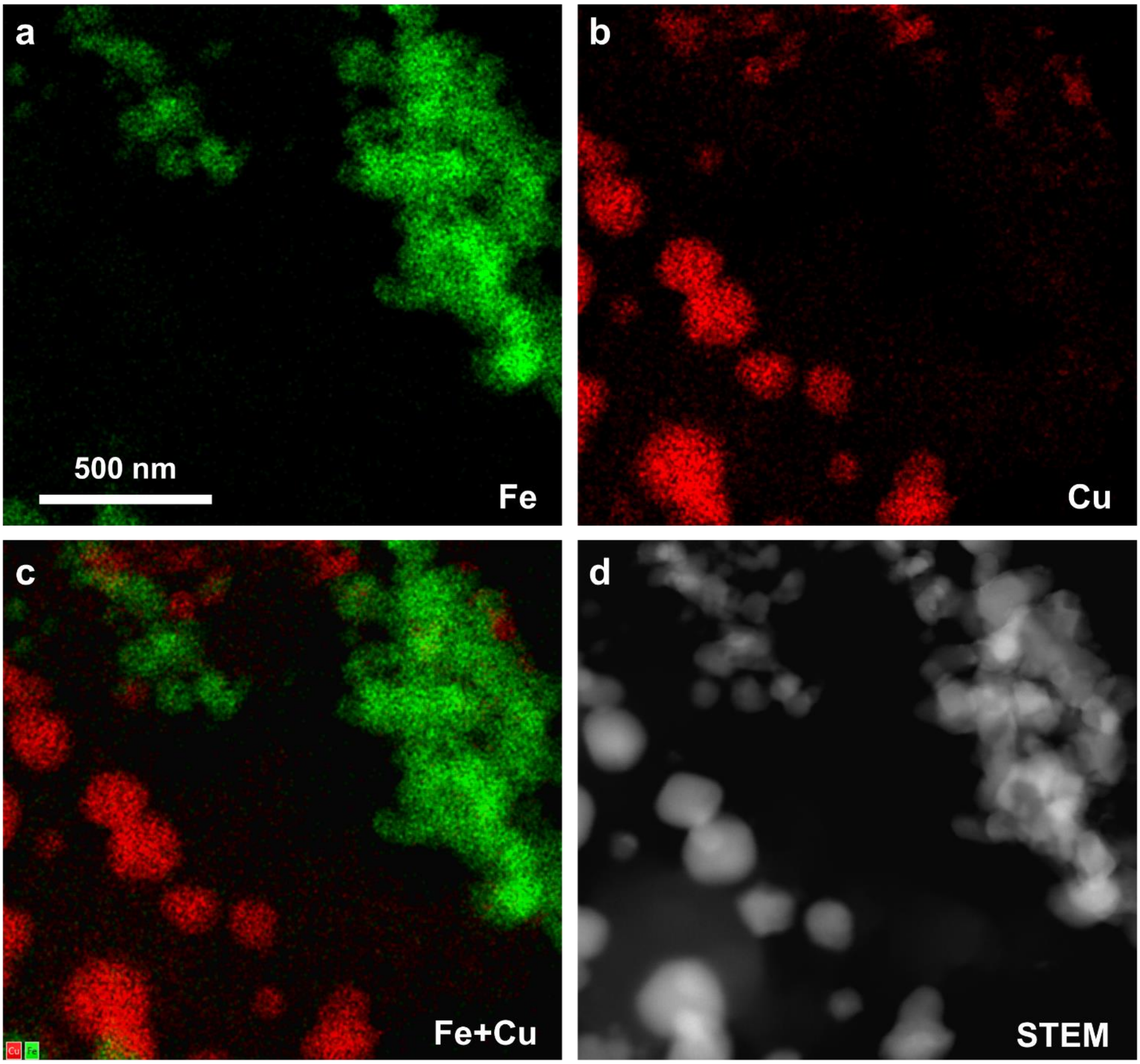

Figure S40. STEM-EDS mapping of Cu and Fe in the $Cu_{0.50}Fe_{0.50}$ sample. (a-c) mapping of Cu and Fe in this area and the corresponding HAADF-STEM image (d).

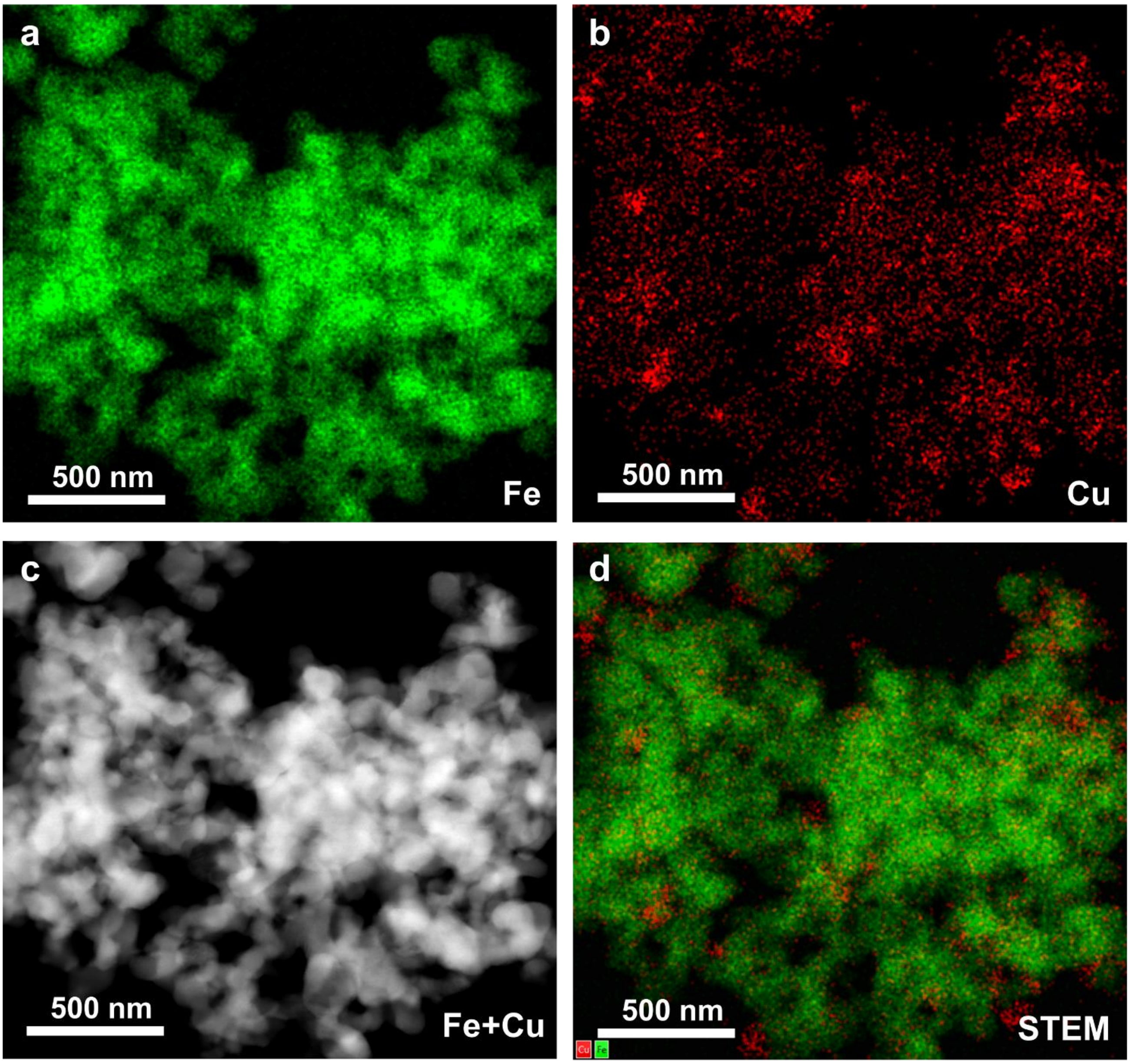

Figure S41. STEM-EDS mapping of Cu and Fe in the $Cu_{0.24}Fe_{0.76}$ sample. (a-c) mapping of Cu and Fe in this area and the corresponding HAADF-STEM image (d).

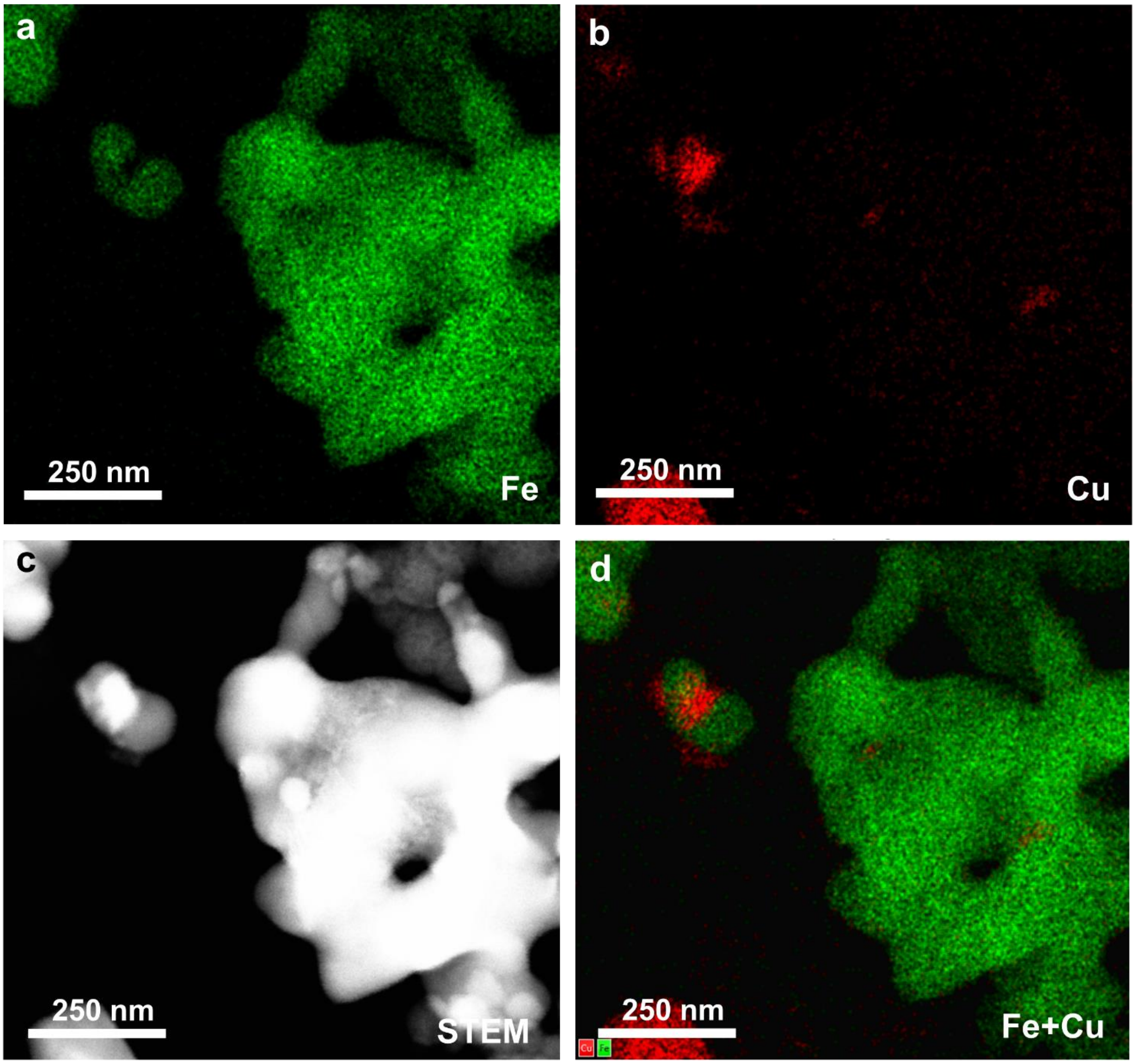

Figure S42. STEM-EDS mapping of Cu and Fe in the $Cu_{0.12}Fe_{0.88}$ sample. (a-c) mapping of Cu and Fe in this area and the corresponding HAADF-STEM image (d).

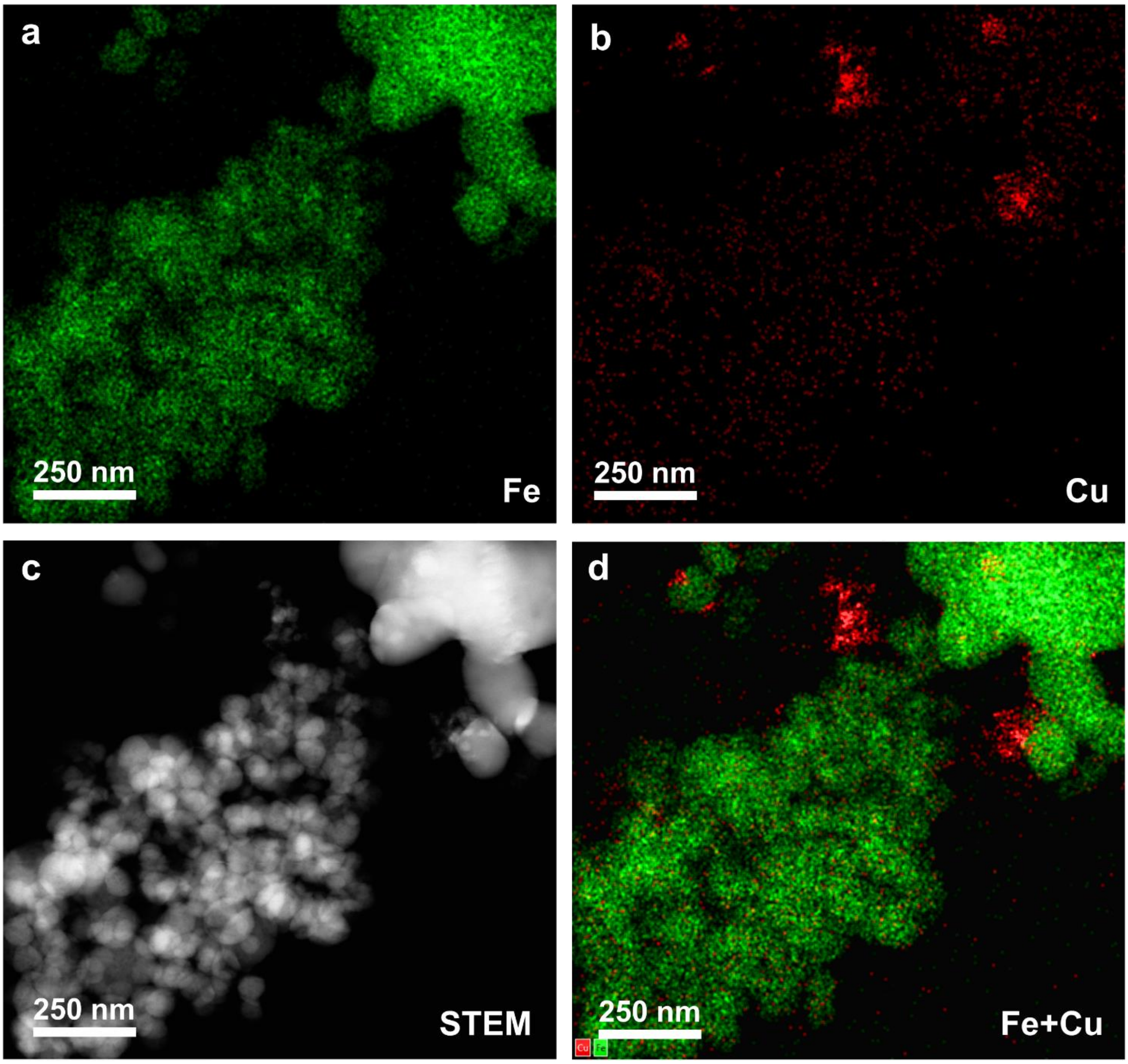

Figure S43. STEM-EDS mapping of Cu and Fe in the $Cu_{0.08}Fe_{0.92}$ sample. (a-c) mapping of Cu and Fe in this area and the corresponding HAADF-STEM image (d).

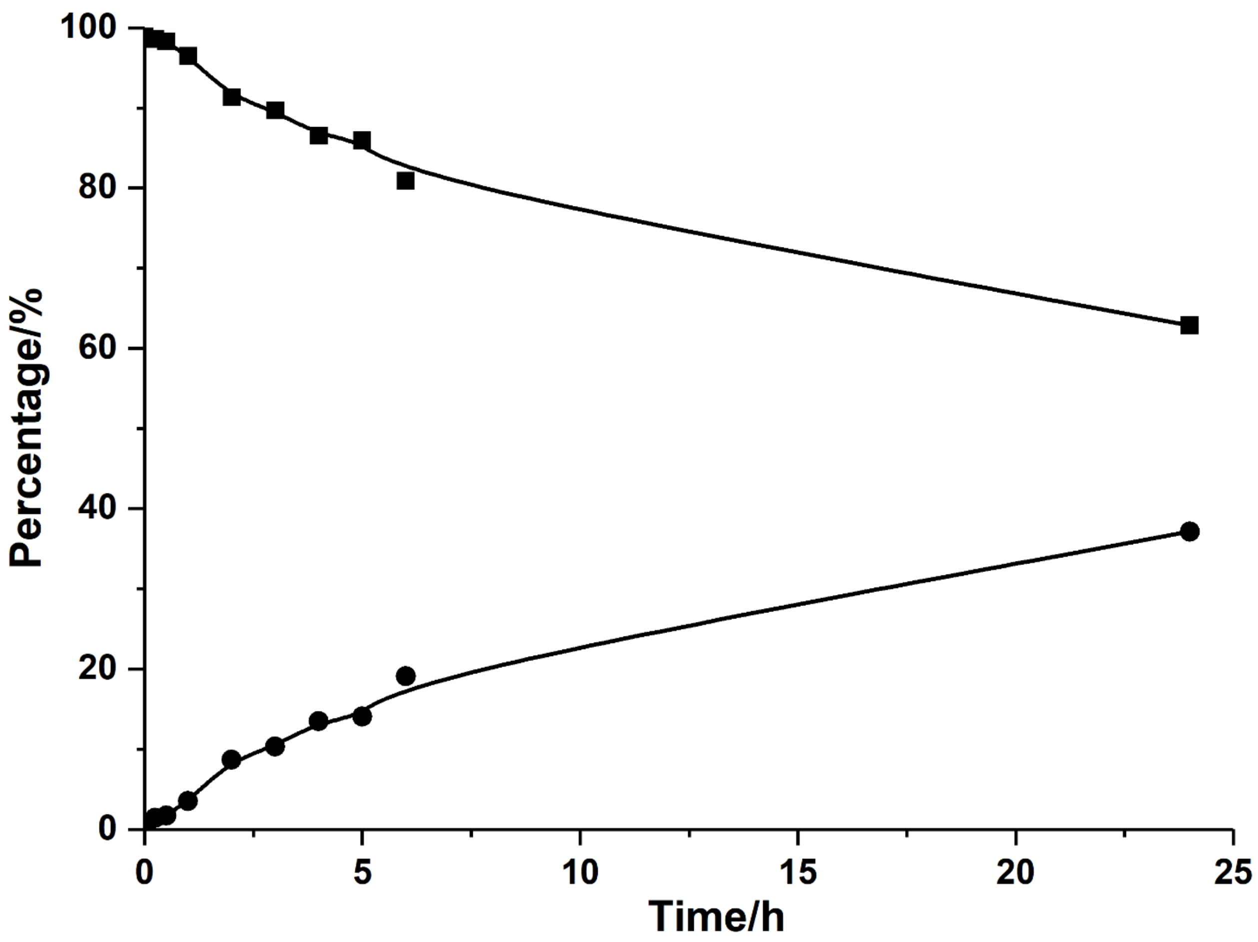

Figure S44. Kinetic curve of the hydrogenation of HMF with $Cu_{0.08}Fe_{0.92}$@C NPs. Reaction conditions: HMF (0.5 mmol, 63 mg), 10 mg catalyst, 10 bar H_2, MeOH (solvent, 5 ml), 110 ºC. Determined by GC using dodecane as an internal standard. HMF (■), BHMF (●).

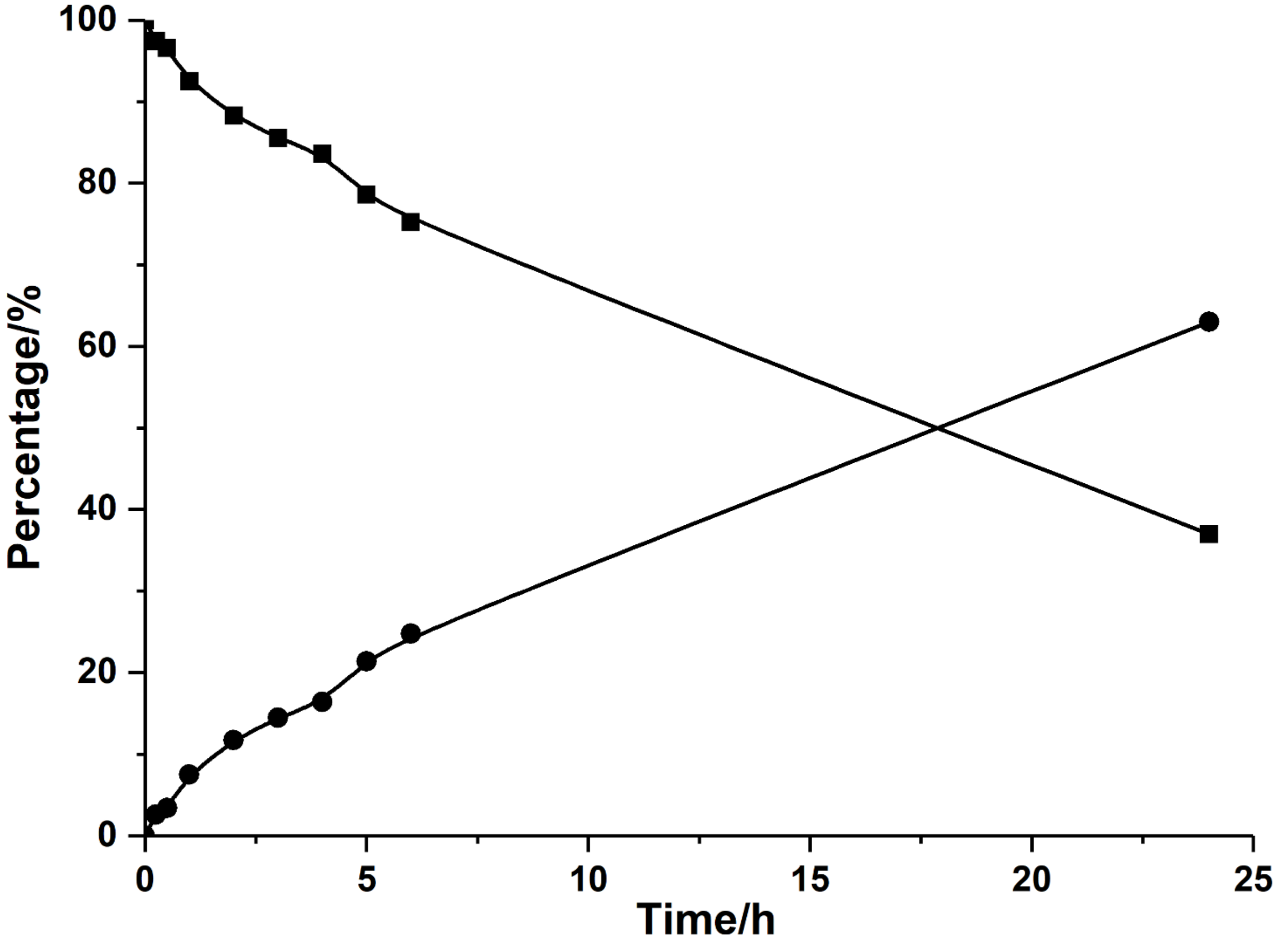

Figure S45. Kinetic curve of the hydrogenation of HMF with $Cu_{0.12}Fe_{0.88}$@C NPs. Reaction conditions: HMF (0.5 mmol, 63 mg), 10 mg catalyst, 10 bar H_2, MeOH (solvent, 5 ml), 110 ºC. Determined by GC using dodecane as an internal standard. HMF (■), BHMF (●).

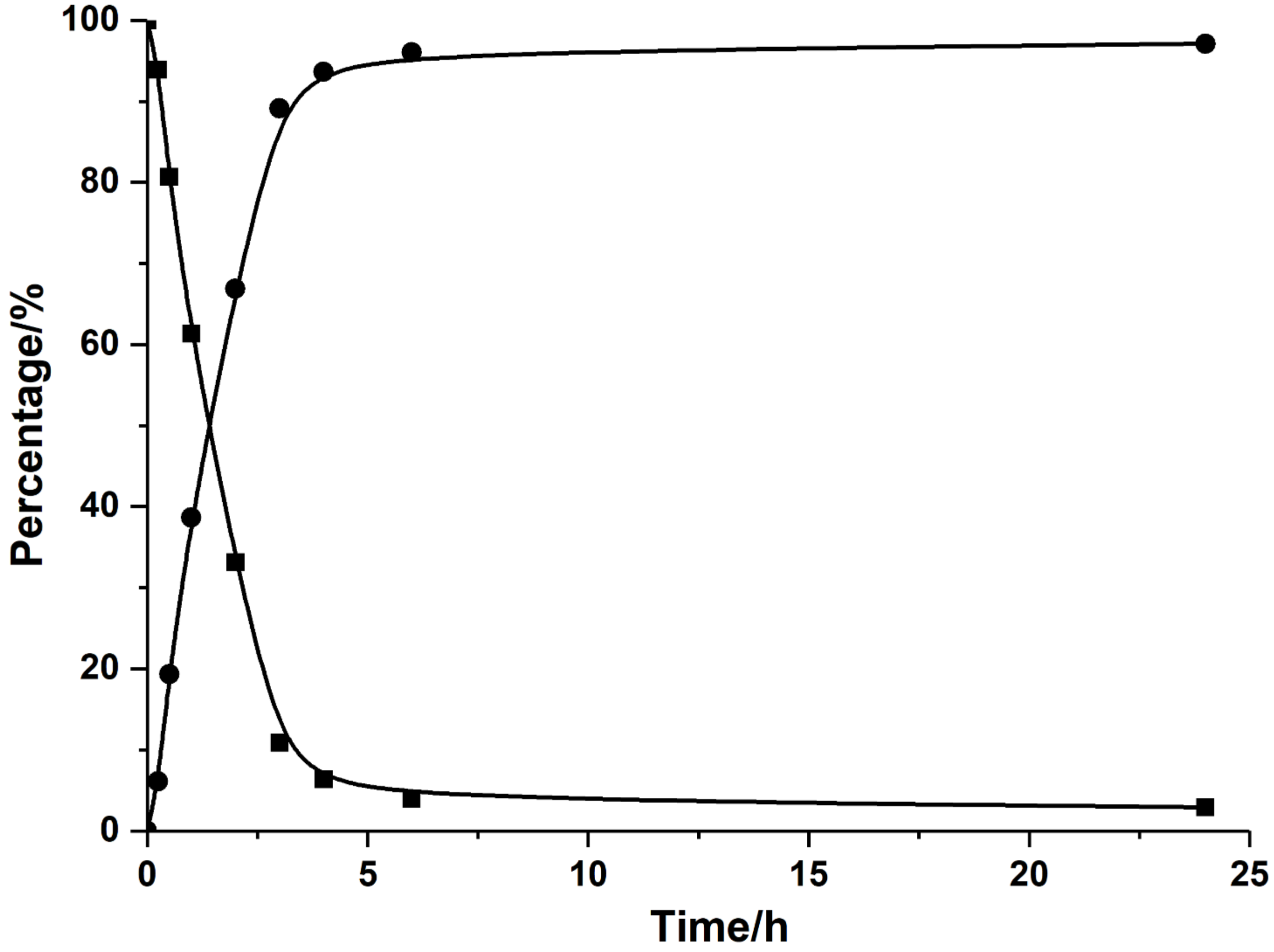

Figure S46. Kinetic curve of the hydrogenation of HMF with $Cu_{0.24}Fe_{0.76}$@C NPs. Reaction conditions: HMF (0.5 mmol, 63 mg), 10 mg catalyst, 10 bar H_2, MeOH (solvent, 5 ml), 110 ºC. Determined by GC using dodecane as an internal standard. HMF (■), BHMF (●).

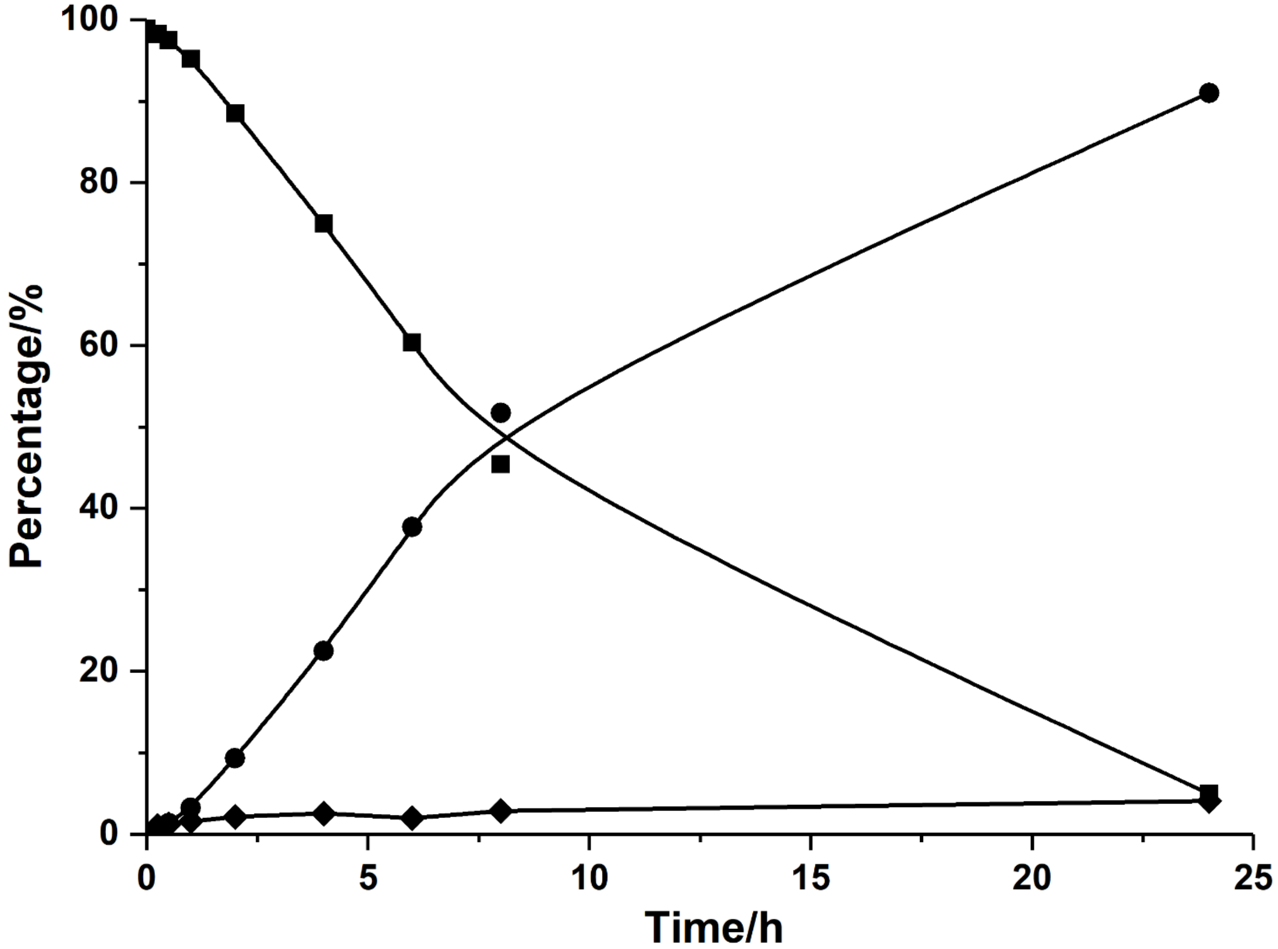

Figure S47. Kinetic curve of the hydrogenation of HMF with $Cu_{0.50}Fe_{0.50}$@C NPs. Reaction conditions: HMF (0.5 mmol, 63 mg), 10 mg catalyst, 10 bar H_2, MeOH (solvent, 5 ml), 110 ºC. Determined by GC using dodecane as an internal standard. HMF (■), BHMF (●), Acetal (♦).

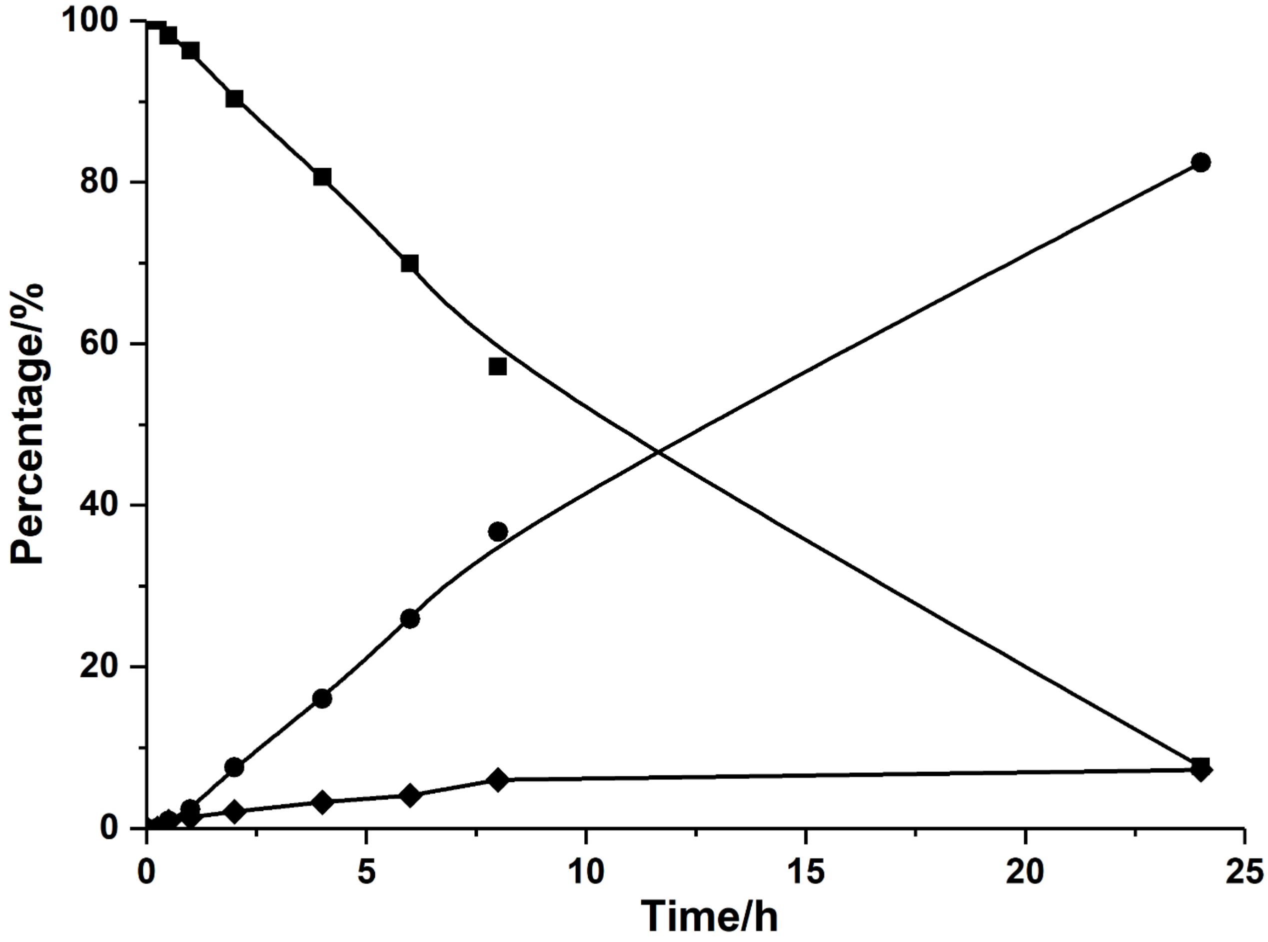

Figure S48. Kinetic curve of the hydrogenation of HMF with $Cu_{0.75}Fe_{0.25}$@C NPs. Reaction conditions: HMF (0.5 mmol, 63 mg), 10 mg catalyst, 10 bar H_2, MeOH (solvent, 5 ml), 110 ºC. Determined by GC using dodecane as an internal standard. HMF (■), BHMF (●), Acetal (♦).

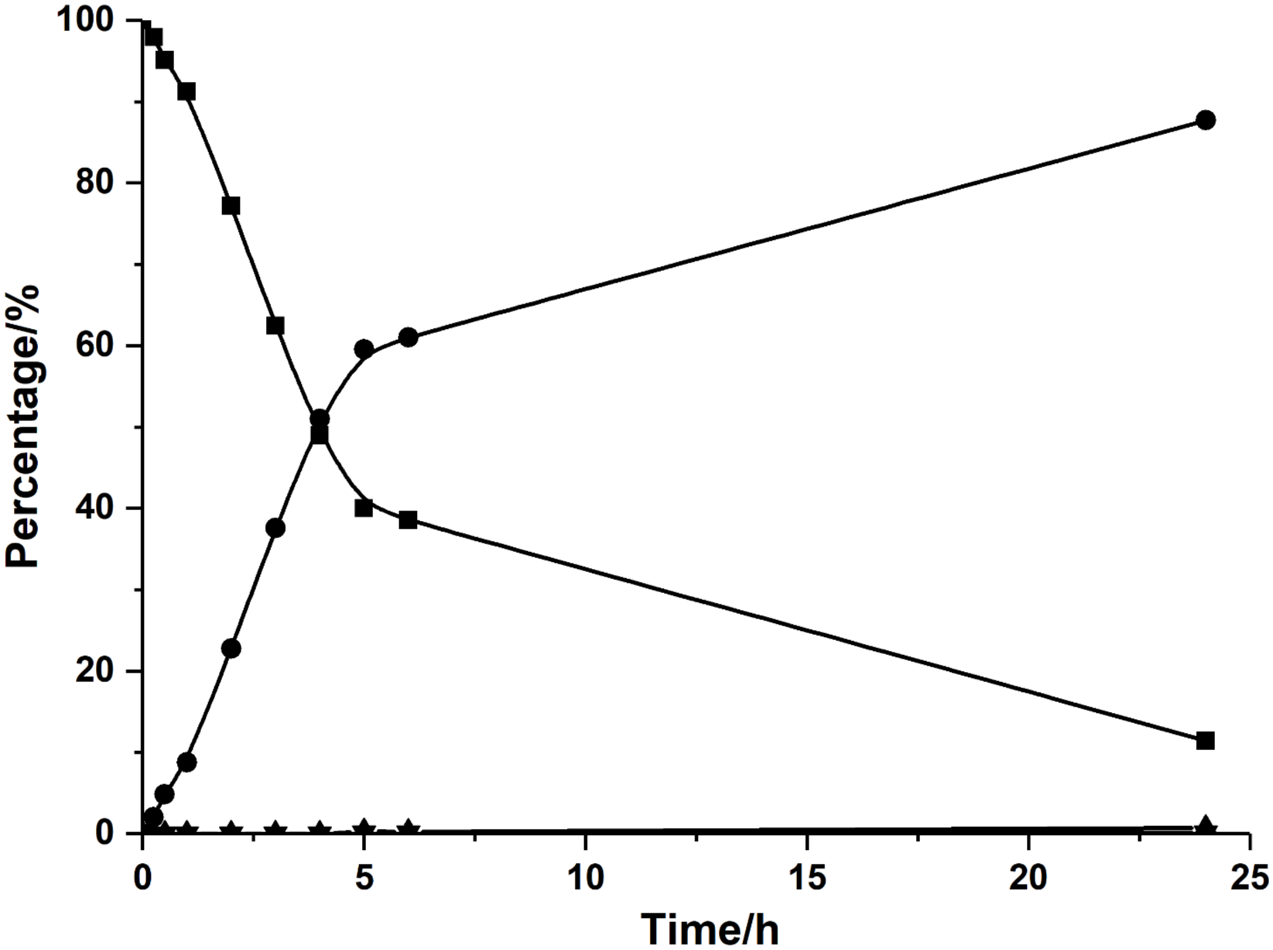

Figure S49. Kinetic curve of the hydrogenation of HMF with Cu@C NPs. Reaction conditions: HMF (0.5 mmol, 63 mg), 10 mg catalyst, 10 bar H_2, MeOH (solvent, 5 ml), 110 ºC. Determined by GC using dodecane as an internal standard. HMF (■), BHMF (●), Acetal (♦).

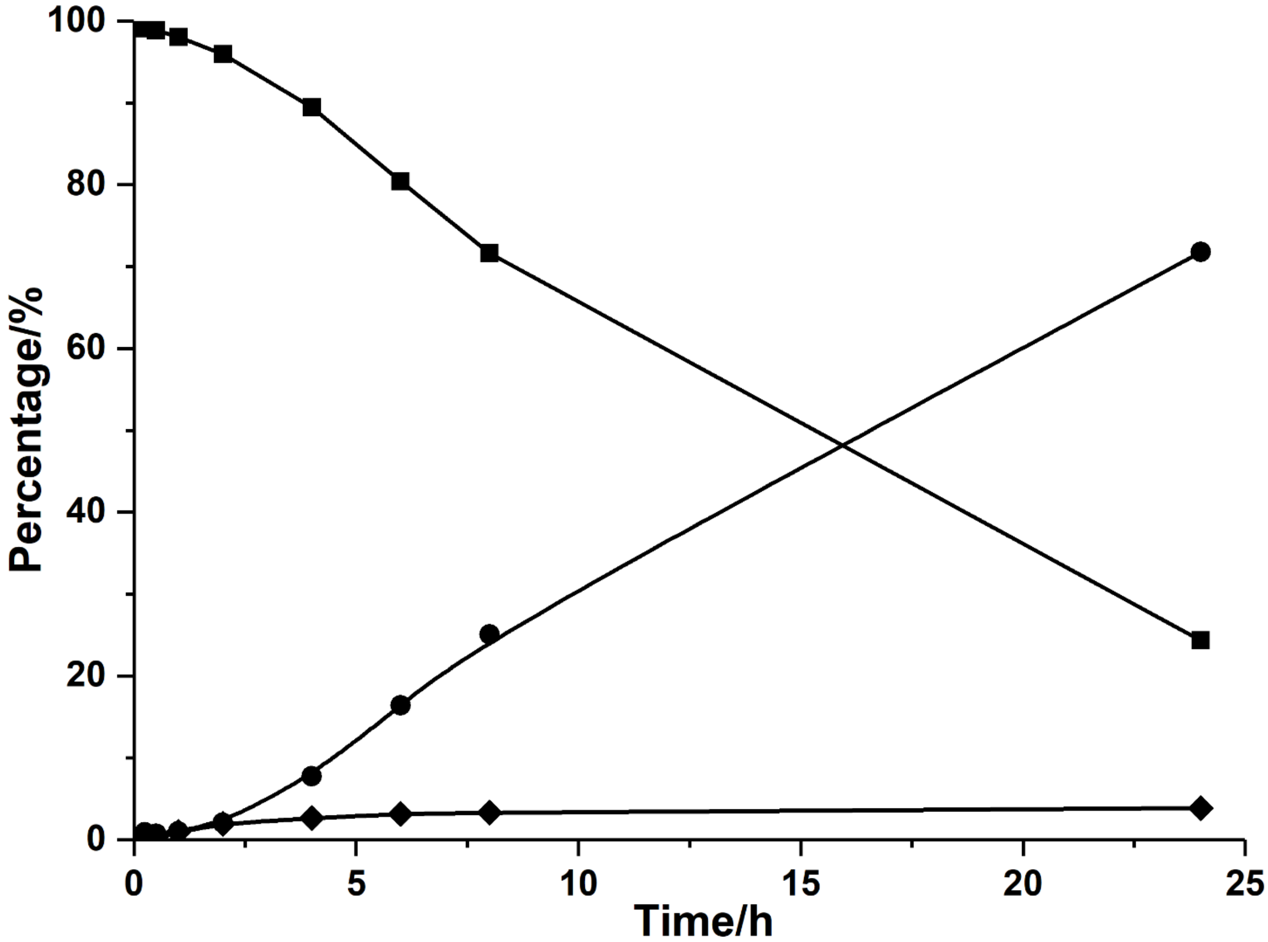

Figure S50. Kinetic curve of the hydrogenation of HMF with Fe/Cu@C catalyst with ~25 wt% of Fe on Cu@C nanoparticles loaded by wetness impregnation. Reaction conditions: 0.5 mmol HMF, 10 mg of catalyst, 5 mL methanol as solvent, 110 ºC and 10 bar of H_2. After 1 h, the catalyst was separated and the reaction was continued. HMF (■), BHMF (●), Acetal (♦).

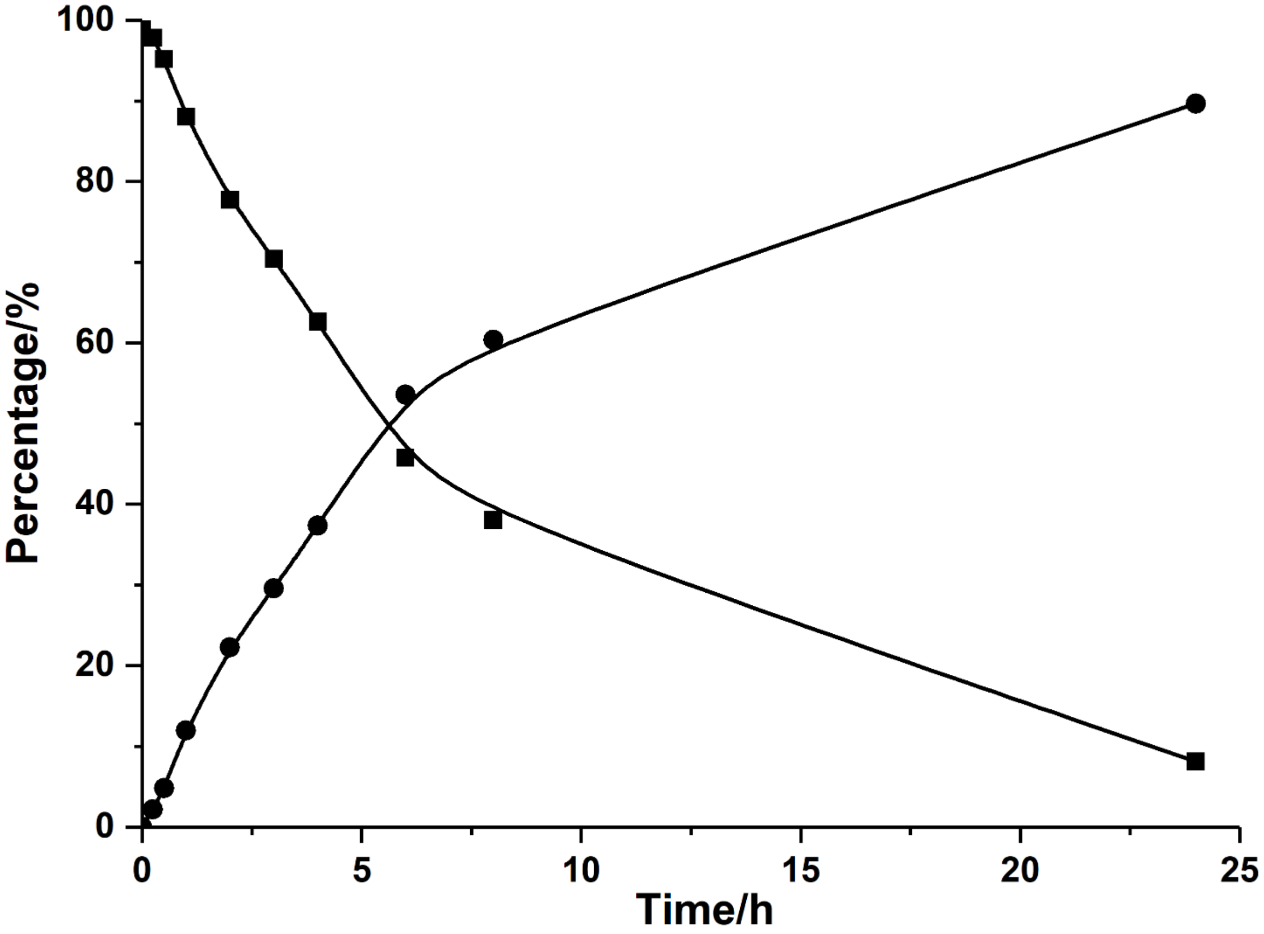

Figure S51. Kinetic curve of the hydrogenation of HMF with mixture of Fe@C and Cu@C NPs (3:1). Reaction conditions: 0.5 mmol HMF, 10 mg of solid catalyst, 5 mL methanol as solvent, 110 ºC and 10 bar of H_2. After 1 h, the catalyst was separated and the reaction was continued. HMF (■), BHMF (●).

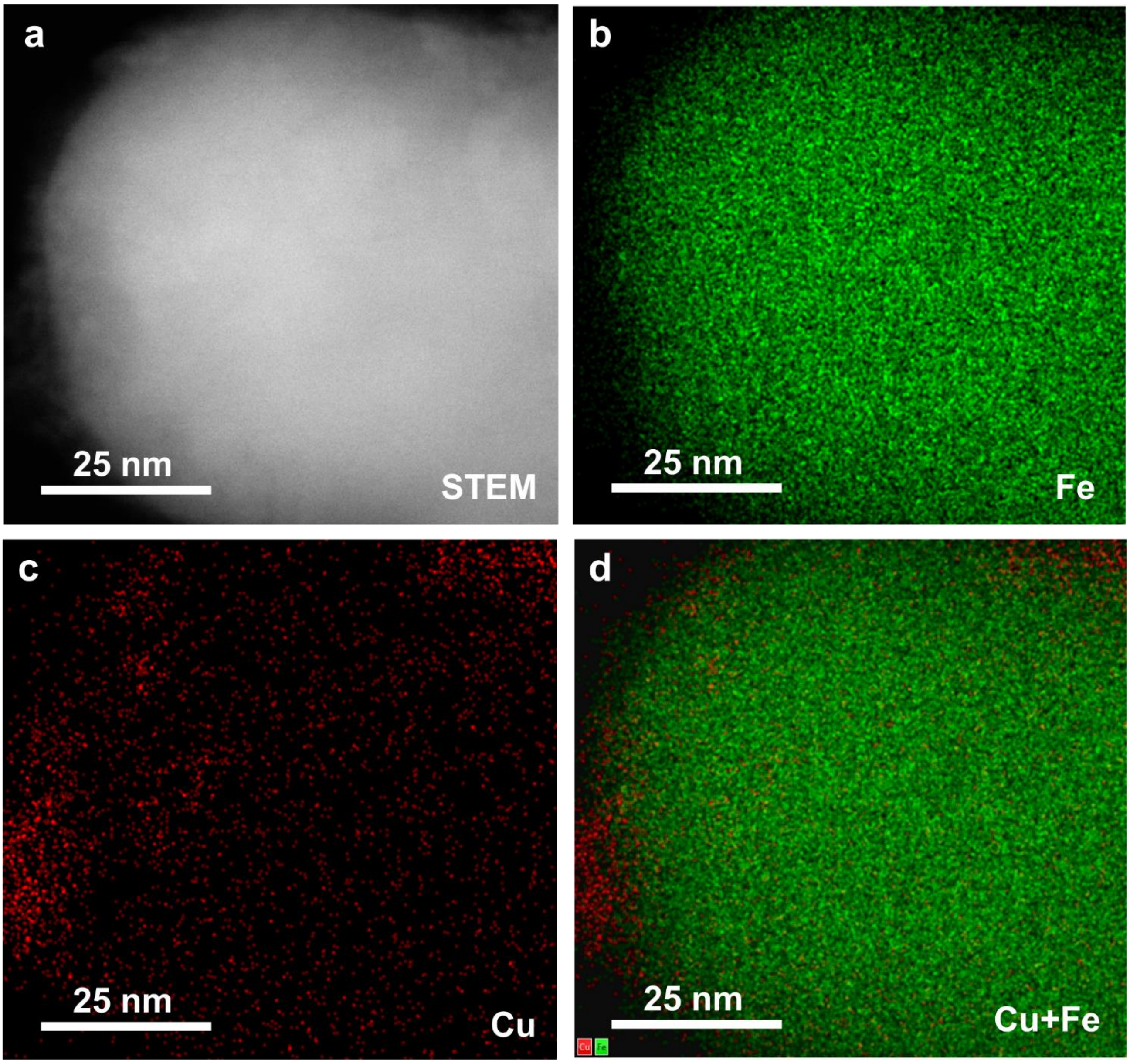

Figure S52. Distributions of Cu species on Fe nanoparticles measured by STEM-EDS mapping in the $Cu_{0.24}Fe_{0.76}$@C sample. As can be seen in (c), Cu patches and highly dispersed Cu species can be observed.

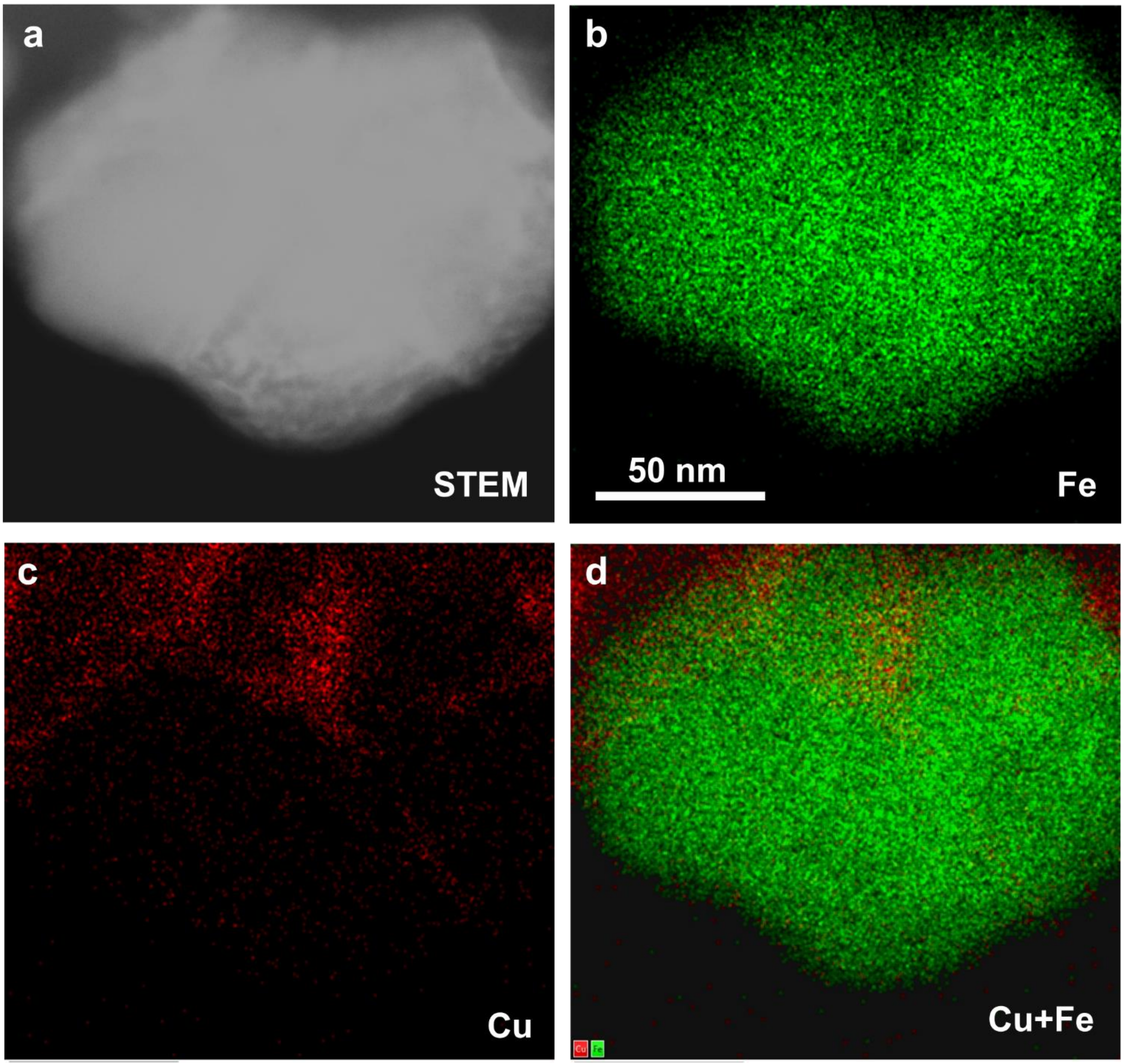

Figure S53. Distributions of Cu species on Fe nanoparticles measured by STEM-EDS mapping in the $Cu_{0.24}Fe_{0.76}$@C sample. As can be seen in (c), Cu patches and highly dispersed Cu species can be observed.

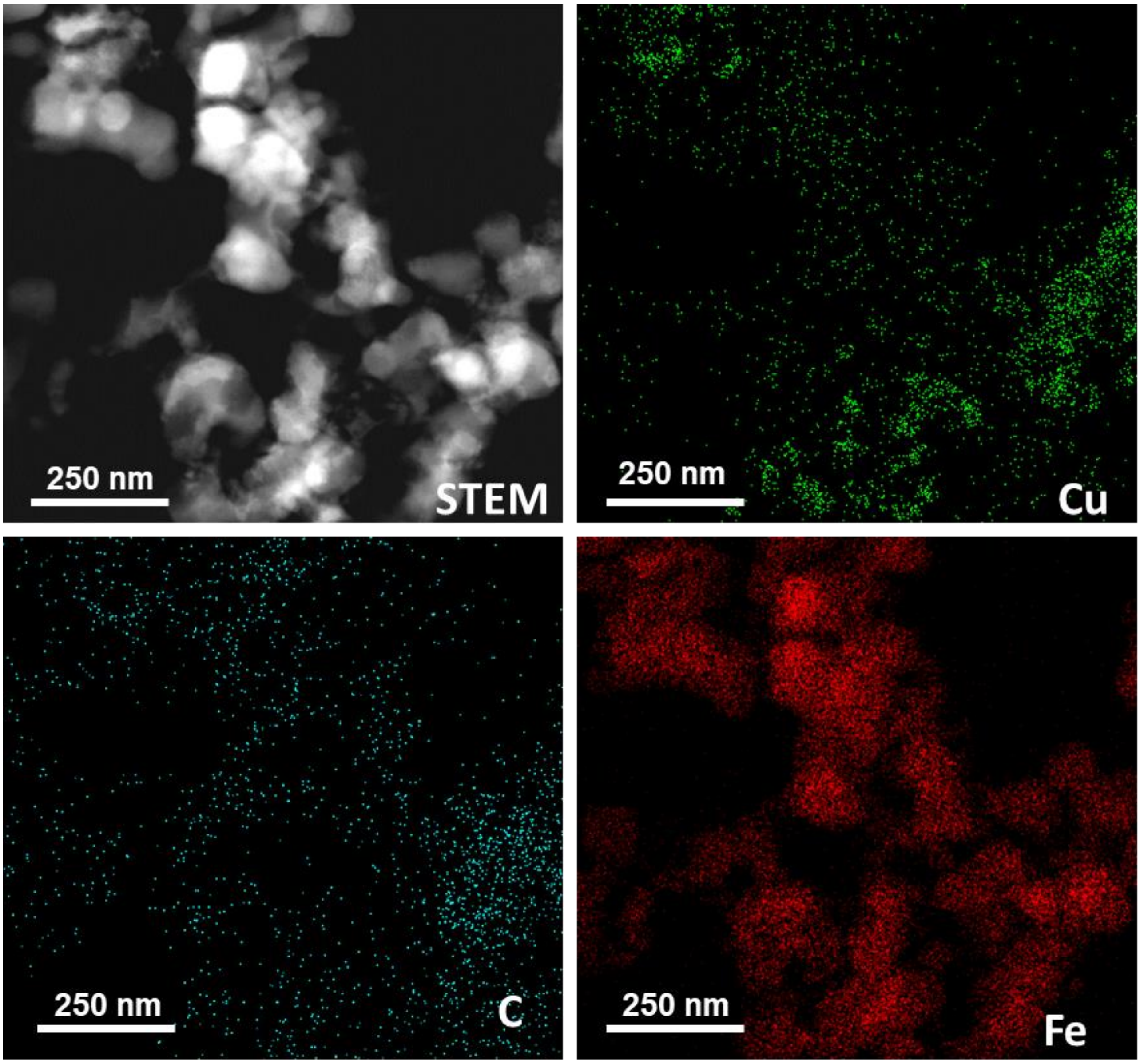

Figure S54. STEM image and the corresponding EDS mapping of a representative area in the $Cu_{0.24}Fe_{0.76}$@C sample.

Table S2. Catalytic performance of non-noble metal catalysts for hydrogenation of 5-(hydroxymethyl)furfural (HMF) to 2,5-Bis(hydroxymethyl)furan (BHMF).

Catalyst	Solid Catalyst /mg	Metal /mg	HMF/ mmol	Mass ratio of HMF to solid catalyst	Temp./ °C	H_2/ MPa	Time /h	HMF Conversion /%	Selectivity to BHMF/%	Ref.
NiFe/CNT	50	5.5	4	10	110	3	18	100	96.1	1
CuZn alloy	100	100	4	5	120	7	3	>99	95	2
NiCu/SiO_2	100	65	4	5	120	7	3	96	88	2
NiCu/SiO_2-ZrO_2	100	39	4	5	120	7	3	85	85	2
NiCu/CeO_2/ZrO_2	100	38	4	5	120	7	3	>99	44	2
Cu@C	20	20	2	12.5	180	5	8	70	77	3
Cu/K/Al_2O_3	100	1.6	0.8	1	60	6	10	99	90	4
Cu/$CoAlO_x$	100	8.5	2.4	3	180	1	5	97.3	95.3	5
Ni-Al oxide	30	14	1.8	7.5	100	2	6	96	71	6
Cu/PMO	100	31	4	5	100	5	3	100	99	7
Cu/ZnO	500	270	11.9	3	140	1.5	1	97.5	94.4	8
$CoAlO_x$	200	60	8	5	120	4	4	89.4	83	9
Cu@POP	200	20.7	5	3.1	150	2	10	100	100	10
CuFe@C	**10**	**10**	**0.5**	**6.3**	**110**	**1**	**6**	**94**	**>99**	**This work**

References for Table S2:

1. Yu, L.; He, L.; Chen, J.; Zheng, J.; Ye, L.; Lin, H.; Yuan, Y. Robust and Recyclable Nonprecious Bimetallic Nanoparticles on Carbon Nanotubes for the Hydrogenation and Hydrogenolysis of 5-Hydroxymethylfurfural. *ChemCatChem* **2015**, *7*, 1701-1707.
2. Bottari, G.; Kumalaputri, A. J.; Krawczyk, K. K.; Feringa, B. L.; Heeres, H. J.; Barta, K. Copper-zinc alloy nanopowder: a robust precious-metal-free catalyst for the conversion of 5-hydroxymethylfurfural. *ChemSusChem* **2015**, *8*, 1323-1327.
3. Chen, B.; Li, F.; Huang, Z.; Yuan, G. Carbon-coated Cu-Co bimetallic nanoparticles as selective and recyclable catalysts for production of biofuel 2,5-dimethylfuran. *Applied Catalysis B: Environmental* **2017**, *200*, 192-199.
4. Sun, K.; Shao, Y.; Li, Q.; Liu, Q.; Wu, W.; Wang, Y.; Hu, S.; Xiang, J.; Liu, Q.; Hu, X. Cu-based catalysts for hydrogenation of 5-hydroxymethylfurfural: Understanding of the coordination between copper and alkali/alkaline earth additives. *Molecular Catalysis* **2019,** *474*, 110407.
5. Wang, Q.; Feng, J.; Zheng, L.; Wang, B.; Bi, R.; He, Y.; Liu, H.; Li, D. Interfacial Structure-Determined Reaction Pathway and Selectivity for 5-(Hydroxymethyl)furfural Hydrogenation over Cu-Based Catalysts. *ACS Catalysis* **2019**, *10*, 1353-1365.
6. Perret, N.; Grigoropoulos, A.; Zanella, M.; Manning, T. D.; Claridge, J. B.; Rosseinsky, M. J. Catalytic Response and Stability of Nickel/Alumina for the Hydrogenation of 5-Hydroxymethylfurfural in Water. *ChemSusChem* **2016**, *9*, 521-531.
7. Kumalaputri, A. J.; Bottari, G.; Erne, P. M.; Heeres, H. J.; Barta, K. Tunable and selective conversion of 5-HMF to 2,5-furandimethanol and 2,5-dimethylfuran over copper-doped porous metal oxides. *ChemSusChem* **2014**, *7*, 2266-2275.
8. Zhu, Y.; Kong, X.; Zheng, H.; Ding, G.; Zhu, Y.; Li, Y.-W. Efficient synthesis of 2,5-dihydroxymethylfuran and 2,5-dimethylfuran from 5-hydroxymethylfurfural using mineral-

derived Cu catalysts as versatile catalysts. *Catalysis Science & Technology* **2015**, *5*, 4208-4217.
9. Yao, S.; Wang, X.; Jiang, Y.; Wu, F.; Chen, X.; Mu, X. One-Step Conversion of Biomass-Derived 5-Hydroxymethylfurfural to 1,2,6-Hexanetriol Over Ni–Co–Al Mixed Oxide Catalysts Under Mild Conditions. *ACS Sustainable Chemistry & Engineering* **2013**, *2*, 173-180.
10. Sarkar, Ch.; Paul, R.; Shit, S. Ch.; Trinh, Q. T.; Koley, P.; Rao, B. S.; Beale, A. M.; Pao, Ch. W.; Banerjee, A.; Mondal J. Navigating Copper-Atom-Pair Structural Effect inside a Porous Organic Polymer Cavity for Selective Hydrogenation of Biomass-Derived 5-Hydroxymethylfurfural. *ACS Sustainable Chem. Eng.* **2021**, 9, 5, 2136–2151

Table S3. BE of surface elements from X-ray photoelectron spectroscopy

Sample	**Fe $2p_{3/2}$ BE (eV)[a-c] (%)[d]**			**Cu $2p_{3/2}$ BE (eV) (%)[d]**		
	Fe^{2+}	Fe^{3+}	Fe^{0}	Cu^{+}/Cu^{0}	Cu^{2+}	α′[e]
Fe@C	709.9 (81.8%)	712.3 (18.2%)	--	--	--	
Fe@C-H_2	709.5 (72.2%)	711.8 (17.9%)	707.0 (9.8%)	--	--	
$Cu_{0.24}Fe_{0.76}$@C	710.1 (62.3%)	712.3 (37.7%)		932.7 (11%)	934.1 (89%)	1852.7 1849.7
$Cu_{0.24}Fe_{0.76}$@C-H_2	710.1 (51.8%)	712.8 (19.8%)	708.1 (28.3%)	931.7 (38.9%)	934.0 (61.1%)	1851.3

a) Peng Li, E.Y. Jiang, H.L. Bai J. Phys. D: Appl. Phys.44 (2011) 075003
b) Mark C. Biesinger, Brad P. Payne, Andrew P. Grosvenor, Leo. W. M. Lau, Andrea R. Gerson, Roger St. C. Smart, Appl. Surf. Sci. 257 (2011) 2717-2730
c) Toru Yamashita, P. Hayes, Appl. Surf. Sci. 254 (2008) 2441-2449
d) In brackets the atomic percent of each component
e) Auger parameter α′= BE(Cu^{+}/Cu^{0}) +KE(Cu LMM); (Cu^{0}) = 1851.3 eV; (Cu^{+}) = 1849.7eV; (Cu^{2+}) = 1852.7eV

Table S4. Catalytic performance of noble metal catalysts for hydrogenation of 5-(hydroxymethyl)furfural (HMF) to 2,5-Bis(hydroxymethyl)furan (BHMF).

Catalyst	Solid Catalyst /mg	Metal /mg	HMF/ mmol	Temp./ °C	H_2/ MPa	Time /h	HMF Conversion/%	Yield to BHMF/%	Selectivity to BHMF/%	Ref.
Au/Al_2O_3	10	0.083	2	120	6.5	2	100	>96	>96	1
Pd/C	8	0.4	1.19	80	10	20	97	82	84.5	2
Pt/C	10	0.5	1	23	1.4	18	-	82		3
$PtSn/SnO_2/RGO$	-	-	8	70	2	0.5	>99	>99	>99	4
Ru/C	250	12.5	5.56	60	5	0.7	100	100	100	5
$Ru(OH)_x/ZrO_2$	15	0.3	0.97	120	1.5	6	99	99	100	6
Ir/TiO_2	50	2.5	1.07	50	6	3	99	95	96	7
CuFe@C	**10**	**10**	**0.5**	**110**	**1**	**6**	**94**	**93**	**>99**	**This work**

References

1. J. Ohyama, A. Esaki, Y. Yamamoto, S. Arai, A. Satsuma, *RSC Adv.* **2013**, *3*, 1033–1036.
2. F. Liu, M. Audemar, K. De Oliveira Vigier, J. M. Clacens, F. De Campo, F. Jérome, *Green Chem.* **2014**, *16*, 4110–4114.
3. M. Balakrishnan, E. R. Sacia, A. T. Bell, *Green Chem.* **2012**, *14*, 1626–1634.
4. J. Shi, M. Zhang, W. Du, W. Ning, Z. Hou, *Catal. Sci. Technol.* **2015**, *5*, 3108–3112.
5. B. Op De Beeck, M. Dusselier, J. Geboers, J. Holsbeek, E. Morré, S. Oswald, L. Giebeler, B. F. Sels, *Energy Environ. Sci.* **2015**, *8*, 230–240.
6. J.. Han, Y. H. Kim, B. Y. Jung, S. H. Hwang, J. Jegal, J. W. Kim, Y. S. Lee, *Synlett* **2017**, *28*, 2299–2302.
7. H. Cai, C. Li, A. Wang, T. Zhang, *Catal. Today* **2014**, *234*, 59–65.

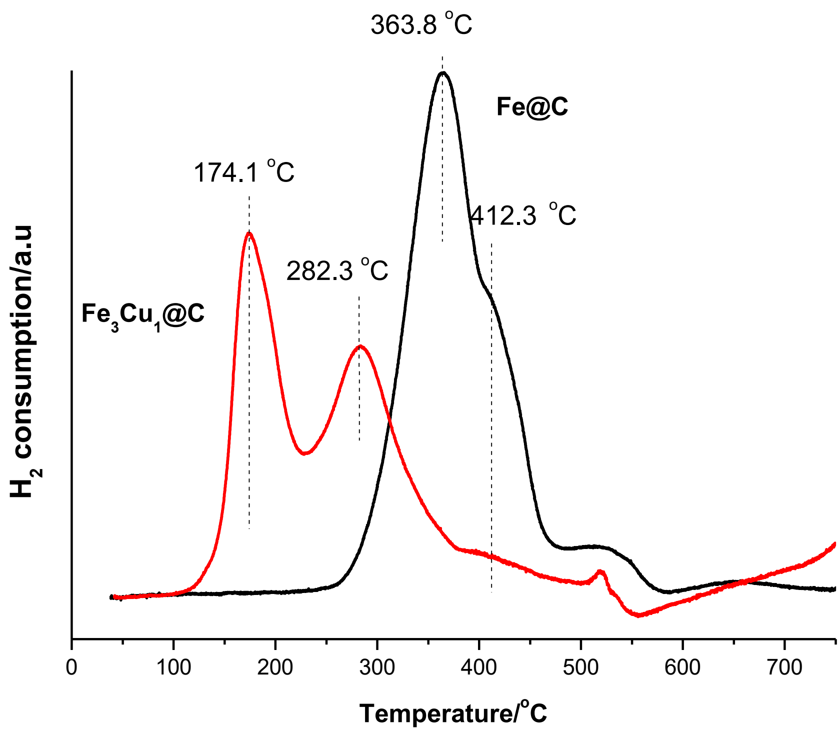

Figure S55. H_2-Temperature-programmed reduction (TPR) profiles of Fe_3Cu_1@C and Fe@C samples.

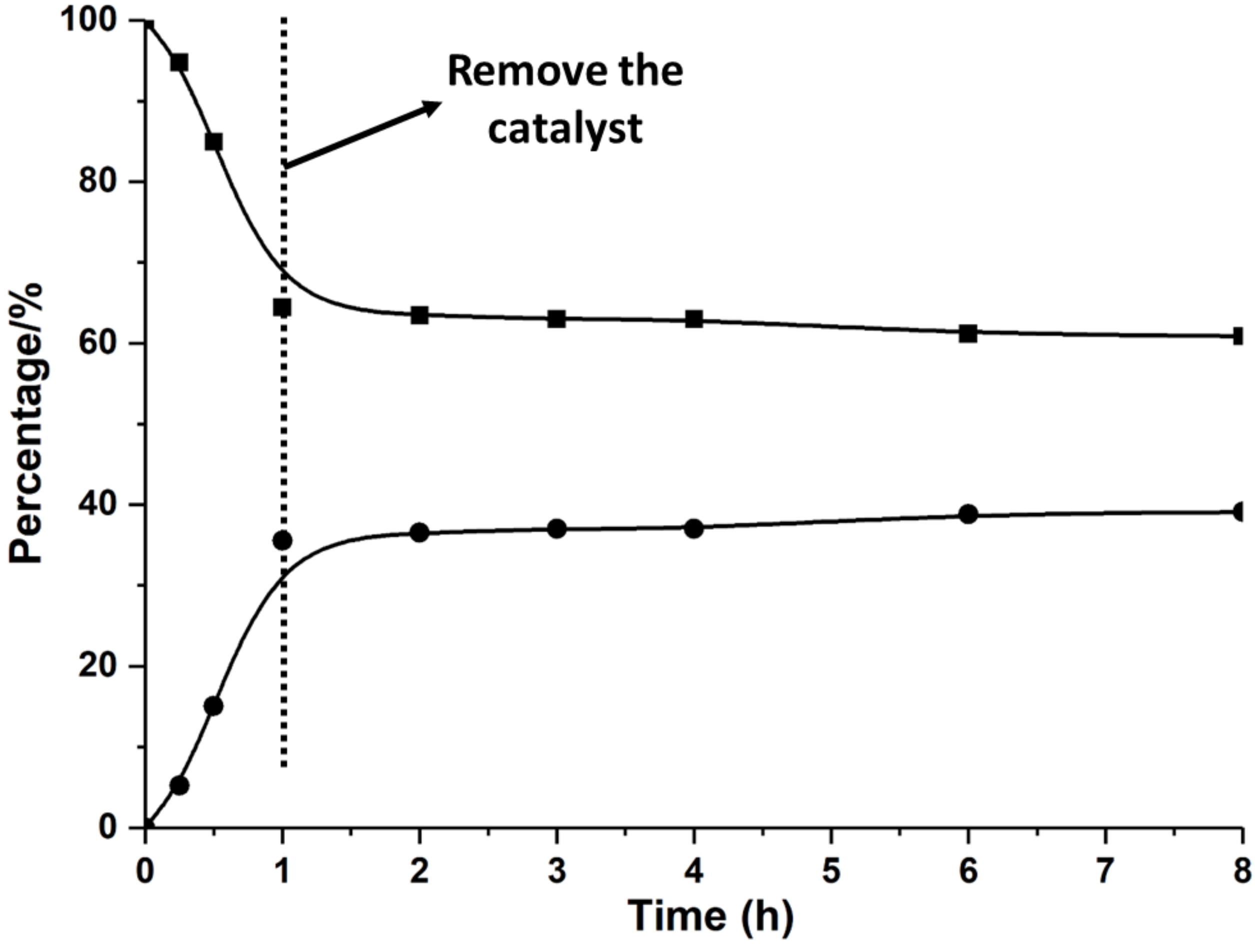

Figure S56. Leaching test with catalyst removal during the reaction course. Reaction conditions: 0.5 mmol HMF, 10 mg of $Cu_{0.24}Fe_{0.76}$@C as the catalyst, 5 mL methanol as solvent, 110 ºC, and 10 bar of H_2. After 1 h, the catalyst was removed and the reaction was continued. HMF (■), BHMF (●).

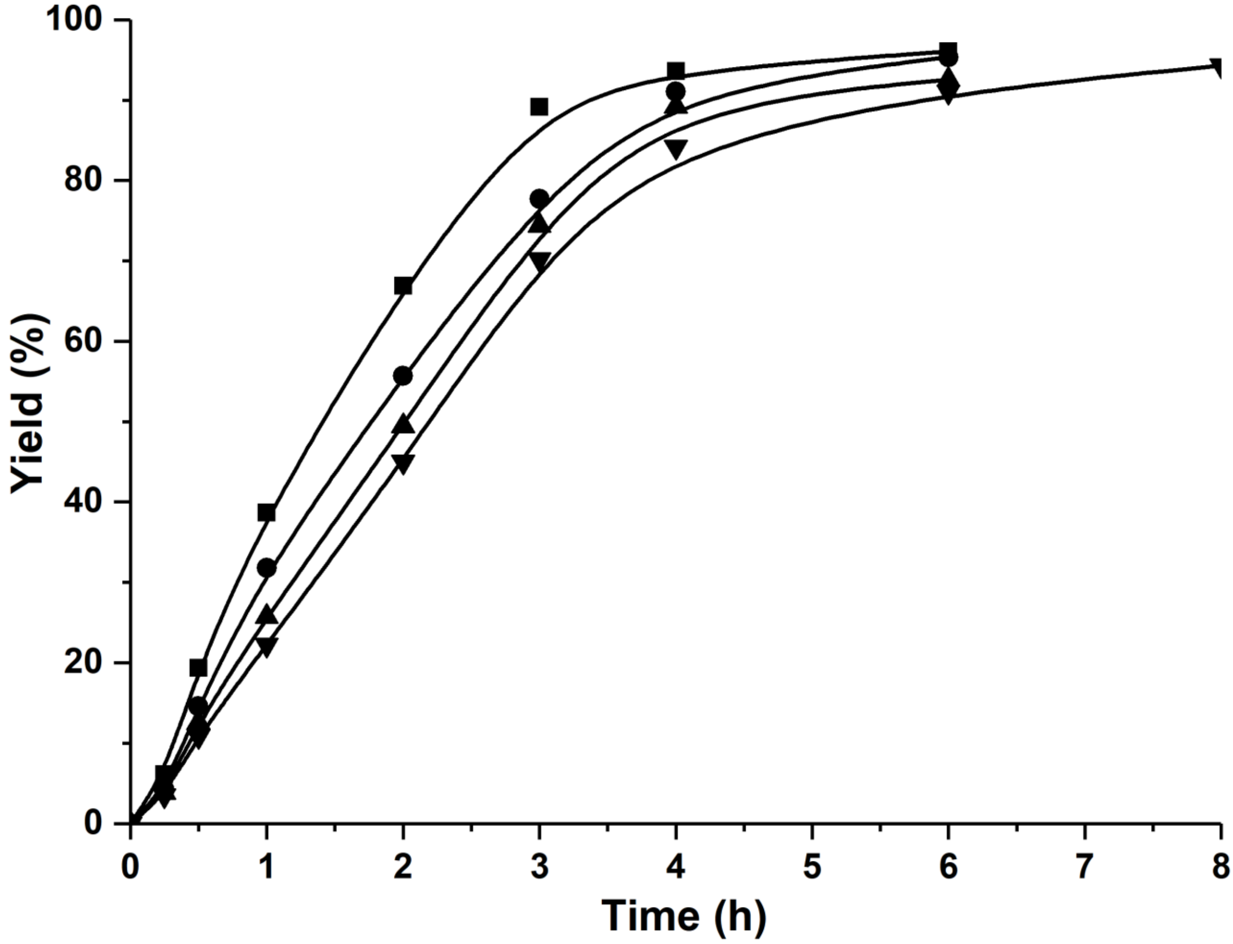

Figure S57. The catalytic performances of recycled $Cu_{0.24}Fe_{0.76}$@C NPs in reduction of HMF to BHMF. Reaction conditions: Reaction conditions: HMF (0.5 mmol, 63 mg), 10 mg of catalyst, MeOH (solvent, 5 mL), dodecane as internal standard, 110 ºC. and 10 bar of H_2. First use (■), second use (●), third use (▲), and fourth use (▼).

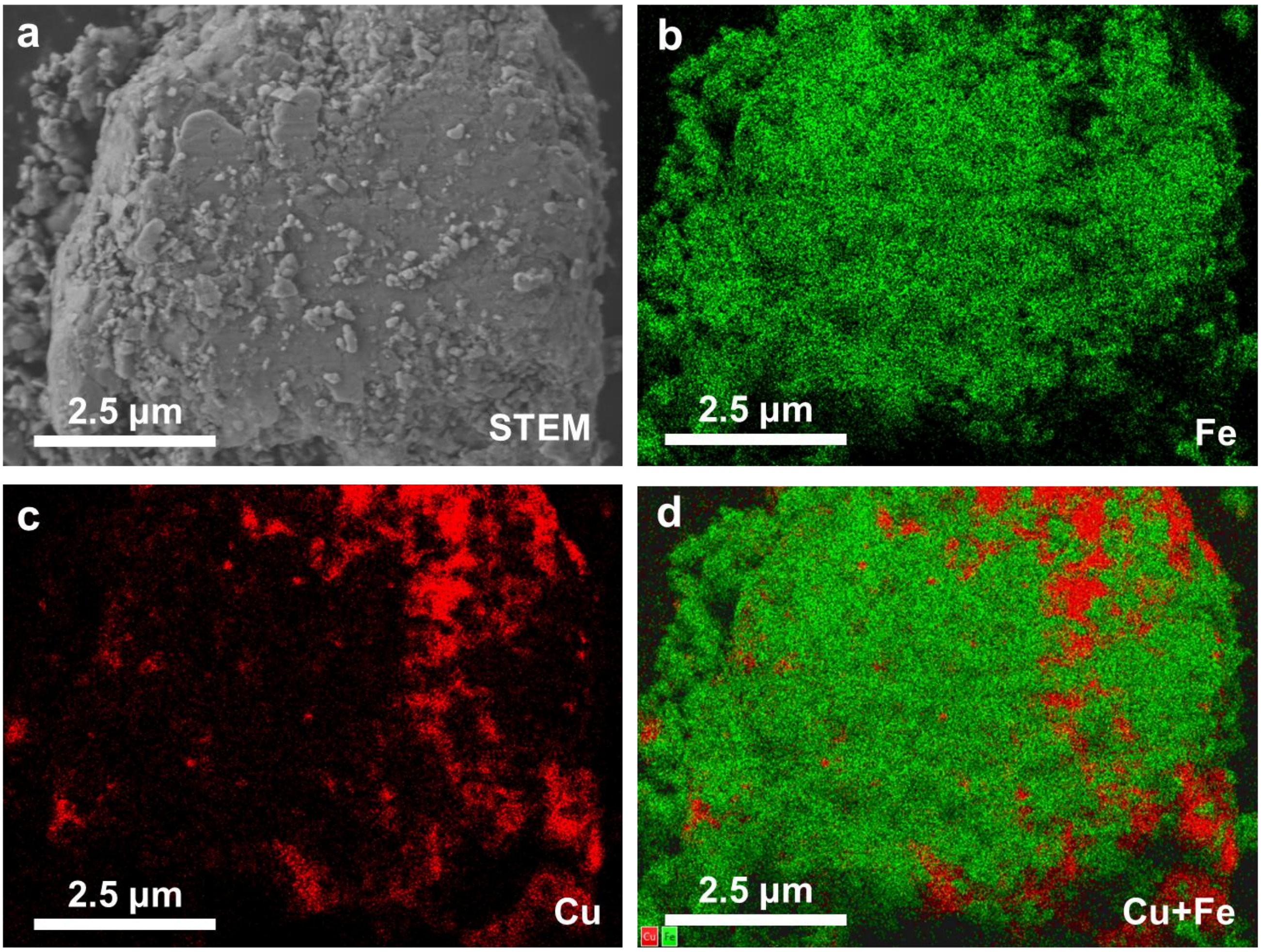

Figure S58. FESEM image and corresponding EDS mapping on the distribution of Fe and Cu in the used $Cu_{0.24}Fe_{0.76}$@C sample after four catalytic runs for hydrogenation of HMF.

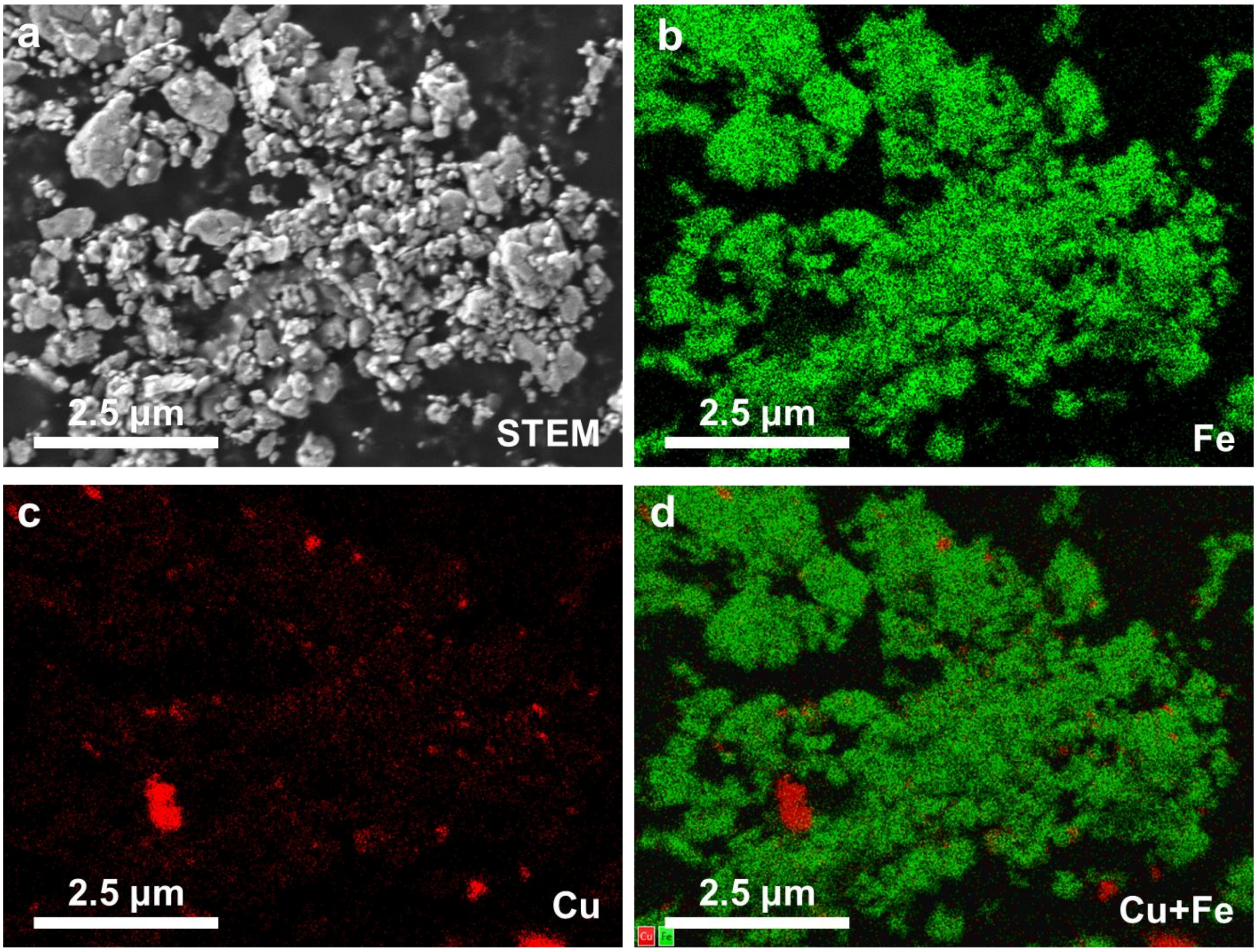

Figure S59. FESEM image and corresponding EDS mapping on the distribution of Fe and Cu in the used $Cu_{0.24}Fe_{0.76}$@C sample after four catalytic runs for hydrogenation of HMF.

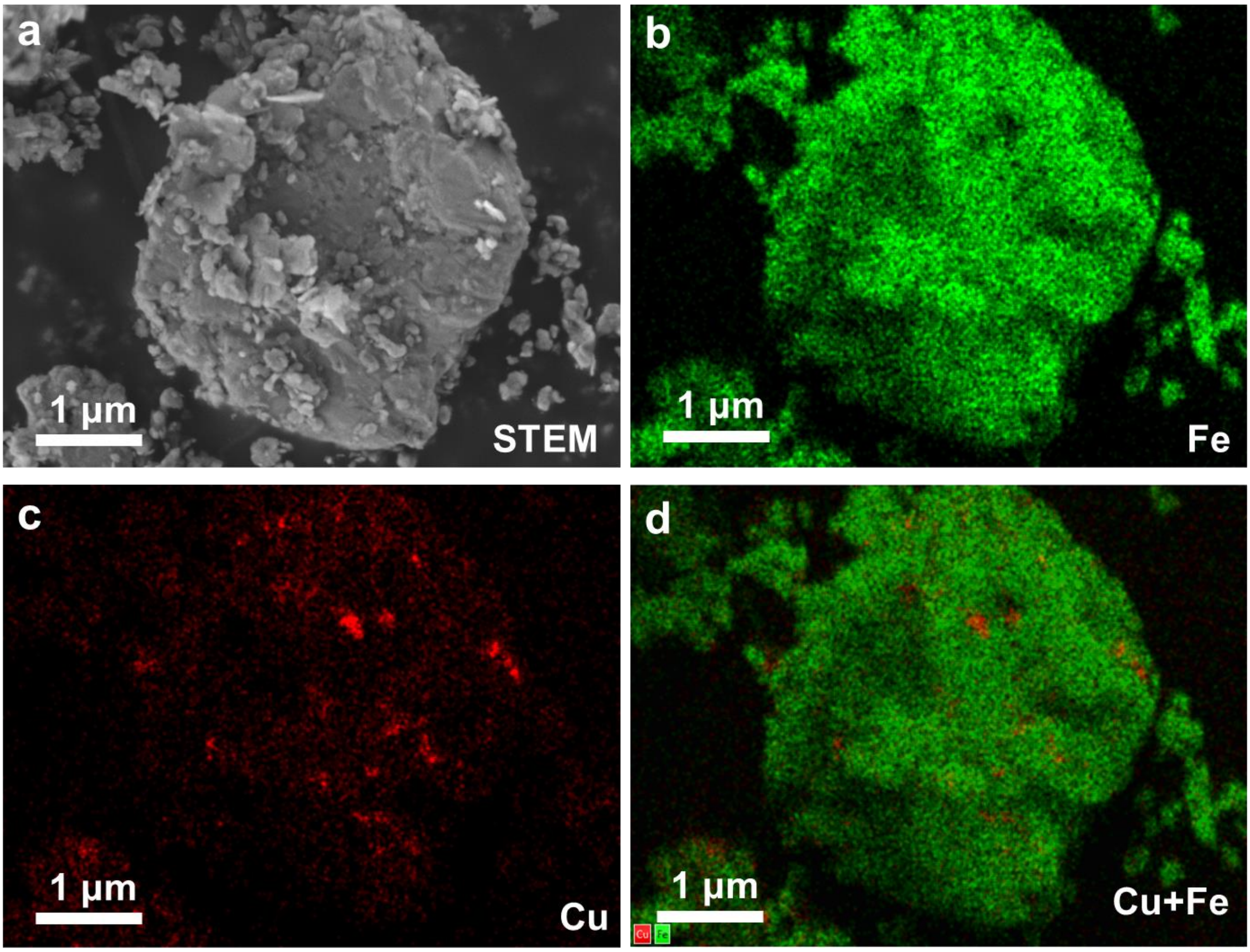

Figure S60. FESEM image and corresponding EDS mapping on the distribution of Fe and Cu in the used $Cu_{0.24}Fe_{0.76}$@C sample after four catalytic runs for hydrogenation of HMF.

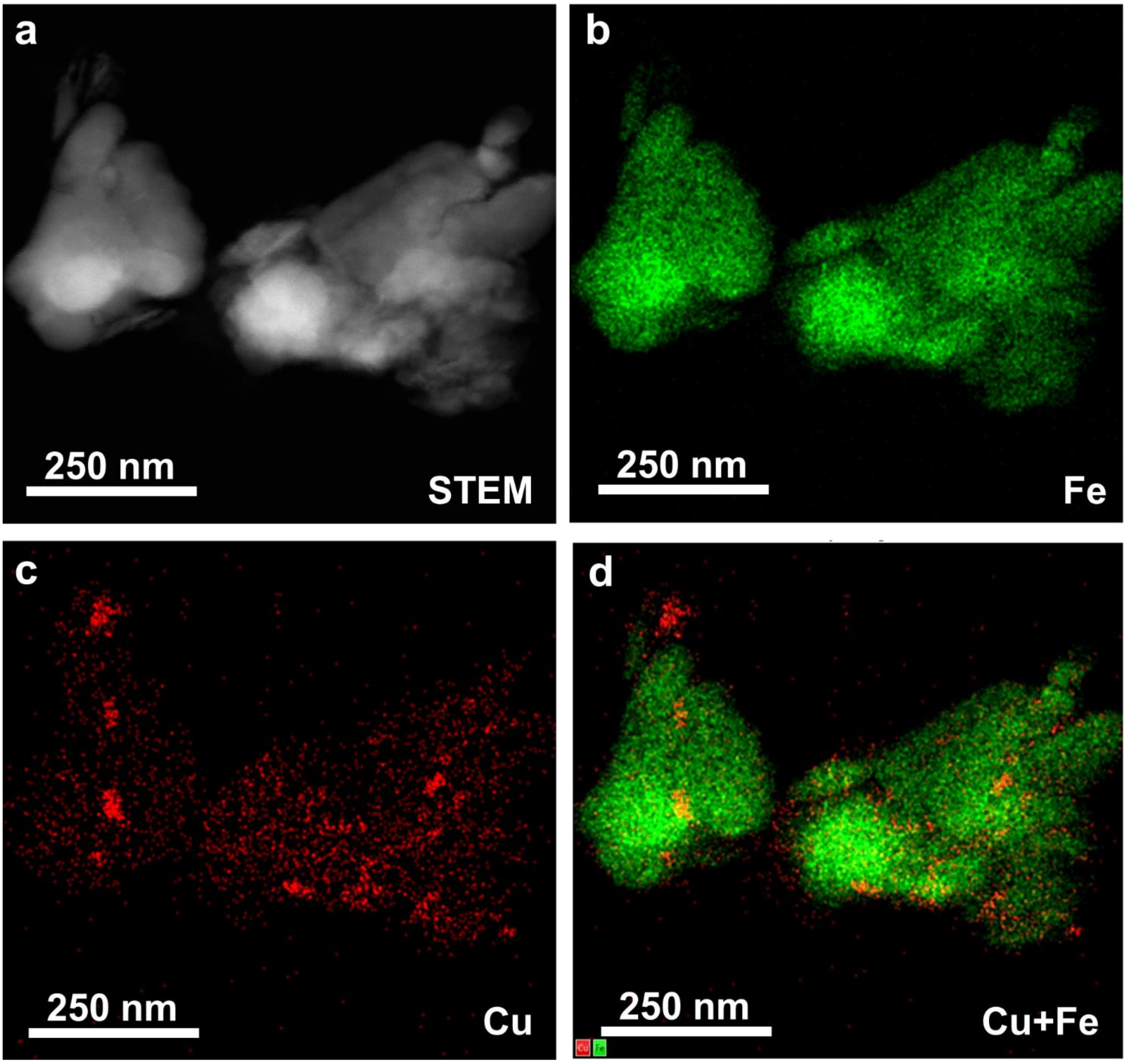

Figure S61. FESEM image and corresponding EDS mapping on the distribution of Fe and Cu in the used $Cu_{0.24}Fe_{0.76}$@C sample after four catalytic runs for hydrogenation of HMF.

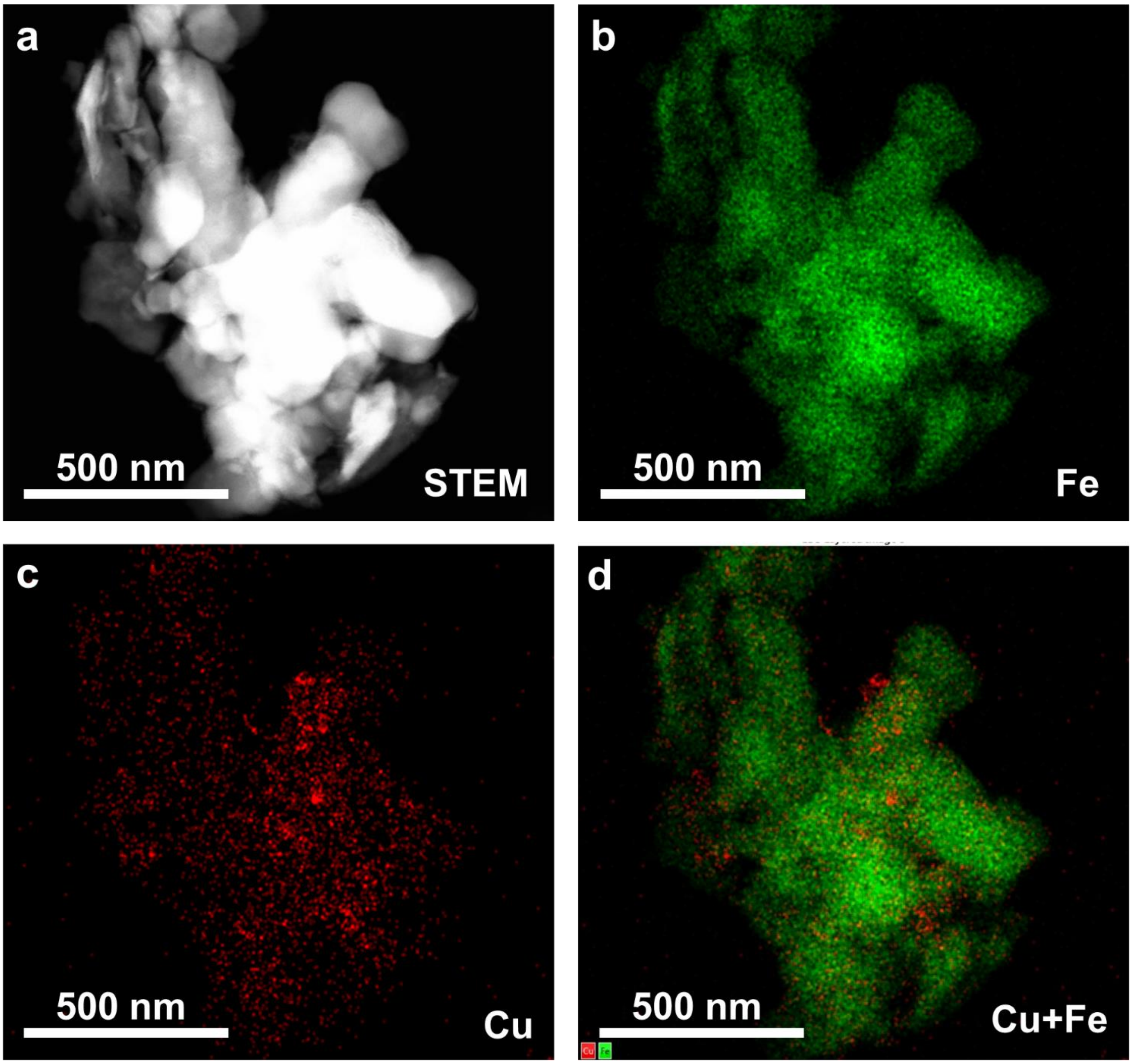

Figure S62. FESEM image and corresponding EDS mapping on the distribution of Fe and Cu in the used $Cu_{0.24}Fe_{0.76}$@C sample after four catalytic runs for hydrogenation of HMF.

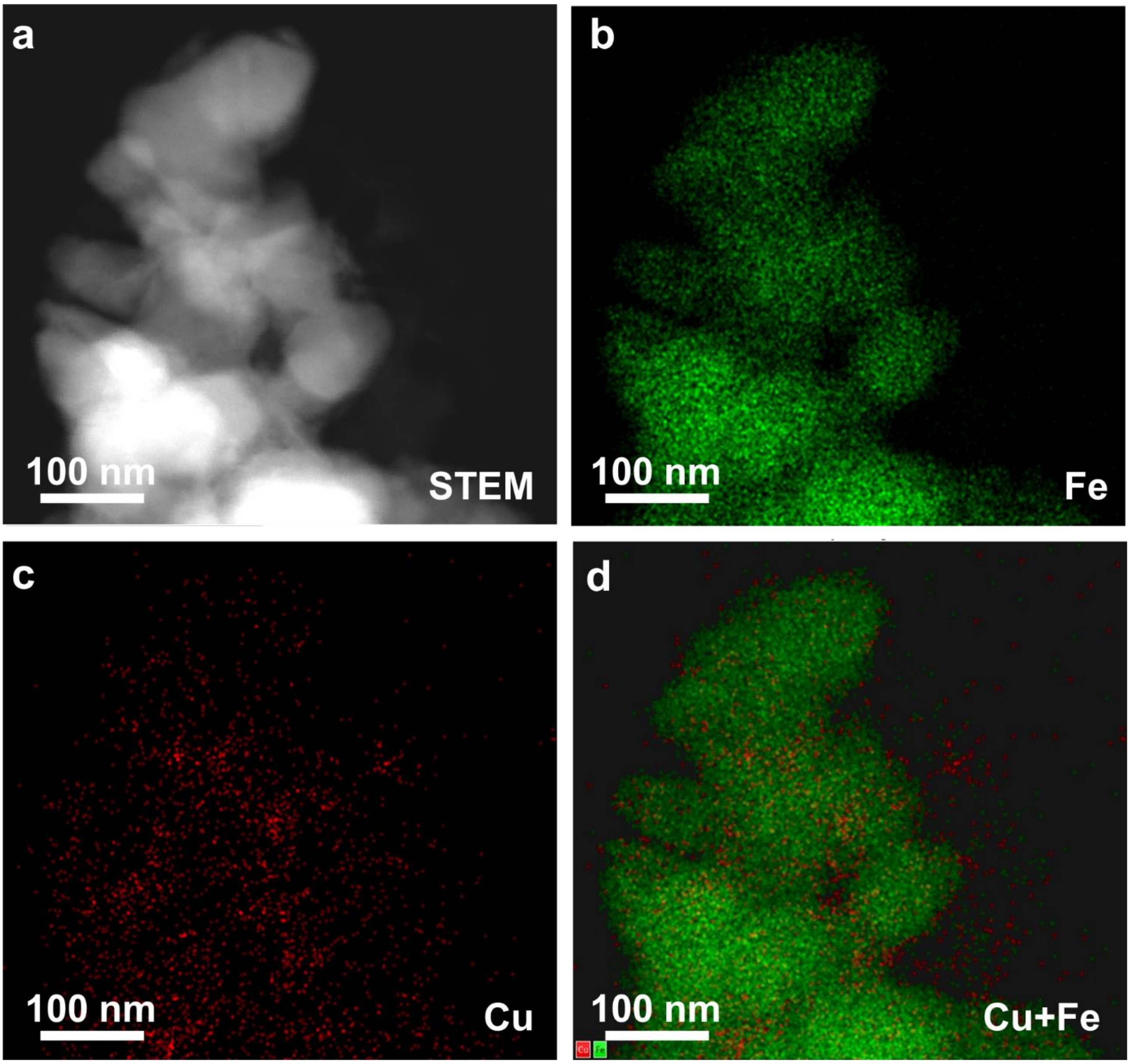

Figure S63. FESEM image and corresponding EDS mapping on the distribution of Fe and Cu in the used $Cu_{0.24}Fe_{0.76}$@C sample after four catalytic runs for hydrogenation of HMF.